HIGH TEMPERATURE CORROSION STUDIES OF SPUTTER DEPOSITED NANOSTRUCTURED COATINGS

A THESIS

Submitted in partial fulfilment of the
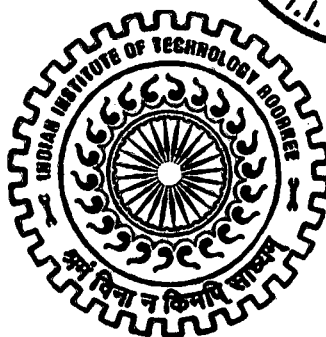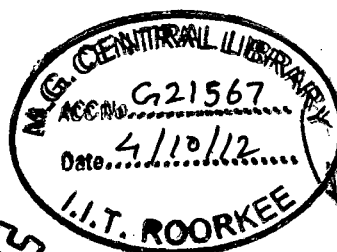*requirements for the award of the degree*
of

DOCTOR OF PHILOSOPHY

in

METALLURGICAL AND MATERIALS ENGINEERING

by

ATIKUR RAHMAN

DEPARTMENT OF METALLURGICAL AND MATERIALS ENGINEERING
INDIAN INSTITUTE OF TECHNOLOGY ROORKEE
ROORKEE-247 667 (INDIA)
NOVEMBER, 2011

INDIAN INSTITUTE OF TECHNOLOGY ROORKEE
ROORKEE
CANDIDATE'S DECLARATION

I hereby certify that the work which is being presented in the thesis entitled **High Temperature Corrosion Studies of Sputter Deposited Nanostructured Coatings** in partial fulfilment of the requirement for the award of the Degree of Doctor of Philosophy and submitted in the Department of Metallurgical and Materials Engineering of the Indian Institute of Technology Roorkee, Roorkee is an authentic record of my own work carried out during a period from July 2009 to November 2011 under the supervision of Dr. R. Jayaganthan, Associate Professor Department of Metallurgical and Materials Engineering and Dr. Ramesh Chandra, Associate Professor, Institute Instrumentation Centre, Indian Institute of Technology Roorkee, Roorkee.

The matter presented in this thesis has not been submitted by me for the award of any other degree of this or any other Institute.

(ATIKUR RAHMAN)

This is to certify that the above statement made by the candidate is correct to the best of our knowledge.

(Ramesh Chandra)   (R. Jayaganthan)
Supervisor   Supervisor

Date:-

The Ph.D. Viva-Voice examination of **Mr. Atikur Rahman**, Research Scholar, has

been held on 22 - 3 - 2012

Supervisors   Chairman SRC   External Examiner

Head of the Deptt./Centre and ODC

High temperature oxidation and hot corrosion are the serious problems in aircraft, marine, industrial and land-base gas turbines. It is because of the usage of wide range of fuels coupled with increased operating temperatures, which leads to the loss of mechanical strength and catastrophic failure of turbine engines. Due to extensive application of the superalloys in land-based and aero gas turbine engines, the high temperature oxidation and hot corrosion behaviour of superalloys has been the subject of intense investigation for the past several years. Most of the studies have focused on the mechanism of oxidation and hot corrosion such as oxide scale growth behaviour of materials based on short-term tests. An understanding of long term high temperature oxidation and hot corrosion behaviour of coatings on superalloys is extremely important for the industrial applications. Hot corrosion may be defined as an accelerated corrosion, resulting from the presence of salt contaminants such as Na_2SO_4, K_2SO_4, NaCl, and V_2O_5 that combine to form molten deposits, which damage the protective surface oxides. Hot corrosion occurs when metals are heated in the temperature range 700–900 °C in the presence of sulphate deposits formed as a result of the reaction between sodium chloride and sulphur compounds in the gas phase surrounding the metals. At higher temperatures, deposits of Na_2SO_4 are molten (m.p. 884 °C) and can cause accelerated attack on Ni-, Fe- and Co-based superalloys. This type of attack is commonly called hot corrosion. For example, alloy components in gas turbines in aircraft, thermal power plants, land-based power generators, boilers, internal combustion engines, gas turbines, fluidized bed combustion and industrial waste incinerators undergo hot corrosion. It is a life-limiting form of accelerated environmental attack that can occur on vanes and blades in the hot sections of gas turbine engines. During hot corrosion, a porous non-protective oxide scale is formed at the surface and sulphides in the substrate. This form of corrosion, unlike oxidation, can consume the material at an unpredictably rapid rate. Consequently, the load-carrying ability of the components reduces quickly, leading eventually to catastrophic failure. It is due to the following reasons; for example, superalloys used for high temperature applications could not meet the requirements of both the high-temperature strength and the

high-temperature erosion–corrosion resistance simultaneously. MCrAlY coatings play a significant role in protection of hot section components in gas turbine engine system, either as overlays or as bond coats. In order to increase the efficiency of gas turbine engines and protection from high temperature oxidation and hot corrosion over a wide range of temperature, nanostructured MCrAlY bond coats have been developed as reported in the literature **(Jiang** S.M et al. 2008). However, limited studies have been reported on the Cr/Co-Al bond coat and Co-Al bond coat on Ni-base superalloy deposited by using magnetron sputtering, which is an excellent technique to produce high-quality films and coatings **(Ulrich** S et al. 2009). Nanostructured MCrAl Y(M=Ni or Co) coatings deposited on superalloy by magnetron sputtering showed an improved high temperature oxidation and hot corrosion resistance at 900 °C as compared to bare superalloy as reported in the literature **(Rahman** A et al. 2008, 2009, 2010 and 2011). Since nanosized grain possesses high density of grain boundaries, it provides the more favorable sites of diffusion for the easier formation of protective scales. The present work has been focused to study the high temperature oxidation and hot corrosion behaviour of nanostructured Cr/Co-Al coatings and Co-Al coatings deposited on Superni-718 in air and molten salts (Na_2SO_4-60%V_2O_5) environment at 900 °C and also bare Superni-718 substrate to assess the performance of coated superalloy. Superni-718 superalloy was developed by Mishra Dhatu Nigam Limited, Hyderabad (India) for the high temperature applications such as turbine blade of jet engine and high-speed airframe parts such as wheels, buckets, spacers, high temperature bolts and fasteners.

A study on the behaviour of aforementioned coatings in air and molten salts environment will be helpful in choosing the suitable coating on substrate to withstand against oxidation and hot corrosion problems manifested in the gas turbine and boiler applications. The outcome of the present research work are critically analyzed and discussed in the light of existing literature to propose an insight into the corrosion mechanism in both coated and bare superalloy. The whole thesis is presented in 7 chapters.

Chapter 1 contains a brief introduction of the oxidation and hot corrosion effects and its deleterious impact on the various engineering equipments and components. The importance of nanostructured coatings for high temperature applications is also briefly discussed. .

Chapter 2 contains oxidation and hot corrosion studies reported by various researchers relevant to the current study. It has been critically reviewed particularly those conducted on Ni- based alloys in air and molten salt environments. The problem has been formulated based on the available literature on oxidation and hot corrosion behaviour of coated and bare superalloy used in high temperature applications.

Chapter 3 presents the experimental techniques and procedures employed for deposition of the coating and their characterisation, oxidation studies in air, and molten salts environment. The specification of the equipments and other instruments used for the present investigation and the techniques used to analyze the corrosion products are discussed below.

Nanostructured coatings were deposited by Magnetron Sputtering process at Institute Instrumentation Centre Roorkee, IIT Roorkee on Superni-718 superalloy. Superni-718 superalloy was procured from Mishra Dhatu Nigam Ltd., Hyderabad (India). In the present work Cr/Co-Al and Co-Al coatings were deposited on Superni-718 at different substrate temperature in the range of 250-700 °C.

The as-deposited coatings were characterised by X-ray diffraction, FE-SEM/EDS, and AFM. The oxidation and hot corrosion behaviour of bare and magnetron sputtered coated superalloy has been studied in the air, and molten salts (Na_2SO_4-60%V_2O_5) in the laboratory furnace for 50-100 cycles under cyclic conditions. Each cycle consisted of 1 hour heating at 900 °C in a silicon carbide tube furnace followed by 30 minutes cooling at room temperature (25 °C), these studies were performed for uncoated as well as coated specimens for comparison. At the end of each cycle, the specimens were critically examined regarding the color, luster, physical changes on the samples, scale adherence/spallation and then subjected to weight change measurements. The molten salt studies were performed by applying a uniform layer (3-5 mg/cm^2) of the mixture of Na_2SO_4-60%V_2O_5 on the preheated specimens (250 °C) with the help of camel hair brush. XRD and FE-SEM/EDS analytical techniques were used to identify the phases and the elemental analysis of the surface scale, respectively. The coated samples were then cut across the cross-section for analyzing its elemental composition by FE-SEM/EDS.

Chapter 4 deals with the detailed investigation of bare substrate and magnetron sputtered Cr/Co-Al coatings on Superni-718 superalloy, which include deposition,

characterisation, oxidation and hot corrosion studies in air and in molten salt (Na_2SO_4 -60% V_2O_5) environments in the laboratory under cyclic condition at 900 °C for 50 and 100 cycles. The techniques such as XRD, FE-SEM/EDS and AFM were used to analyze the as-deposited coatings and the corroded specimens are characterized by XRD, and FE-SEM/EDS. This chapter is divided into two sections. The first section **(Section 4.1)** describes the deposition of nanostructured Cr/Co-Al coating on superni-718 at 250, 350, 450, 500, and 700°C substrate temperatures, and their high temperature oxidation behaviour at 900 °C for 50 and 100 cycles in air and compare with bare substrate. With increase in substrate temperature, the surface mobility of condensed atoms increases, which could easily diffuse from island side to lower potential zone of substrate, resulting in denser coating with reduced porosity or voids in coatings. XRD and CoAl binary phase diagram confirmed that on the surface of coatings before oxidation has β-CoAl phase. Thickness of coatings was approximately 4.5 to 5 μm was calculated by FE-SEM cross-sectional analysis. Coated superalloy at 250, 350, and 450°C has higher oxidation resistance in air environment at 900 °C for 50 hrs as compare to bare superalloy, due to formation of protective and adherent scale such as Al_2O_3, Cr_2O_3, CoO, and $CoCr_2O_4$ spinel. Among them Cr/Co-Al coated sample at 350 °C has highest oxidation resistance. Cr/Co-Al Coated superalloy at 700 °C substrate temperature has highest oxidation resistance in air environment at 900 °C for 100 hrs as compare to Cr/Co-Al coated sample at 500 °C and bare superalloy, due to formation of dense, protective and adherent scale such as Al_2O_3, Cr_2O_3, CoO, and $CoAl_2O_4$ spinel as a major phase and $CoCr_2O_4$ spinel as a minor phase. Also, Cr/Co-Al Coated superalloy at 700 °C before oxidation has dense morphology of coating, since it belongs to structure zone 3, which is confirmed by surface as well as cross-sectional FE-SEM micrograph. **Section 4.2** describes the study of cyclic hot corrosion of nanostructured Cr/Co-Al coatings on Superni-718 substrate in molten salt (Na_2SO_4-60%V_2O_5) environment at 900 °C for 50 and 100 cycles and is compared with bare Superni-718 superalloy. The better hot corrosion of Cr/Co-Al coated sample at 700 °C substrate temperature might be attributed to the formation of three dimensional pyramidal scale morphology on corroded dense surface and continuous oxide scale formed on cross-section. The scale mainly consisting of $NaAlO_2$, $CoAl_2O_4$, $CoCr_2O_4$, CoO, Al_2O_3 and Cr_2O_3.

Chapter 5 contains the investigation of deposition, characterisation, oxidation, and hot corrosion of Co-Al coatings on Superni-718 at different substrate temperature and bare

Superni-718 substrate in the laboratory under cyclic condition at 900 °C for 100 cycles. The techniques such as XRD, FE-SEM/EDS and AFM were used to analyze the coated samples before and after oxidation and hot corrosion. The thickness of coating was calculated by FE-SEM cross-sectional analysis and was approximately 4 μm. It showed a good adhesion with the substrate. This chapter is divided into two sections. The first section **(Section 5.1)** describes degradation behaviour of sputtered Co-Al coatings on Superni-718. Co-Al coatings were deposited at 500-700 °C substrate temperature. At the substrate temperature 800 °C, the deposited coatings peeled off due to the induced thermal stress in the coatings, which is confirmed by FE-SEM/EDS.

Oxidation kinetic was established at 900 °C for 100 cycles under cyclic conditions. The sputtered Co-Al coated sample at 700 °C has provided a maximum oxidation resistance in air at 900 °C for 100 hrs. The presence of Al_2O_3, Cr_2O_3 and CoO and respective spinels might have contributed for better oxidation resistance. **Section 5.2** describes the microstructural characterization and cyclic hot corrosion behaviour of sputtered Co-Al nanostructured coatings on superalloy at 500-700 °C substrate temperature in molten salt (Na_2SO_4-60%V_2O_5) environment at 900 °C for 100 cycles. The bare and sputtered Co-Al coated sample depicts least and improved hot corrosion resistance in molten salt environments at 900 °C for 100 hrs. The Co-Al coated sample at 700 °C shows better hot corrosion resistance might be due to dense coating before hot corrosion and after hot corrosion attributed to the formation of dense oxide scale with phases like Al_2O_3, Cr_2O_3, CoO, $NiCr_2O_4$, $CoAl_2O_4$ and $CoCr_2O_4$. Spinel phases might have blocked the all possible paths/defects in scale which has formed during cyclic hot corrosion and to enhance the hot corrosion resistance.

Chapter 6 describes the comparative results of the bare Superni-718 substrate and magnetron sputtered Cr/Co-Al and Co-Al coated Superni-718 at different substrate temperature in air, and molten salt environments (Na_2SO_4-60%V_2O_5) at 900 °C under cyclic conditions.

Chapter 7 includes conclusions of the present investigation and scope for the future work.

ACKNOWLEDGEMENTS

LIST OF FIGURES

Diffractometer (Bruker AXS, D8 Advance).

after 50 cycles in molten salts environments at 900°C, (b) corroded Cr/Co-Al coatings on Superni-718 at 500 -700°C substrate temperature and bare Superni-718 substrate, after 100 cycles in molten salts environment at 900°C.

900 °C for 100 cycles.

LIST OF TABLES

(II) PAPER PUBLISHED IN NATIONAL / INTERNATIONAL CONFERENCE PROCEEDING

1. **Atikur Rahman**, V. Chawla, R. Jayaganthan, R. Chandra, and R. Ambardar, High Temperature Oxidation Behaviour of Nanostructured Co-Al Coating on Superalloy, 2nd International Conference on Production and Industrial Engineering CPIE-2010 (3rd-5th December, 2010), NIT Jalandhar, pp.232-236..

2. **Atikur Rahman**, R. Jayaganthan, R. Chandra, and R. Ambardar, Cyclic Oxidation Resistance of Co-Al Coatings deposited on Superni-718 by Magnetron Sputtering Process, 49th National Metallurgist Day and 65th Annual Technical Meeting NMD-ATM-2011 (13th -16th November, 2011), Indian Institute of Metals Hyderabad, Theme 1.2, pp.51.

ABBREVIATIONS

Bal	Balance
SEI	Secondary Electron Image
EDAX	Energy Dispersive X-ray Analysis
EDS	Energy Dispersive X-ray Spectroscopy
hr	Hour
HVOF	High Velocity Oxy-Fuel
K_p	Parabolic Rate Constant
LPPS	Low Pressure Plasma Spray
m.p.	Melting Point
min	Minute
FE-SEM	Field Emission Scanning Electron Microscopy
VPS	Vacuum Plasma Spray
Wt%	Weight Percentage
Wt. Gain	Weight Gain
XRD	X-ray Diffraction
LTHC	Low temperature hot corrosion
HTHC	High temperature hot corrosion

CONTENTS

CHAPTER 6 COMPARATIVE DISCUSSION

CHAPTER 7 CONCLUSIONS

SUGGESTIONS FOR FUTURE WORK

REFERENCES

CHAPTER 1

INTRODUCTION

1.0 INTRODUCTION

Corrosion is known as oxidation or dry corrosion. Metals and alloys experience accelerated oxidation when their surfaces are covered with a thin film of fused salt, such as Na_2SO_4, NaCl and V_2O_5 in oxidizing atmosphere at elevated temperatures. These fused salts damage the protective oxides / scales. This mode of attack is called hot corrosion, where porous non-protective oxide scale is formed at the surface and sulphides in the substrate. This form of corrosion unlike oxidation, can consume the metal at an unpredictably rapid rate.

High temperature oxidation and hot corrosion are serious problems in gas turbines, internal combustion engines, and fluidized bed combustion, paper and pulp industries. No alloy is immune to high temperature oxidation and hot corrosion attack indefinitely, although there are some alloy compositions that require a long initiation time at which high temperature oxidation and hot corrosion process move from the initiation stage to the propagation stage.

Hot corrosion has been observed in gas turbines, internal combustion engines, boilers, fluidized bed combustion and industrial waste incinerators since 1940's. However, it became a topic of importance and popular interest in the late 1960's when gas turbine engines of military aircrafts suffered severe corrosion attacks while operating over and near sea water during the Vietnam conflict **(Rapp 1986 and 2002).**

Corrosion occurs when molten compounds (Na_2SO_4 melting point $884^{\circ}C$) dissolve the protective oxide layers, which naturally form on materials during boiler/gas turbine operation. Moreover, the vanadium compounds are also good oxidation catalysts and allow oxygen and other gases in the combustion atmosphere to diffuse rapidly to the metal surface

and cause further oxidation. As soon as the metal is oxidized, the cycle starts over again resulting into high corrosion rates **(Natesan 1976, Sharma 1996).**

In energy generation processes, the mechanism of hot corrosion is dependent on the formation of a liquid phase that is predominantly Na_2SO_4 or K_2SO_4. The sulphur released from the coal, forms SO_2 with a minor amount of SO_3 and reacts with the volatilized alkalis to form Na_2SO_4 vapor, which then condenses together with fly ash on the super-heater and reheater tubes in the boiler. Such a liquid phase dissolves the chromium oxide in the protective coating, which allows the base metal to react with sulphate ions to form sulphide ions and non-protective oxides **(Natesan 1976 and Rapp et al. 1981).**

Superalloys (Ni -, or Co- and Fe-based) are used as structural components in various applications such as gas turbines, steam boiler, heat exchangers, aeroengines and industrial springs as they possess superior mechanical properties, and corrosion and oxidation resistance to some extent. During operation, blades and vanes of gas turbines are subjected to severe thermal cycling and mechanical loads. In addition, they are also attacked chemically by both high temperature oxidation and hot corrosion. It is impossible to impart both high temperature strength and high temperature oxidation and corrosion resistance to the superalloys simultaneously along with ease of manufacturing. It is possible only with the composite materials to meet such requirements, where the base material provides the necessary mechanical strength and the coating provides the protection against wear, erosion-corrosion, and oxidation.

Therefore, protective superalloy coatings are currently used on superalloys in energy conversion and gas turbines to protect their surfaces from oxidation and hot corrosion. However, to realize the enhanced efficiency, which is unattainable with the conventional MCrAlY (M=Ni or Co or Fe) coatings, of gas turbine engines, nanostructured MCrAlY (M=Ni or Co or Fe) coatings with superior performance in terms of high temperature oxidation resistance and thermo-mechanical fatigue life are required. It is well known in the literature that the nanostructured coatings provide a better corrosion resistance at high temperature due to the formation of continuous protective layer assisted by the enhanced

diffusivity of atoms in the coating (**Geng et al. 2003, Ren et al. 2006, Chen et al. 2000, Peng et al. 2003, Ajdelsztajn et al.2002**).

Nanostructure Coatings form protective oxide scales with superior adhesion to the substrate (**Gao et al. 2004**) . The high density of grain boundaries provides fast diffusion paths, promoting selective oxidation of protective oxide scales. The fine-grained coatings and/or the fine-grained oxide scales show a fast creep rate at high temperatures, which can release the stresses accumulated in the scales, therefore reducing the scale spallation tendency. The oxides formed on nanocrystalline coatings are micro pegged onto the grain boundaries to form a complex interface that results in better scale adhesion to the metal substrate. Nanocrystalline alloy coatings, oxide-dispersive alloy coatings and metal-oxide composite coatings show superior high-temperature corrosion resistance. Engineering alloys rely on the formation of protective oxide films such as Al_2O_3 and Cr_2O_3 to resist high temperature and corrosive environments. Unfortunately, relatively large concentrations of Al or Cr are needed to form a complete Al_2O_3 or Cr_2O_3 scale in conventional coating. In the Ni-20Cr-Al alloy system, for instance, greater than 6 wt% Al is required to form a complete Al_2O_3 scale. With nanocrystalline coatings, the Al content that is required to form a complete protective oxide scale can be substantially reduced. Experimental results indicate that when the grain size of Ni-20Cr-Al coatings was ~60 nm, alloys containing ~2 wt% Al could form a complete α- Al_2O_3 scale at 1000°C in air. This concentration is only one-third of the required Al% for the Ni-20Cr alloy with normal grain size.

Over the past two decades, there has been considerable research on the development of coatings with finer microstructures approaching the nanometer scale. The nanocrystalline Al–Fe–Ti–Cr–Zn–Cu high entropy alloy is stable even after sintering at 800°C for 1 h and has a high hardness of 2GPa as compared to microcrystalline Al–Fe–Ti–Cr–Zn–Cu system (**Kamaraj M et al 2008**). Nanostructured coatings are more resistant to high-temperature oxidation and corrosion than their counterpart conventional coatings (**Gao et al. 2001, Liu et al. 1999, Zhang et al. 2005**). Short-term (50–200 h.) test results on Fe–Ni-Cr–Al and Ni–Cr–Al coatings have shown that the protective oxide layer formed on the

nanocrystalline coatings exhibited better spallation resistance during cyclic oxidation testing compared to the conventional cast materials of the same chemical compositions of the coatings. The oxide layer formed on the nanocrystalline coating on 310 SS samples exhibited excellent spallation resistance during cyclic oxidation testing at 1000°C for up to 100 one hour thermal cycles (**Liu et al. 1999**). The effect of heat treatment on the corrosion behaviour of binary Al–Fe alloys containing iron at levels between 0.04 and 0.42 wt.% was investigated by **Rajan et al.(2006).**

Several investigators have recently assessed the oxidation resistance of nanocrystalline Ni–Cr–Al coatings (**Liu et al. 1998, Chen et al.1999, Chen et al.2000, Liu and Gao 1998**). The results of these investigations indicate that the grain size and Cr/Al contents have a strong influence on the selective Al oxidation behavior of these coatings. Typically, ultra-fine grain size and higher Cr/Al ratio promote selective oxidation of Al and formation of a continuous protective alumina scale, α -Al_2O_3, on the external surface.

Liu et al.(1998) have studied the effect of grain size on protective oxide scale formation and spallation behavior of oxide scale on a Ni–20Cr–3Al coating. Their 50 one-hour thermal cycling test results at a peak temperature of 1100°C showed that fine grain size promoted formation of either alumina, Al_2O_3, or chromia, Cr_2O_3, as opposed to formation of a mixed oxide scale. The oxide scale formed on the ultra fine grain coated surface varied from α -Al_2O_3 to Cr_2O_3 as the coating grain size increased from 50 to 500 nm. Specifically, the finer coating grain structure promoted selective oxidation of Al through rapid diffusion of Al along the grain and sub-grain boundaries.

Numerous techniques are now available for the preparation of nanostructured coatings and among them, vacuum-based deposition techniques fall into two basic categories: chemical vapor deposition (CVD) and physical vapor deposition (PVD). Chemical vapor deposition (CVD) is a process where one or more gaseous adsorption species react or decompose on a hot surface to form stable solid products.

The main steps that occur in the CVD process can be summarized as (**Hitchman et al. 1993**):

  a) Transport of reacting gaseous species to the surface

  b) Adsorption of the species on to the surface

  c) Heterogeneous surface reaction catalyzed by the surface

  d) Surface diffusion of the species to growth sites

  e) Nucleation and growth of the films

  f) Desorption of gaseous products and transport of reaction products away from the surface

Plasma-assisted chemical vapor deposition (PVCVD) technique was used to synthesize such nanostructured films at the beginning. However, in CVD techniques, molecular species in the gas phase chemically react at a film surface, leading to the formation of a condensed film as well as the emission of volatile by-products. It also makes use of aggressive chemicals as metal sources for the deposition of coatings. Due to the undesirable characteristics of chemicals emanating from CVD, physical vapor deposition (PVD) technique is considered to be more suitable for industrial-scale synthesis of these films (**Li et al. 2005**). It may be mentioned that CVD is a more complex method of forming thin films and coatings than PVD. In PVD, the synthesis of thin films is usually carried out from the same material and its purity depends on the starting materials, base vacuum, and purity of the ambient gas atmosphere (**Xue Jun Min et al.2002**). On the other hand, CVD technique, some un-reacted chemicals and products other than the desired one are often left behind after the deposition of coatings.

The development of new materials can only be produced by means of sophisticated and therefore less economical production methods. The deposition of solids from the vapor phase enables the production of a wide range of new materials without resorting to the problems of liquid phases (**Knotek et al. 1987**). Therefore, physical vapor deposition (PVD) is a versatile synthesis method and it is gaining more prominence in semiconductor and coating technology. PVD is capable of depositing thin film materials with structural control over

atomic or nanometer scale by careful monitoring of the processing conditions. Materials with high melting points and high reactivity can be deposited easily by PVD processes. Also, homogeneous multicomponent phases as well as multilayer coatings can be easily produced with completely new material properties. By controlling the substrate temperature, materials can be deposited in different structures, such as amorphous, microcrystalline and the nanocrystalline structures **(Knotek et al. 1987).**

PVD involves the generation of vapor phase species either via evaporation, sputtering, laser ablation or ion beam. In evaporation, atoms are removed from the source by thermal or electron means; in sputtering, atoms are ejected from the target surface by the impact of energetic ions. In the former case, the vapor phase species that experience collisions and ionization are condensed onto a substrate following nucleation and growth phenomena. Thermal evaporation has a limitation in multi component materials since one of the metallic elements typically evaporates before the other due to the differences in vapor pressures of the evaporating species. On the contrary, sputtering is capable of depositing high melting point materials such as refractory metals and ceramics, which are difficult to fabricate using evaporation. Since the sputtered atoms carry more energy than the evaporated atoms, the sputter-grown films usually have higher density. In general, sputtering seems to be the most appropriate technique to deposit ternary compounds because the transformation of the original materials into a gaseous state does not involve an intermediate liquid phase, but instead occurs directly as a result of an atomic momentum transfer at the target **(Huang et al. 2005A).**

Magnetron sputtering is of particular importance due to its easy handling, high reproducibility and high flexibility of large-scale as well as complex geometry shape production **(Shum et al. 2004)** and also the configuration of the magnetic field confines the electrons and gives a high degree of ionization near the target. The indirect result of this process is that the vapor flux ejection from the target is higher and, consequently, the deposition rate is increased; recent developments, such as an unbalanced magnetron, give further benefits in this respect. Another advantage in magnetron sputter deposition lies in the fact that such systems can be made to work at lower pressure than D.C. glow and R.F

discharges to obtain a high-quality, low impurity films at a reasonable deposition rate **(Brizoual et al. 1999).** Also the importance of sputtering methods is that it involves a number of parameters such as sputtering pressure, sputtering power, substrate-target distance and substrate temperature, etc. whereby a number of combination of these parameters may be used to obtain high quality films with required properties.

Magnetron sputtered **Cr/Co-Al and Co-Al** nanostructured coatings on Superni-718 substrate have been chosen for the present investigation due to the formation of intermetallic β-CoAl phases in the Co–Al based superalloy coatings show high melting point (1640°C), which is beneficial for providing, oxidation resistance at very high temperature above 1000°C in the actual service applications, especially in gas turbines. The CoAl based nanostructured superalloy coatings could serve as potential protective coatings for the components in energy conversion systems such as stationary gas turbines of power plants, internal combustion engines, heat exchangers and jet engines operating at high temperatures, and in severe corrosive environments. High temperature resistant alloys based on the intermetallic compound CoAl alloyed with the refractory metals such as Cr, Mo or Re can be used as protective coatings for prospective energy conversion systems operating up to 1300°C in corrosive environments.

CHAPTER 2

LITERATURE REVIEW

This chapter deals with a comprehensive review of the literature with reference to oxidation theory, hot corrosion chemistry, high temperature oxidation and hot corrosion of nickel-based superalloy and nanostructured coatings in molten salt environments.

2.1 OXIDATION THEORY

2.1.1 Thermodynamics

Metals in general are not stable in an environment containing oxygen. A few exceptions exist for gold and silver at moderately low temperatures. For most metallic elements, a general reaction between the metal (M) and oxygen (O) in the gas can be written as

$$aM + b/2O_2 = M_aO_b \qquad (2.1)$$
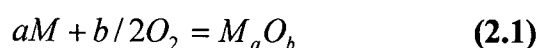
The Gibb's Free Energy (ΔG) associated with such a reaction is generally negative. A convenient way to graphically display the relative stabilities of these reactions for various types of elements is to use a Richardson/Ellingham diagram as shown in **Fig. 2.1**. From this diagram, the elements such as aluminum, silicon and chromium are near the bottom for unit activity of the metal, which shows the oxides of these metals are more stable than the oxides of the elements above them and it is this large affinity for oxygen that makes them the desired alloying element for oxide scale formation.
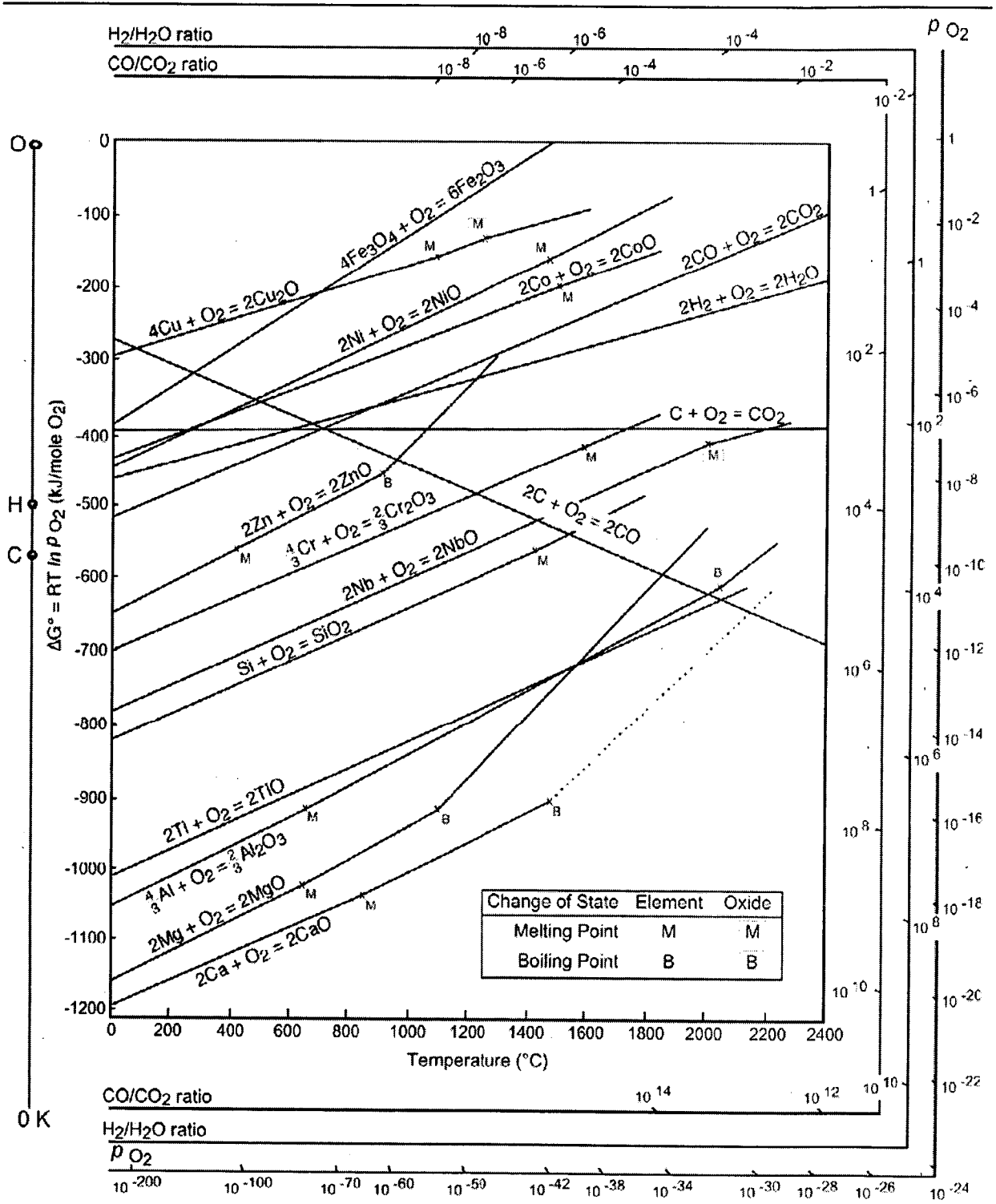
Fig. 2.1   Richardson-Ellingham diagram for oxides

2.1.2 Oxidation Product

The above section gives insight to which element in the alloy will form the stable oxide, but the morphology of the product is important to form a protective barrier. Upon exposure to oxidizing conditions, the surface elements will react with the oxidant to produce the oxide scale. This product should form a dense continuous scale to separate the two reactants (metal and oxygen). The single purpose of the scale is to act as a diffusion barrier and limit the transport of metal and oxygen atoms from further reaction. The integrity of this oxide scale must be maintained through changes in environment such as thermal cycling and exposures to oxidizing atmospheres with fluctuation in oxygen potential.

2.1.3 Transport

Further oxidation of the metal requires transport of one of the reactants through the scale, the dense oxidation product. Solid state diffusion is the process by which this occurs. The driving force for metal cation and/or oxygen anion diffusion through the scale is the chemical potential or activity gradient created across the scale as demonstrated in **Fig. 2.2**. Thermodynamic equilibrium fixes the activities at the interfaces, where the activity of the metal in the oxide is equal to that of the metallic element in the alloy at the metal-oxide interface, and the apparent oxygen partial pressure will be the dissociation pressure for that oxide. A similar treatment can be utilized at the gas-oxide interface to calculate activity of the metal where the pressure of the oxygen is that in the atmosphere. From these chemical potential gradients, two types of transport can exist. One type is the inward diffusion of the oxygen ions and the other is the outward transport by the cation of the metal species. Electro neutrality is required, and therefore, the fluxes across the scale are accompanied by transport of electronic defects. **Fig.2.2** shows the respective fluxes of ionic and electronic species.

Metal
M

Oxide
MO

Gas
O_2

Cations →

← Cation Vacancies

Electrons →

← Anions

$a_M' = 1$

p_O''

$$(p_{O_2}')_{M/MO} = \exp\left(\frac{2\Delta G_{MO}^\circ}{RT}\right)$$

$$a_M' = \left(\frac{1}{p_{O_2}''^{\,1/2}}\right)\exp\left(\frac{\Delta G_{MO}^\circ}{RT}\right)$$

x

$M = M^{2+} + 2e^-$
or
$M + O^{2-} = MO + 2e^-$

$M^{2+} + 2e^- + \tfrac{1}{2}O_2 = MO$
or
$\tfrac{1}{2}O_2 + 2e^- = O^{2-}$

Overall reaction: $2M + O_2 = 2MO; \Delta G_{MO}^\circ$
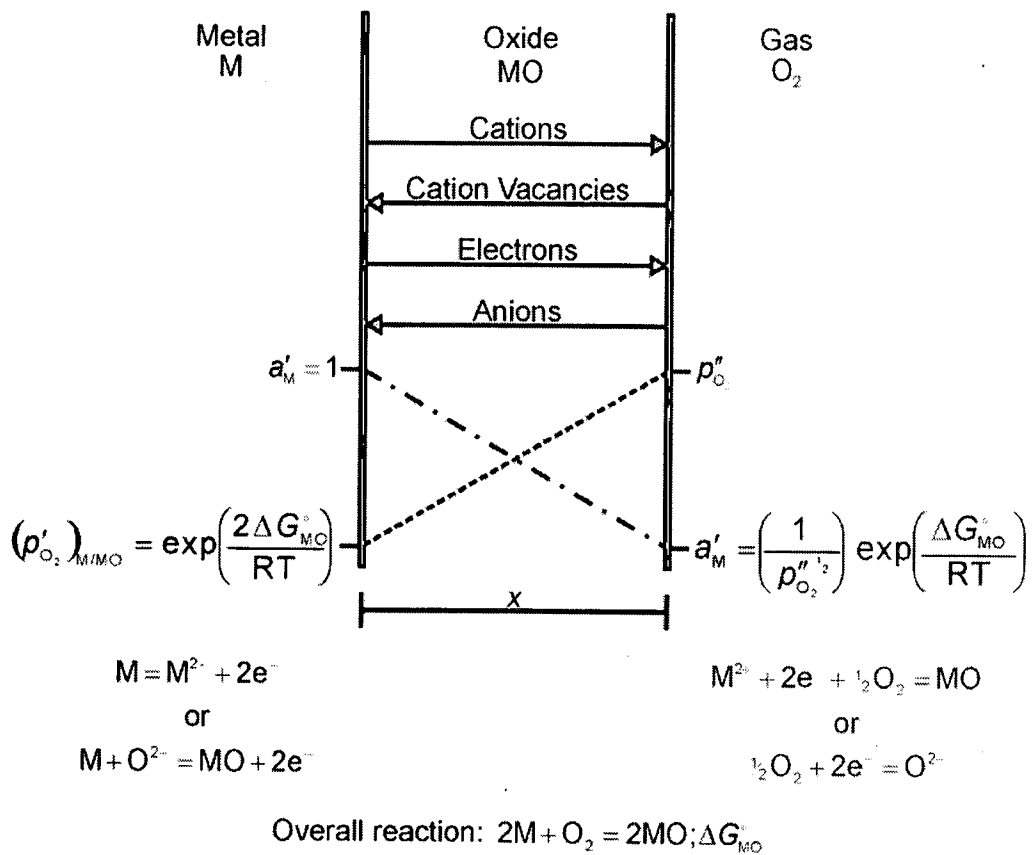
Fig.2.2 Schematic diagram of species transport and equilibrium reactions

Wagner quantified the diminishing growth rate as the decrease in the thickening of the oxide scale with time (**Wagner C. 1952**). As the scale thickens, the diffusion distance increases ultimately reducing the reactant flux establishing an ever decreasing scale growth rate. He formulated the parabolic rate law, where

$$x^2 = 2 \cdot k_p \cdot t \qquad\qquad (2.2)$$

Here the square of the scale thickness, x^2 is proportional to time, t and the proportionality constant is k_p, the parabolic rate constant. It is experimentally easier to continuously monitor oxidation by mass change rather than scale thickness.

Similar to **Eq. (2.2)**,

$$\left(\frac{\nabla m}{A}\right)^2 = K'' \cdot t \qquad\qquad (2.3)$$

the parabolic rate law can be expressed in terms of oxygen uptake normalized per unit surface area, $\left(\dfrac{\nabla m}{A}\right)^2$. A comparison of parabolic rate constants for selected oxide scales as a function of reciprocal temperature is presented in **Fig.2.3**. In this graph, the parabolic rate constant for mass gain (k'') is used instead of the k_p.
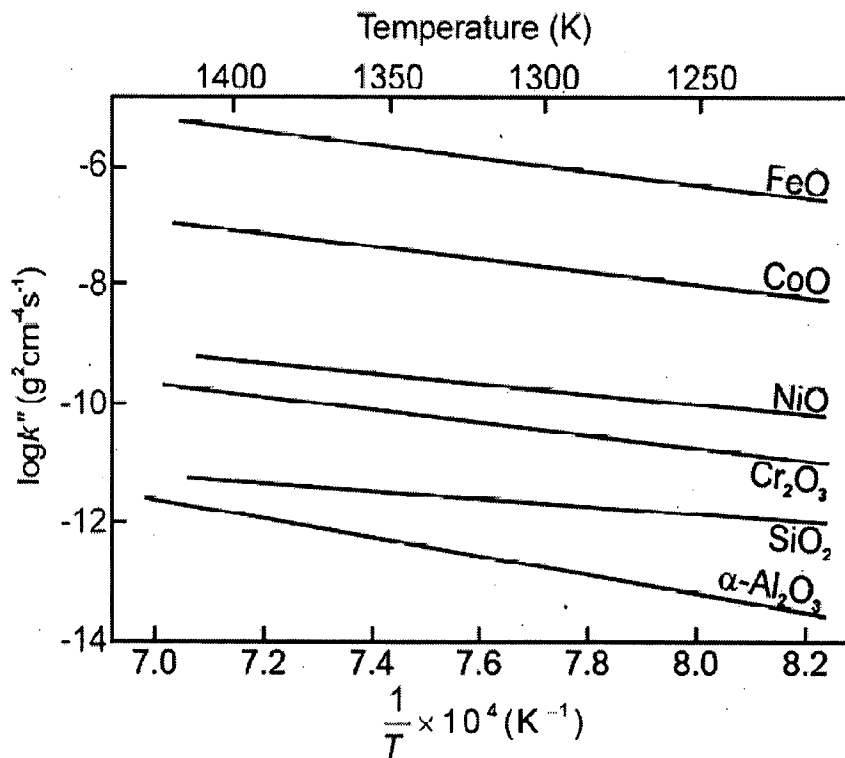
Fig.2.3   Plot of isothermal parabolic growth constant versus inverse temperature for various oxide scales.

Other rate equations exist for the various types of oxide scales. Different treatments of the transport, rate controlling step and the nature of the scale itself need to be considered. For the oxidation of a large number of metals at low temperature, a logarithmic rate law can be used to describe the kinetics. This equation

$$x = k_{\log} \cdot \log(t - t_o) + A \qquad (2.4)$$

and $k_{\log}, t_o$ and A are constants. This rate equation represents the behavior of metals at temperatures in the range of 300-400°C. In this temperature range, the oxide scales thicken rapidly followed by insignificant growth. Rate limiting transport of electronic defects or voids in these thin scales is theories that explain this type of behavior.

A linear law exists for a growth rate of a scale that is independent of time or oxide thickness. Here

$$x = k_l \cdot t \qquad (2.5)$$

And k_l is the rate constant for this linear behavior. Transport across a boundary layer or a phase boundary reaction could be the limiting step for this process that results in the linear growth rate. Another phenomenon resulting in growth kinetics independent of scale thickness is the continual cracking of the oxide scale. From these different rate equations for the oxidation of metals, the parabolic rate equation most accurately describes the behavior of high temperature alumina formers.

2.1.4 Selective Oxidation

The ability for an alloy to form a protective oxide is a thermodynamic and kinetic issue. From thermodynamics, the predicted oxide scale will be of the element that has the largest affinity for oxygen. For this investigation, let us focus on alloys that form an alumina layer. During the initial stage of oxidation, all of the elements in the alloy will oxidize and the initial scale will be composed of elements in proportions as they are present in the alloy or

coating. Once this transient oxide forms a continuous layer on the alloy, a drop in oxygen activity at the oxide metal interface will only allow the thermodynamically more stable oxide to continue to form. The capability of the alloy to maintain this oxide depends on the amount of this element in reserve and its ability to diffuse to the scale for further reaction. The concentration in the alloy to achieve this can be represented by

$$N_B^{Critical} = \frac{V_m}{32v}\left(\frac{\pi k_p}{D_B}\right)^{1/2} \tag{2.6}$$

where $N_B^{Critical}$ is the concentration of the oxide forming element in the alloy, D_B is the diffusivity of B in the alloy, k_p is the parabolic rate constant, V_m is the specific volume of the metal and v is the ratio of oxygen to B in the oxide. This relation is derived by equating the transport of B to the metal-oxide interface from the alloy to that required for continual scale growth determined by k_p. If the actual concentration of B, N_B, in the alloy or coating should drop below $N_B^{Critical}$, diffusion of B in the substrate to the metal oxide interface would not be sufficient. As a result, the local oxygen partial pressure would increase to oxidize other alloy elements or dissolution of oxygen in the alloy could cause internal oxidation of B. This phenomenon has been described by **Evans et al. (1999)** as intrinsic chemical failure, or InCF.

If the scale should spall, direct exposure of the underlying alloy, which has been depleted of the scale forming element, B, would result. The critical concentration to reform the same oxide is determined by

$$N_B^+ \geq \left(\frac{\pi g^+}{2v}N_S^o\frac{D_o V_m}{D_B V_{ox}}\right)^{1/2} \tag{2.7}$$

Here N_S^o is the oxygen solubility in the substrate, N_B^+ is the concentration of element B in the alloy, D_o and D_B are the diffusivities of oxygen and B in the alloy respectively, V_{ox} and V_m are the specific volumes of the oxide and metal respectively and g^+ is an empirical parameter for lateral growth of oxide precipitates. This critical concentration of B is

determined by the ability to transport B in the alloy to initial oxide nuclei that results in lateral growth. This initial lateral growth of the oxide particles is the mechanism by which a continuous layer is developed. This concentration of the preferred scale forming element limits the oxidation life for the alloy or coating. Once this element is depleted below N_B^+ , the alloy loses the ability to reform the lost B oxide scale and other alloying elements are oxidized.

Rapid degradation of the component begins as a result of the nonprotecting nature of these other oxide scales. Failure by this type of depletion of scale forming elements is referred to as mechanically induced chemical failure, or MICF (**Evans et al.1999**)

Since growing the B oxide after spallation entails a lateral growth component of the oxide, the concentration required to heal the scale, N_B^+ , is generally larger than that to maintain the scale growth, or

$$N_B^+ > N_B^{Critical} \qquad (2.8)$$

From this, one can deduce that any spallation of the alloy reduces the service life of the component.

2.1.5 Oxide Scale Adherence

The adherence of an oxide scale to the metallic substrate is the greatest concern for oxidation resistance. From thermodynamics, the minimum work required to separate these two phases is the work of adhesion. It can be defined by the **Adam N.K (1941)** equation as

$$W_{ad} = \nabla G^{ad}{}_{ox/m} = \gamma_{ox} + \gamma_m - \gamma_{ox/m} \qquad (2.9)$$

Where W_{ad} is the work of adhesion, $\nabla G^{ad}_{ox/m}$ is the free energy change, γ_{ox} is the oxide-gas surface energy, γ_m is the metal-gas surface energy and $\gamma_{ox/m}$ is the oxide-metal interfacial energy. The nature of oxide scale bonding to the substrate, which has a great influence on the

$\gamma_{ox/m}$ is not completely understood. **McDonald and Eberhart (1965)** have performed sessile-drop experiments of liquid metals on an alumina substrate. Their results show a linear relation of the W_{ad} to the free energy of formation for the native oxide of the metal.

.   Part of their analysis shows that, the neighboring atom of the oxide to that across the interface of the metal determines the type of bonding. Metal-aluminum bonds across the interface would result in a weak Van der Waals bonding, but the metal-oxygen bonding across the interface is expected to be ionic in nature. These results are for liquid metals on a static alumina substrate, and caution is necessary when applying these results to solid metallic substrates and a growing scale. Another bonding theory proposes that electrostatic forces can develop from the electric field generated during the scale growth (**Fromhold Jr. A. T 1972**)

The nature and strength of the chemical bonding at the oxide-metal interface is extremely sensitive to the impurity levels. Sulfur is the element of major concern where a concentration of only a few parts per million can have profound effects on the cyclic oxidation life of a material (**Smialek 1991**). However, there exists a controversy over the mechanism by which 'S' causes deleterious effects. (**Grabke et al. 1991 and 1995**) have only detected 'S' on the metal surface of interfacial voids. Here, the sulfur is not the cause of the void formation, but it reduces the metal surface energy for void stabilization and growth. As these voids grow, a decrease in the average adherence results from reducing the contact area or complete separation by void coalescence could occur. In contrast to these results, sulfur has been detected at the intact metal-oxide interface for alumina (**Smeggil et al. 1986, Luthra et al.1986 and Hou et al.1992**) and chromia (**Fox et al.1991**) forming scales. This interfacial sulfur must be responsible for the weakening of bonds at the interface, or it may have an embrittling effect when it segregates to the interface (**Briant et al. 1982**).

Reactive elements (REs), elements with a large affinity for oxygen, have been studied in detail for the past half century. Alloys with the addition of small amounts of oxygen active elements such as Hf, Zr, Y or Ce exhibit great increases in the cyclic oxidation life. With low level ($\leq$100ppm) additions, scale adhesion has also been greatly improved (**Whittle and Stringer 1980, Funkenbusch et al.1985**). These improvements can be achieved by alloying, ion implantation, or oxide dispersion of the RE oxides.

There have been a number of proposed mechanisms to explain this reactive element effect that include: (1) RE form oxide pegs at the metal-oxide interface to mechanically fix the scale(**Felten 1961**); (2) RE can act as a vacancy sink to eliminate void precipitation at the metal-oxide interface(**Tien and Pettit 1972**) ; (3) RE have also been shown to alter the growth mechanism of the oxide scale(**Golightly et al. 1976 and Schumann et al.1996**) : (4) REs increase the scale plasticity for stress relaxation(**Antill 1967**) ; (5) REs segregate to the metal oxide interface to form a graded seal and strengthen the metal-oxide bond(**Antill 1967**) and (6) REs act as a sulfur getter to prevent segregation to the interface(**Smeggil 1986**) .

The strength of the oxide to metal bond is a critical issue due to the large load that is applied to the interface. This load originates from the stresses that form in the oxide layer. There are two types of stresses that need to be considered. First is the growth stresses that form while the scale is growing during the high temperature exposure, and the second is the thermal stress. Growth stresses can result from a number of different mechanisms. One mechanism was proposed by **Pilling and Bedworth (1923)** where the volumetric change during oxidation of a metal would result in a stress due to the constraint imposed on the oxide scale by the geometry of the metal substrate. They compared metals based on the Pilling and Bedworth ratio (PBR) where

$$\text{PBR} = \frac{\text{Volume per metal ion in oxide}}{\text{Volume per metal atom in metal}} \qquad (2.10)$$

Metals with PBR greater than one would have oxide scales that grow in compression and less than unity would form tensile stresses in the scale. Also from their explanation, scales that form by cationic diffusion would have new oxide form at the oxide-gas interface and would not be subjected to the constraints and form stress free. A second source of growth stresses occurs at the early stages of oxidation. Here lattice strains from epitaxial growth are significant, but as the scale thickens, the contribution would be minimal. Another mechanism could be a gradient in point defects in the oxide scale that results in the change in lattice parameter.

This would only occur in oxides that accommodate significant deviations from stoichiometry. Changes in the substrate due to recrystallization or phase transformations can alter the stress state. For chromia formers, alloy grain growth has been shown to disrupt the oxide **(Horibe 1975)**, and for alumina formers, phase transformations in nickel aluminide coatings have a similar affect **(Tolpygo 2000)**. Compressive growth stress can develop when oxide forms within oxide, as the case of anion diffusion along grain boundaries or micro cracks. The following effect has been noted on chromia formers **(Caplan 1975)**. Single crystal scale (no grain boundaries) grown on pure Cr remained planar and adherent. In contrast, a polycrystalline scale on the same alloy would buckle on the substrate as a response to the stress. These above mechanisms only deal with an oxide on a planar, semi-infinite surface which is not the case of the 3 dimensional components. **(Hancock and Hurst 1974)** have formulated an explanation for convex and concave surfaces as a function of cationic or anionic diffusion in the scale. Cationic transport results in the recession of the metal-oxide interface since the new oxide forms at the oxide-gas interface. This condition with a convex surface results in a compressive stress, while the concave surface would result in initial compression that would transfer into a tensile stress. For anionic diffusion, new oxide forms at the metal-oxide interface and on a convex surface, this new oxide pushes the original oxide resulting in a tensile stress in the outer region of the scale. On the concave surface, a compressive stress develops that increases with time.

The second type of stress occurring in the scale is the thermal stress. This situation is analogous to the bi-metal strip where two dissimilar metals are bonded together. As a result of the different coefficients of thermal expansion (CTE) the strip bends with a change in temperature. For metal-oxide systems a mismatch in CTE is present, but a constraint is applied to the interface. There is no bending since the thickness of the metal is generally orders of magnitude larger than the thickness of the oxide and oxide usually forms on both sides of the specimen. For a planar surface, the stress in the oxide can be determined by (**Oxx 1958**)

$$\sigma_{ox} = \frac{E_{ox}.\Delta T.(\alpha_{ox} - \alpha_m)}{1 + 2.\left[\dfrac{E_{ox}}{E_m}\right]\left[\dfrac{t_{ox}}{t_m}\right]} \qquad (2.11)$$

Where σ is the stress in the oxide, E is Young's modulus, ΔT is the change in temperature, α is the coefficient of thermal expansion (CTE) and t is the thickness. Subscripts ox and m denote oxide and metal respectively. Since $t_{ox} \ll t_m$, the second term in the denominator can be assumed to equal zero and this equation can be reduced to

$$\sigma_{ox} = E_{ox}.\Delta T.\Delta\alpha \qquad (2.12)$$

Where $\Delta\alpha$ is the difference in the oxide and metal CTEs. With this large difference in thickness between scale and substrate, one can conceive that the oxide is forced to conform to the dilatation of the substrate. The magnitudes of these stresses are on the order of 4 to 5 GPa compression for an alumina scale on a Ni-base alloy after cooling to ambient temperature from 1000 to 1200°C which places a considerable load on the metal-oxide interface. The metal-oxide system responds to the growth and residual stresses differently. Growth stresses, are present at elevated temperatures where the strengths of the metallic substrate and the oxide are low. Plastic deformation and creep of the scale and the substrate

have been reported for alumina scales on FeCrAlY alloys (**Sarioglu 1998**). For this case, a growth stress of approximately 1GPa has been measured in the scale. At room temperature, the thermal stress has reached a maximum and any additional strain from the growth stress increases the total residual stress in the oxide. Also, the tendency of the alloy and oxide to deform under these loads is reduced. If the residual stress is too large for the interface bonding, cracking and spallation of the scale are the results, as demonstrated in **Fig.2.4.**

Failure by the initiation of an interfacial buckle with subsequent cracking of the oxide scale is depicted in **Fig.2.4 (a)** and the initiation of wedge cracks in the oxide scale followed by interfacial cracking is shown in **Fig.2.4 (b).** If the interface is strong enough, the residual stress can cause deformation of the scale and substrate without scale loss as shown in **Fig.2.4(c).** Because of the large residual stresses, adherence of the oxide becomes an important issue during thermal cycling.

Gas

⟶ Oxide ⟵

Alloy

· Gas   Gas   Gas

Oxide   Oxide   Oxide

Alloy   Alloy   Alloy

(a)   (b)   (c)
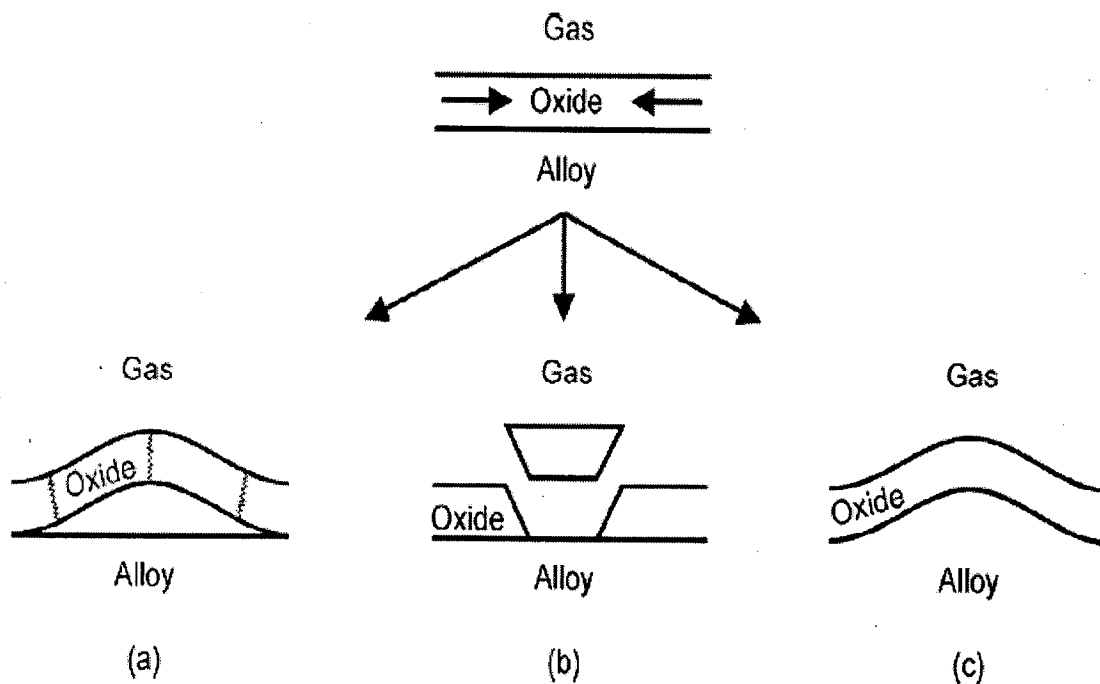
Fig.2.4 Schematic diagram of oxide and substrate response to the compressive

stresses in the scale.

2.2 OXIDATION OF SUPERALLOYS

Superalloys are now widely used in a variety of applications at temperatures ranging from 923 to 1373 K in aggressive atmospheres such as the combustion products of fuel and air, high temperature catalytic reactors etc. **(Jena 1984)**. In order to function satisfactorily in such a severe environment, superalloys must possess properties such as outstanding high temperature strength, creep and fatigue resistance, excellent ductility, good impact resistance and adequate resistance to hot-corrosion **(Jena 1984)**. Superalloys are used extensively in oxidizing environments; for example, as disks in turbine engines. The superalloys have been developed to achieve oxidation resistance by utilizing the concept of selective oxidation. The selective oxidation approach to obtain oxidation resistance in superalloys consists of oxidizing essentially only one element in the superalloy and relying upon this element's oxide for protection. For effective protection, it is anticipated that the oxide should cover the whole surface of the alloy and it must be an oxide through which the diffusion of the reactants takes place at comparatively slow rate. Nickel-, cobalt- and iron-base superalloys make use of the selective oxidation of the aluminium or chromium to develop oxidation resistance **(Pettit and Meier 1985)**. Further, **Pettit and Meier (1985)** have reported that the selective oxidation processes are affected by a number of factors such as alloy composition, alloy surface conditions, gas environment and cracking of the oxide scale. Cyclic oxidation conditions whereby the oxide scales crack and spall, as well as certain phases present in the superalloys, both affect the capability to selectively oxidize aluminium or chromium in the superalloys.

The superalloys exhibit outstanding strength and surface stability at temperature up to 85% of their melting points. Usually the superalloys are used at temperatures above 540 °C **(Metal Handbook, 1990)**. However, compared with steels, corrosion resistance of the superalloys is relatively less known **(Smith et al. 1999, Castello et al. 2000)**. The superalloys are broadly classified as nickel-, cobalt- and iron-based alloys.

Pettit and Meier (1985) opined that during isothermal oxidation of Ni-base superalloys, Cr_2O_3 and Al_2O_3 scales are expected to be formed. Whereas, under cyclic conditions, depletion of chromium and aluminium leads to the formation of NiO scale, some

alloys move toward the NiO scale formation much more rapidly than others. They further concluded that the application of aluminide coatings to two nickel based superalloys B-1900 and Mar M200 makes them remain in alumina scale formation range for even longer times than obtained for the uncoated.

The time over which nickel base superalloys can maintain protective, external scales of alumina or chromia is affected by temperature, the gas environment and alloy composition.

Superalloys contains a number of significant alloying elements in addition to Cr and Al, including Mn, Ti, Si, and the refractory elements, Mo, W, Ta, Zr, and Hf. In many cases, these elements exert significant influence on the oxidation resistance of Cr_2O_3 and Al_2O_3 forming alloy. Some alloying elements are beneficial and some are deleterious to superalloy oxidation resistance depending upon their amount and working condition. A number of studies have been carried out on the effect of their additions on the oxidation behaviour of different alloys. **Smialek et al. (1987)** has given an extensive review of this behaviour.

Levy et al (1989) reported studies on the cyclic oxidation resistance of three single-crystal nickel base superalloys and DS Mar M 200 at 1093°C using a tube furnace and burner rig. The same ranking of the alloys was reported in both tests with the single-crystal superalloys having better oxidation resistance than the directionally solidified alloy DS Mar M 200. They further opined that tube furnace tests can be used in place of burner-rig tests to rank alloys. Oxidation tests at 900°C using the tube furnace produced a ranking of the alloys consistent with the 1093°C results.

The oxidation behaviour of a single-crystal Ni-base superalloy has been studied using discontinuous thermo gravimetric analysis and prolonged exposure in air at 800 and 900°C by **Li et al (2003A)**, and over the temperature range from 1000–1150°C by **Li et al (2003B)**. They observed that the mass gain at 900°C was lower than that at 800°C due to the formation of a protective inner α-Al_2O_3 layer at 900°C. The scale formed at 900°C was found to be more uniform than that formed at 800°C, which consisted of several layers: an NiO outer layer, spinel-rich sub-layer, a $CrTaO_4$-rich layer and an α-Al_2O_3 inner layer. Whereas in the temperature range of 1000–1150°C, the outer NiO layer was observed to be replaced by an spinel, a sub-layer of mainly α-Al_2O_3, with unchanged composition of inner

layers of the scale. Further, no internal oxides or nitrides were observed below the inner α-Al_2O_3 layer after 1000 hours at 1000°C, and after 200 hours at 1100 and 1150°C.

Li et al. (2003C) studied the oxidation kinetics and oxidation layer of a cast Ni-base superalloy K35 at 800°C by still TGA method. The results showed that oxidation kinetics of the superalloy obeyed the parabolic law. They further observed that oxidation rate of the superalloy was dependent on the growth dynamics of Cr_2O_3. Moreover, the oxide layer was found to be thin and, consisted of Cr_2O_3 mainly with a bit of $NiCr_2O_4$ and $TiO.TiO_2$. Internal oxidation of the alloy was also observed.

Zhao et al (2005A) investigated the oxidation behaviour of a new nickel-based superalloy in air at 950°C and 1000°C for 140 hours and reported that the alloy obeyed the parabolic rate law at 950°C, whereas small deviations were observed at 1000°C. No oxide spallation was observed at 950°C, while minor spallation was seen at 1000°C. The oxide scale was found to be consisted of Cr_2O_3, (Ni, Co) Cr_2O_4, TiO_2, SiO_2, TiO_2 and Al_2O_3. Internal oxidation of the superalloy was also indicated at both the temperatures of the investigation.

2.3 HOT CORROSION

The first technical publication on hot corrosion was reported by **Simons et al. (1955)** he suggested that hot corrosion is an electrochemical process in which the molten salt acts as an electrolyte. **Seybolt (1968)** attributed Na_2SO_4 induced hot corrosion of Ni–Cr alloys to accelerated oxidation of the Cr-depleted alloy following preferential internal sulfidation of Cr. **Bornstein and DeCrescente (1969)** reported that accelerated kinetics were not observed during the oxidation of three different presulfidised superalloys and proposed a hot corrosion mechanism based on the (basic) dissolution of the protective oxide scale by a reaction involving Na_2O, the basic minority component of the fused salt. **Goebel and Pettit (1970A) and Goebel et al. (1973)** extended this mechanism to include acidic fluxing and oxide reprecipitation to account for the catastrophic oxidation caused by Na_2SO_4 for alloys containing strong acidic components, such as V or Mo. These mechanisms are still accepted

today, and some quantitative aspects of oxide solubility and electrochemical reaction steps have been added in the literature.

Accelerated corrosion can also be caused by other salts, viz. vanadate or sulphates-vanadate mixtures and in the presence of solid or gaseous salts such as chlorides **(Bornstein et al. 1973)**. However, turbine manufacturers and users became aware of hot corrosion in late 960's, **(Stringer 1977)** have conducted experimental as well as field tests to identify the ature of attack and explained its temperature dependence and the corresponding norphologies. Hot corrosion was first associated with Na_2SO_4 in mid 1950's **(Luthra and hores 1980)**. Hot corrosion became a topic of importance and popular interest in the late 960s when gas turbine engines in military aircraft suffered severe corrosion during the ietnam conflict while operating over sea water **(Rapp 1986)**. When metals are heated in the mperature range 700–900°C, sulphates deposits are formed as a result of the reaction stween sodium chloride and sulphur compounds in the gas phase surrounding the metals **Iancock 1987)**.

According to **Shih et al. (1989)** metals and alloys often experience an accelerated cidation in high-temperature gas environments when covered with a thin layer of molten salt posit, usually alkali sulphates. This type of oxidation is commonly called hot corrosion.

Hot corrosion is a degradation of metals and /or an alloy owing to the oxidation ocesses which are affected by liquid salt deposits, predominantly Na_2SO_4. The primary urce of Na_2SO_4, in marine and aircraft engines, is due to reaction between NaCl in ingested r and sulfur in fuel according to the following reactions **(Khajavi 2004)**

$$2NaCl + SO_2 + \tfrac{1}{2} O_2 + H_2O \rightarrow Na_2SO_4 + 2HCl \qquad (2.13)$$

$$2NaCl + SO_3 + H_2O \rightarrow Na_2SO_4 + 2HCl \qquad (2.14)$$
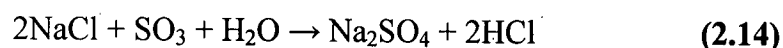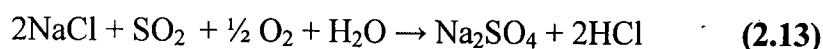
To protect the turbine engines from the high temperature corrosion attack facilitated by impurities, thermal sprayed coatings are to be deposited over the hot section components of turbine engines and boiler tubes. The thermal sprayed coatings consist of oxides and voids originating from spraying process are found at the splat boundaries, through which the coatings were mainly attacked **(Uusitalo et al. 2004).**

2.3.1 High Temperature Hot Corrosion (HTHC)- Type I

It has been known since the 1950s and it is an extremely rapid form of oxidation that takes place at temperatures between $815^{\circ}C$ and $926^{\circ}C$ in the presence of pure Na_2SO_4 (m.p $886^{\circ}C$) **(Khajavi 2004).** HTHC starts with the condensation of fused alkali salts (Na_2SO_4) on the surface of the component; the most significant source of sodium is marine, industrial atmosphere as well as fuel. During combustion of fuels, sodium from air and sulfur from the fuel combine to form a sodium Sulphate **(Eliaz et al., 2002).** Na_2SO_4 formation lies basically in the reaction

$$SO_2 + 2NaCl + O_2 \rightarrow Na_2\ SO_4 + Cl_2 \qquad (2.15)$$
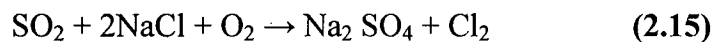
Type I, or high-temperature hot corrosion, is characterized by a macroscopically uniform corrosion front, which involves an internal layer of internal oxidation, which may also contain internal sulfides and carbides. The external oxide is not protective, and is composed of the oxides of the base metal (nickel or cobalt); and the oxides of the other constituents, particularly chromium and aluminum **(Stringer 1998).**

Sidhu et al. (2006J) reported that the macroscopic appearance of HTHC is characterized in many cases by severe peeling of metal and by significant color changes. For instance, a greenish tone appears on the surface of metals and alloys due to the formation of NiO in the area of accelerated attack. Microscopically, the morphology of Type I is characterized by a sulphidation and depletion region beneath the porous, non-protective scale.

2.3.2 Low Temperature Hot Corrosion (LTHC)- Type II

Low temperature hot corrosion (LTHC) was recognized in the mid-1970s as a separate mechanism of corrosion attack **(Khajavi 2004)**. Low temperature hot corrosion mainly observed within the temperature range 650-800°C and requires a significant high partial pressure of SO_3, for Nickel/Cobalt-based superalloys. The formation of low melting eutectic compounds occurs due to the combination of sodium sulfate and nickel/Cobalt sulfate (melting temperature of the $Na_2SO_4 \pm CoSO_4$ eutectic is 540°C) **(Eliaz et al. 2002)**.

The formation of $Na_2SO_4 + NiSO_4$ eutectics 671°C has been reported for nickel-based superalloys, the morphology of attack is pitting when the LTHC takes place, low temperature corrosion characteristically shows no denuded zone, no or little inter-granular attack, and a layered type of corrosion scale and also no subscale sulfide particles **(Mishra 1986)**. Chromium (25-40%) and silicon are particularly beneficial in coatings for protection against Type II corrosion. It should be noted that the classification of the form of the attack (type I or type II) is primarily based on the morphology of the attack, and not the temperature. Type II, or low-temperature hot corrosion is characterized by a pitting attack **(Stringer 1998)**.

2.3.3 Hot Corrosion of Superalloys

The hot corrosion of superalloys usually involves two distinct stages of attack **(Pettit and Meier 1985, Pettit and Giggins 1987)**, namely, an initiation (incubation) stage and propagation stage. Such conditions are depicted schematically in **Fig.2.5.**

No alloy is immune to hot corrosion attack indefinitely although there are some alloy compositions that require a long initiation times before the hot corrosion process moves from the initiation stage to the propagation stage. During the initiation stage of hot corrosion, superalloys are being degraded at rates similar to those that would have prevailed in the absence of the deposits. Elements in the alloy are oxidised and electrons are transferred from metallic atoms to the reducible substances in the deposit. Consequently, the reaction product barrier that forms beneath the deposit on the alloy surface usually exhibits primarily those features resulting from the gas–alloy reaction **(Pettit and Giggins 1987)**. Numerous factors

affect the time at which the hot corrosion process moves from the initiation stage into the propagation stage as shown in **Fig. 2.5.** These factors also play the dominant role in determining the type of reaction product that is formed in the propagation stage. This fact is responsible for variety of hot corrosion processes that have been observed when superalloys are exposed to different environments **(Pettit and Meier 1985)**.

The propagation stage of the hot corrosion sequence is the stage for which the superalloy must be removed from service since this stage always has much larger corrosion rates than for the same superalloy in the initiation stage **(Pettit and Meier 1985 and Pettit and Giggins 1987)**. Since superalloys always contain elements that have high affinities for oxygen, an oxygen gradient is established across the deposit. Hence, an important effect of the deposit is to separate the superalloy from the gas environment. This situation usually results in a lower oxygen activity over the surface of the alloy than what would have been established in the absence of a deposit **(Pettit and Meier 1985, Pettit and Giggins 1987)**.

HOT CORROSION CHRONOLOGY

Initiation Stage

Salt deposit

Reaction product barrier

Alloy

Important factors

- ❖ Alloy composition
- ❖ Fabrication condition
- ❖ Gas composition & velocity
- ❖ Salt composition
- ❖ Salt deposition rate
- ❖ Condition of salt
- ❖ Temperature
- ❖ Temperature cycles
- ❖ Erosion
- ❖ Specimen geometry

Propagation Stage

Lesser protective

reaction product

Alloy
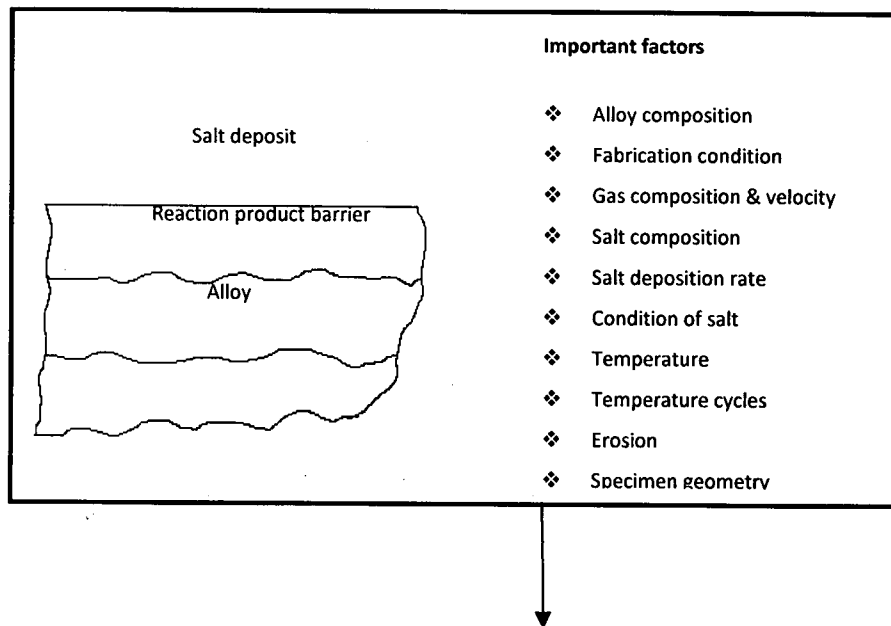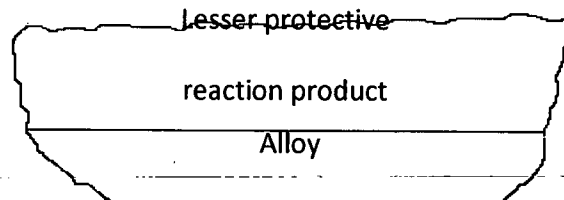
Fig. 2.5   Schematic diagram illustrating the conditions that develop during the initiation and the propagation of hot corrosion attack and to identify the factors that determine the time at which the transition from the initiation to the propagation stage occurs **(Pettit and Meier 1985).**

2.3.4 Mechanism of Hot Corrosion

From the literature review, it has been observed that there are varieties of conditions which can be considered for hot corrosion degradation of the superalloys. Researchers have proposed number of mechanisms for this type of degradation such as failure of oxide scale, sulphidation-oxidation and salt fluxing, oxide solubility, and effect of vanadium **(Goebel and Pettit 1970A, Goebel and Pettit 1970B, Beltran and Shores 1972, Rapp and Goto 1981, Pettit and Meier 1985, Rapp 1986, Stringer 1987, Otsuka and Rapp 1990, Zhang et al. 1993, Eliaz et al. 2002).**

These mechanisms can be considered in relation to each other rather than as completely different and unrelated corrosion process. The salt fluxing mechanism was firstly proposed by **Goebel and Petit (1970A and 1970B).** According to this model, the protection efficiency of the surface oxide layer might be lost as a result of fluxing of this layer in the molten salt. This fluxing may be either due to combination of oxides with O^{2-} to form anions (basic fluxing) or by decomposition of the oxides into the corresponding cations and O^{2-} (acidic fluxing). **Fig.2.6** schematically illustrates oxide solubility with the superposition of four different sets of basicities at the salt/gas interface II, and at the oxide/metal interface I **(Goebel et al. 1973).** As compared to basic fluxing, acidic fluxing causes more severe oxidation. The acidic fluxing takes place when the O^{2-} activity in the molten salt is markedly lowered. In contrast to basic fluxing, the acidic fluxing can be self-sustaining because the displacement of the salt from the stoichiometry does not become progressively more difficult as the reaction proceeds **(Stringer 1987).**

It is important to notice that the concentration of oxygen ions available for basic fluxing is limited by the amount of deposit present upon the surface of the superalloy. Hence basic fluxing reactions are not self-sustaining but require a continuous source of Na_2SO_4 in order toprecede this type of degradation indefinitely. As opposed to the basic fluxing, the acidic

fluxing can be self-sustaining, since the displacement of the salt from stoichiometry does not become progressively more difficult as the reaction proceeds **(Stringer 1987, Pettit and Meier 1985).**

Therefore, acidic fluxing is more severe as compared to basic fluxing. In general, the hot corrosion of the superalloys with high contents of aluminium and chromium is often reported to occur according to the basic fluxing mechanism. On the other hand, the hot corrosion of alloys with high contents of tungsten, molybdenum and vanadium is often reported to follow the acidic fluxing mechanism (**Eliaz et al. 2002**) and these elements, when oxidised in the presence of Na_2SO_4, deposit on superalloys causing catastrophic self-sustaining hot corrosion (**Pettit and Meier 1985**).

Al_2O_3 precipitation by

$$2AlO_2^-$$
$$\downarrow$$
$$Al_2O_3 + O^{2-}$$

AlO_2^-

Basic fluxing mechanism

Al_2O_3

Alloy $\leftarrow Na_2O_4 \rightarrow$ Gas

Al_2O_3 precipitation by

$$MoO_4^{2-} \rightarrow MoO_3 + O^{2-}$$
and
$$2Al + 3O^{2-}$$
$$\downarrow$$
$$Al_2O_3$$

Al^{3+}

MoO_4

MoO_3

Acidic fluxing mechanism
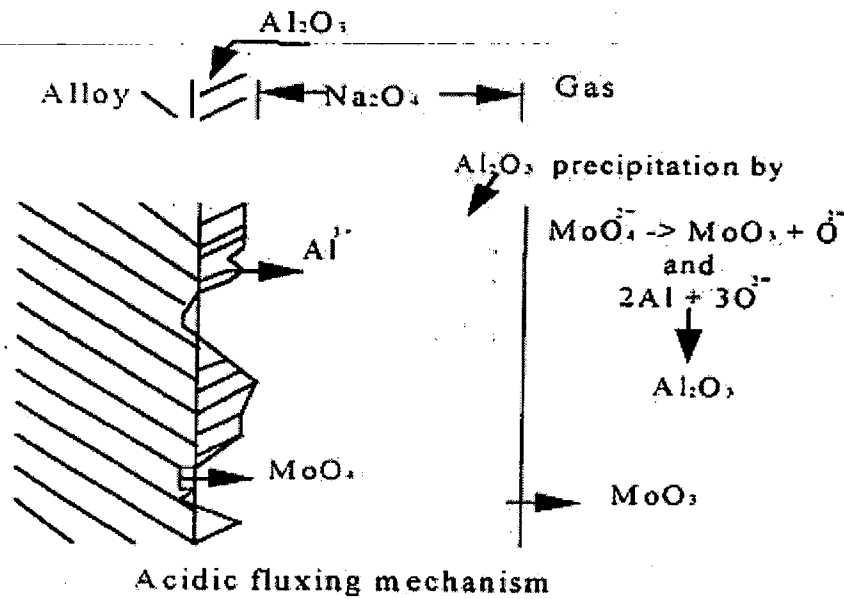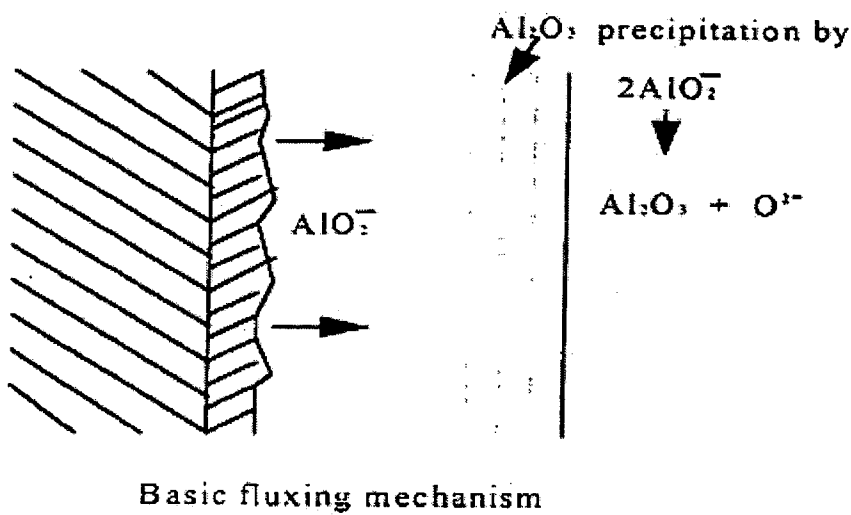
Fig.2.6   Schematic diagrams of basic and acidic fluxing mechanisms with respective

typical morphology of corrosion attack (**Goebel et al. 1973**)

Stott et al. (1994) proposed that sulphur-containing species, penetrating through localized short-circuit paths in the oxide, develop sulphide ducts from the scale–metal interface to the scale–gas interface. The sulphide ducts provide easier diffusion paths for the base-metal ions through the oxide to the surface, and eventually allow more rapid growth of sulphide nodules above the oxide. However, **Natesan (1985)** reported that no transport of sulphur into the oxide, or sulphide duct formation was necessary to form massive mixed iron and chromium sulphides at the oxide–gas interface. Based on theexperimental results of sulphidation–oxidation of Incoloy 800, he reported that adsorption of sulphur by the oxide scale accelerates the transport of cations such as Fe and Ni from the substrate to the gas/scale interface and if the sulphur partial pressure in the gas is above that needed for base-metal sulphidation, the transported cations react with sulphur to form sulphides as an outer scale, external to the preformed chromium oxide layer.

Hot corrosion in sulphates, chloride and vanadate environment of a cast nickel base superalloy had been reported by **Deb et al. (1996)** Weight gain studies were carried out in air for the uncoated samples and coated with 100% Na_2SO_4, 75% Na_2SO_4-25% NaCl and 60% Na_2SO_4 + 30% $NaVO_3$+10% NaCl. The presence of sulphur in the form of sulphates can cause internal sulphidation of the alloy beneath the external oxide layer. Chlorides cause the formation of volatile species, which form voids and pits at grain boundaries, thus forming an easy path for flow of corrodents. The presence of vanadate in conjunction with sulphates and chloride provides additional fluxing action. This destroys the integrity of the alloy and weakens its mechanical properties.

Rapp and Goto (1981) proposed that protective scales on alloy become non-protective when the solubility gradients of the protective oxides in the molten deposit are negative, due to possibility of continuous dissolution and re-precipitation of oxide. On the basis of oxide solubilities measurement in molten Na_2SO_4 as a function of the acidity of the

salt, they suggested that a negative gradient of the solubility of the protective oxide in the salt film at the oxide/salt interface should lead to oxide dissolution at this interface and to precipitation of a non-protective oxide away from the interface, where the solubility is lower.

Fluxing arises in this case only because of the local variation of sodium oxide activity and/or oxygen partial pressure across the salt film, without any necessity of sulphide-forming reaction. This mechanism can explain a self-sustaining process of dissolution of the protective oxide to maintain an accelerated corrosion attack **(Stringer 1987).**

Different research workers have examined the effect of vanadium on high temperature hot corrosion of metals and alloys. **Bornstein et al. (1973) and Goebel et al. (1973)** suggested that a self-sustained acidic dissolution of the protective Cr_2O_3 or Al_2O_3 scales could take place when the salt film contains vanadium, because V_2O_5 is a strong acidic oxide.

Zhang and Rapp (1987) further suggested that every oxide forms an acidic solute with much higher solubility in the presence of vanadate, which contributes to the more accelerated attack of oxides by mixed sulphate-vanadate, melts than by a pure sulphate melt

2.3.5 Chemistry of Salts

2.3.5.1 Sulphate Chemistry

As described by **Rapp (1986 and 2002)**, oxy-anion melts of alkali nitrates, carbonates, hydroxides, and sulphates exhibit an acid/base character wherein the acid components may be considered as $NO_2(g)$, $CO_2(g)$, $H_2O(g)$ or $SO_3(g)$, respectively. Although the use of the Lux-Flood selection of NO_3^-, CO_3^{2-}, OH^- and SO_4^{2-} as the basic components is common for such fused salts, the oxide ion can alternatively be chosen as the Lewis base in common for all of these salts. For a melt of pure Na_2SO_4 (m.p. 884°C), there exists equilibrium as given below:

$$Na_2SO_4 \rightarrow Na_2O + SO_3(g) \qquad\qquad (2.16)$$
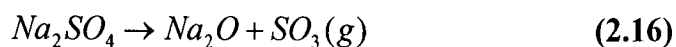
According to **Rapp (1986)**, in examining the expected stability of the protective oxide Cr_2O_3, with respect to dissolution either as acidic solutes such as $Cr_2(SO_4)_3$ or as basic solutes such as Na_2CrO_4 or $NaCrO_2$, the phase stability diagram for the Cr-S-O system can be superimposed on that for Na-S-O, as shown in **Fig. 2.7**. The two abscissa scales at the bottom and top of figure provide alternate parameters for melt basicity (or acidity). Under no conditions, the metal chromium remains stable in contact with Na_2SO_4 at 1200 K (927°C) **(Rapp 1986)**.

2.3.5.2 Vanadate Chemistry

Among the transition metals vanadium is unique, in that it forms a low-melting oxide V_2O_5. This low melting temperature (670°C under 1 atm of oxygen) results from the peculiar crystal structure of the compound in which vanadium is 5-coordinated with oxygen and in which there occur four different vanadium-oxygen bond lengths. The phase stability diagram for the Na-V-S-O system at 900°C reported by **Hwang and Rapp (1989)** has been shown in **Fig. 2.8**.

The dashed lines present the isoactivity lines for the vanadate species in the salt solution.
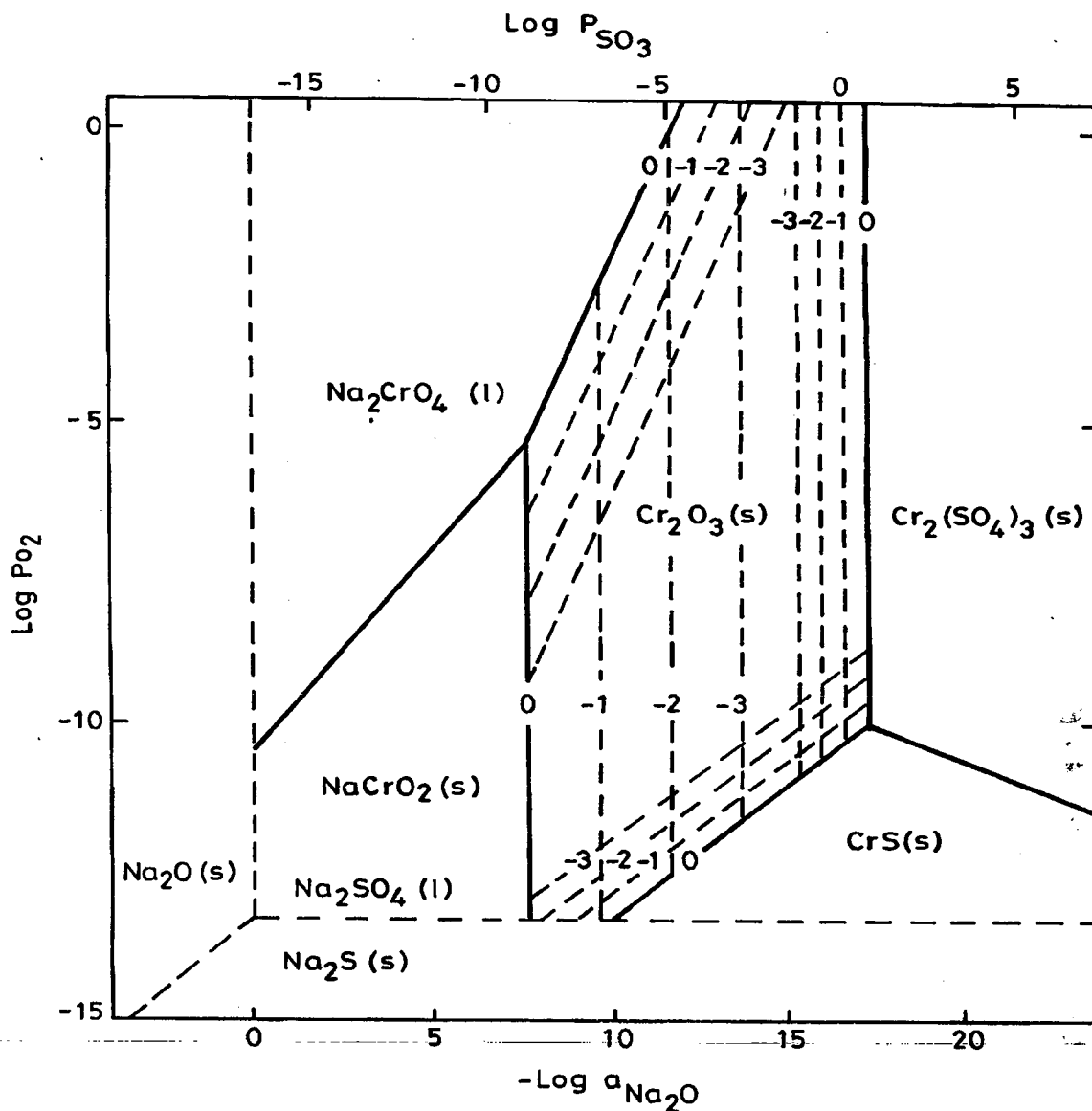
Fig. 2.7   Na-Cr-S-O phase stability diagram for 1200 K **(Rapp 1986).**
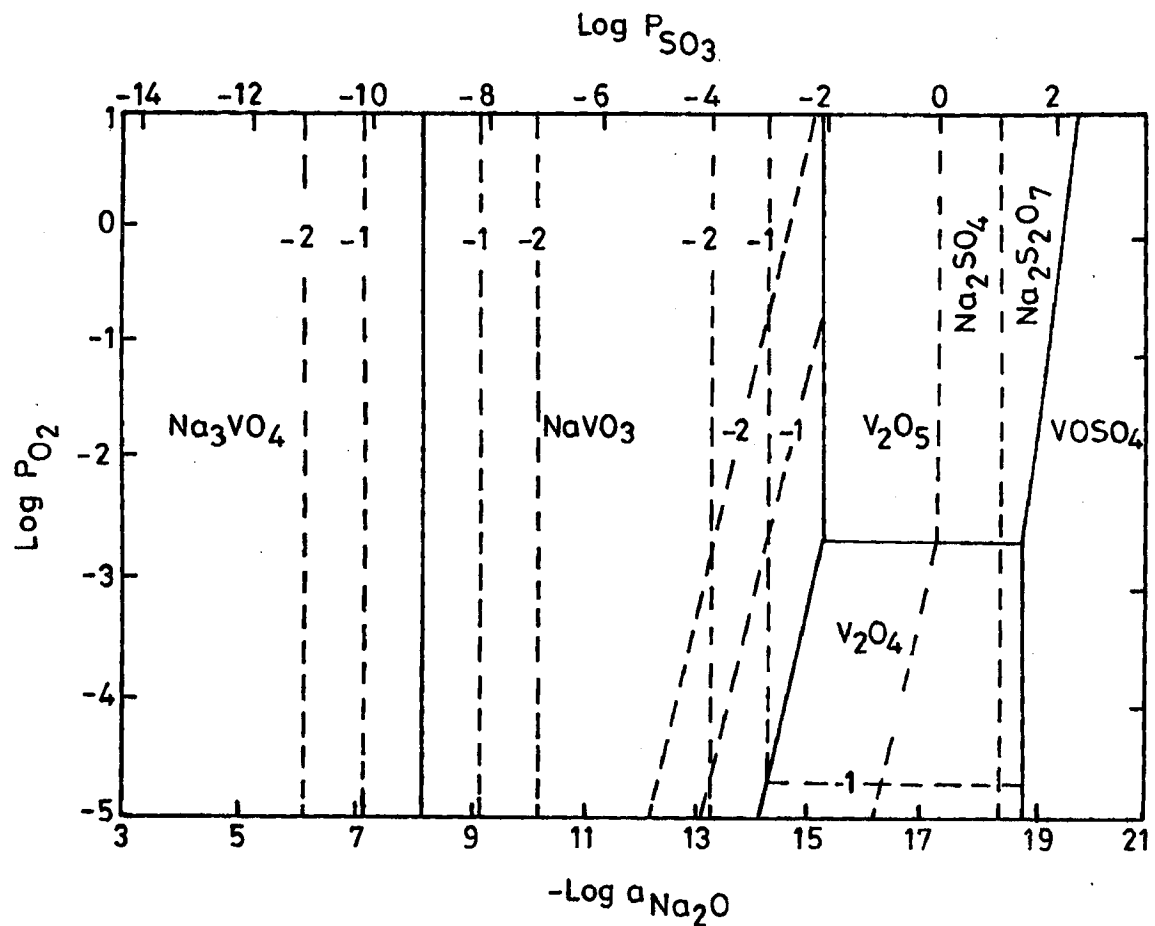
Fig. 2.8   Phase stability diagram for Na-V-S-O system at 900°C **(Hwang and**

Rapp 1989).

They determined the dependence of the equilibrium concentrations of various vanadate solutes in the sodium sulphate-vanadate solutions on the melt basicity by considering following equilibrium reactions:

$$Na_2SO_4 \rightarrow Na_2O + SO_3 \qquad (2.17)$$

$$Na_3VO_4 \rightarrow Na_2O + NaVO_3 \qquad (2.18)$$

$$2NaVO_3 \rightarrow Na_2O + V_2O_5 \qquad (2.19)$$
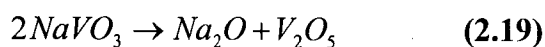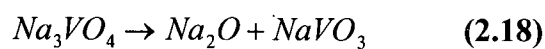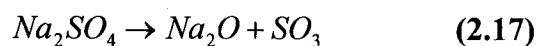
The equilibrium concentration of each vanadium compound varies continuously with melt basicity. Na_3VO_4 is the dominant component in the melt at basicity less than 8.2 and V_2O_5 is dominant at basicity greater than 16.3. For basicities between 8.2 and 16.3, $NaVO_3$ is the most important vanadium solute **(Hwang and Rapp 1989)**.

2.3.5.3 Hot Corrosion in Molten Salt (Na_2SO_4-60%V_2O_5) Environment

Kolta et al. (1972) studied the kinetics of reactions between Na_2SO_4 and V_2O_5. They concluded that the rate of reaction depends both on the temperature (600-1300°C) and the molar ratios of Na_2SO_4 and V_2O_5. They further revealed that with increase in the reaction period (>30 min.), the reaction rate decreased and finally reached to zero order. They attributed this decrease in the reaction rate to the formation of vanadosulphate complexes such as $(NaV_3O_8)_2.Na_2SO_4$ and $(NaVO_3)_2.Na_2SO_4$, which are decomposed at higher temperatures giving the meta- and pyro-vanadates respectively.

The effect of vanadium and sodium on the accelerated oxidation of nickel base alloys has been reported by **Bornstein et al (1975)**. They observed the initial rapid rate of oxidation between V_2O_5 and metal substrate which is attributed to the reduction of V_2O_5 by the substrate. Inter-metallic systems Ni_3Al and $NiAl$ were particularly found to be susceptible to V_2O_5 corrosion. According to them, the sulphidation attack alters the composition of the melt to produce more oxide ions i.e. $M + SO_4^- = MS + O^- + 3/2O_2$. Severity of attack is found to decrease with increase in the initial oxide ion content of the melt. Oxides such as Cr_2O_3 have been suggested to react preferentially with oxide ions. **Natesan (1976)** reported that molten sulphate-vanadate deposits are extremely corrosive to high-temperature materials in the combustion systems.

Luthra and Spacil (1982) carried out a thermo-chemical analysis of deposits in gas urbines for liquid fuels containing Na, S and V. They observed that the predominant species in he salt deposits formed on the gas turbine surfaces were Na_2SO_4, V_2O_5 and $Na_2V_2O_6$. This nvironment is also pertinent to the boilers. According to **Otero et al (1987)**, Na_2SO_4-60%V_2O_5 deposit was detected on a number of components in actual service which were operated at high temperature and were in contact with high-temperature gases from

combustion of dirty fuels, containing certain amounts of impurities, i.e. Na, V, S etc. The presence of sulphur and its oxidised compounds were reported to favour the formation of isolated lobes with radial morphology having great permeability to facilitate the access of oxygen which further led to reduction in the protective nature of scale. The presence of vanadium and its oxidised products was observed to generate compounds with acicular morphology, identified to look like alkaline vanadate complexes. These acicular shapes further contribute to reduce the protective character of the scale.

Kofstad (1988) has proposed that during combustion, the vanadium contaminants are oxidized to the higher valence vanadium oxides (V_2O_4 and V_2O_5) which react with sodium salts to form low melting point sodium vanadates (lowest M.P. $535°C$) such as $(Na_2O)_xV_2O_4(V_2O_5)_{12-x}$, $(Na_2O)_5(V_2O_4)_x(V_2O_5)_{12-x}$, $NaVO_3$, $Na_4V_2O_7$ and Na_3VO_4. Metal oxides dissolved in the vanadates may suppress the melting points and eutectic temperatures even further. He further reported that the slags developed on valves in diesel engines consist predominantly of sodium sulphate and sodium vanadates and have melting points as low as $400°C$.

Hwang and Rapp (1989) studied the solubility of oxides in the mixed sodium sulphate-vanadate solution containing 30 mole% vanadates. They reported that the basicity of the melt, oxygen partial pressure and proportion of V^{5+} and V^{4+} states of vanadate in the sulphate-vanadate solution decide the solubilities of oxides. **Kofstad (1988)** revealed that the solubilities of metal oxides may be high and are dependent on the Na: V ratio. The solubilities of Cr_2O_3 and Fe_2O_3 are highest ($\approx$ 50 mol. %) at Na: V ratios close to 5 : 12. For NiO, the solubility is about 60 mol. % at Na : V = 3 : 2 which decreases to about 55 mol.% at Na : V = 5 : 12. As V_2O_5 is acidic, it will react with more basic oxides to form the corresponding vanadates.

In this aggressive environment (Na_2SO_4-60%V_2O_5), the hot corrosion behaviour of superalloy IN-657 at 1000 K ($727°C$) has been investigated by **Otero et al (1990 and 1992)**. They reported that corrosion rate of the alloy in contact with molten salt mixtures has been approximately reduced by one order of magnitude over exposure times of 210 hrs when the amount of molten salt is kept constant. During the initial stages of the exposures, the

corrosion rate was found to be increased with increasing the temperature up to 1000 K (727°C) and further reported to have decreased at higher temperature. After 100 hours of exposure, the influence of temperature was insignificant. **Zhang and Rapp (1994)** measured the solubility of CeO_2 as a function of melt basicity in a Na_2SO_4-10mol. %$NaVO_3$ solution at 900°C and 1 atm. oxygen. A comparison of the solubility in Na_2SO_4-10mol. %$NaVO_3$ with the solubilities in both pure Na_2SO_4 and in Na_2SO_4-30mol. %$NaVO_3$ was made. Their results indicated that CeO_2 dissolves in the salt solution either as a basic or as an acidic solute.

Sidhu (2003) studied the hot corrosion behaviour of boiler tube steels namely ASTM-SA210 grade A1, ASTM-SA213-T-11 and ASTM-SA213-T-22 in air and molten salt environments of Na_2SO_4-60%V_2O_5 at 900°C. They found that all the steels show less resistance in the molten salt environment than in air. They reported that the presence of vanadium, sodium and sulphur accelerates the rate of corrosion of boiler steels in the molten salt environment. **Sidhu et al. (2007)** evaluated the hot corrosion behaviour of HVOF sprayed Cr_3C_2-NiCr and NiCrBSi coated Superni- 718 at 900°C under cyclic conditions in the presence of the Na_2SO_4-60%V_2O_5 salt mixture. He concluded that the Cr_3C_2-NiCr coating oxidizes partially along the splat boundaries up to the coating-substrate interface, whereas in the case of NiCrBSi coating, only the upper layer of the coating oxidizes and the remaining portion of the coating remains similar to as-sprayed coating.

2.4 PREVENTIVE MEASURES AGAINST HOT CORROSION

The corrosion control in highly aggressive applications requires careful selection of materials. Nickel-based superalloys have good mechanical properties and superior corrosion resistance at higher temperatures and are used as base materials for hot section components in turbines. However, the hot corrosion is inevitable when these alloys are used at higher temperatures for longer periods of time in an extreme environment **(Goebel et al. 1973).**

Heath et al. (1997) proposed a number of countermeasures corresponding to the variety of corrosive environments including

- Proper selection of alloy,

- Optimum design of components,
- Use of chemical additives to neutralise the corrosive components in the flue gases,
- Shielding the substrate, and
- Protective coatings.

The important factors that influence hot corrosion are as follows: (a) alloy composition; (b) alloy fabrication condition; (c) deposit composition; (d) amount of deposit on superalloy; (e) gas composition and velocity; (f) temperature; (g) temperature cycles; and (h) erosion. **(Gurrappa 1999). Eliaz et al. (2002)** also, in their review of hot corrosion in gas turbine components, suggested several approaches to control the hot corrosion of gas turbine components. These approaches are proper selection of structural alloys, application of coatings, washing of hot parts, air filtering, and control of both fuel cleanliness and composition.

Another method of hot corrosion prevention is to coat the alloy with a protective layer, which has been used in the current investigation. This is the preferred approach, even when relatively less hot corrosion-resistant alloys are used **(Eliaz et al. 2002)**. For adequate corrosion protection of a metal in an aggressive environment, it is important to select materials and techniques that are compatible. For example, addition of an organic inhibitor (e.g. pyridines, pyrimidines, quinolines) is sufficient to mitigate corrosion of metals in many corrosive media. However, these inhibitors have shown only limited success due to solubility and/or thermal stability problems in high –temperature, concentrated salt solutions **(Priyantha et al. 2003)**.

Hot corrosion preventive and control methods used in the aggressive environment can be classified as. corrosion inhibitors, selection of proper alloy, cathodic protection and protective coatings **(Priyantha et al. 2003, Bai et al. 2004)**. MCrAlYs are amongst the most important protective coating materials applied to counteract hot corrosion and high temperature oxidation. Like other coatings designed to resist oxidative environments at high temperatures, MCrAlYs should be capable of developing a thermodynamically stable, slow-growing and adherent surface oxide layer **(Zhao et al. 2004B)**.

2.5   PROTECTIVE COATINGS

The coatings at high temperature develop a protective oxide layer on the metal surface to limit loss of metal by oxidation. Generally, these protective oxides (namely Al_2O_3, Cr_2O_3, and SiO_2) minimize the diffusion of gaseous or liquid species towards the component and conversely prevent elemental diffusion from the alloy towards the external surface where they could react with the substrate. Moreover, inter-diffusion effects between coating and substrates are supposed to be minimum as far as the properties of the coated component are concerned **(Mevrel et al. 1989).**

Early failure of the thermal power plant components frequently occurs due to the complex reactions between the metallic materials and the hostile combustion environment. It is important to clarify the degradation mechanism of the high temperature materials by typical salts, so as to reduce the tube material consumption by developing more protective structural materials and coatings, with an ultimate goal to increase the energy recovery efficiency **(Li et al. 2005).** Materials for high temperature service need excellent mechanical properties, including high temperature strength, good creep resistance, microstructure stability, and strong corrosion resistance. These requirements sometimes cannot be achieved by alloy development alone. An alternative approach in which mechanical strength is accomplished by alloy development and corrosion resistance by surface coating or surface treatment is often used **(Tsaur et al. 2005).**

Due to the increasing aggressive service environments, coatings must be applied to Ni-based superalloy gas turbine components for high temperature oxidation and hot corrosion resistance **(Zheng et al. 2006).**

Coatings are playing a significant role in today's aero and industrial turbine engines to extend the life or enhance the performance of components; about **75%** of all the components in jet engines are coated **(Zheng et al. 2006 and Gurrappa 2000).** The most common metallic coatings used in the hot section of turbine engines are MCrAlY type overlay coatings, which can be specifically designed and produced to meet the particular environmental operating conditions independent of substrates **(Guo et al. 2006A).**

2.6 NANOSTRUCTURED COATINGS FOR HIGH TEMPERATURE

It is well known in the literature that the nanostructured MCrAlY (M=Ni or Co or Fe) coatings provide a better corrosion resistance at high temperature due to the formation of continuous protective layer assisted by the enhanced diffusivity of atoms in the coating **(Geng et al. 2002, Ren et al. 2006, Chen et al. 2000, Peng et al. 2003, Ajdelsztajn et al.2002)** which is unattainable with the conventional MCrAlY (M=Ni or Co or Fe) coatings. Therefore, protective nanostructured superalloy coatings (MCrAl-type) are used on superalloys in energy conversion and gas turbines to protect their surfaces from oxidation and hot corrosion and to enhance the efficiency which in turns enhances the life of the components.

Nanostructure coatings form protective oxidation scales with superior adhesion to the substrate **(Gao et al. 2004)**. The high density of grain boundaries provides fast diffusion paths, promoting selective oxidation of protective oxide scales. The fine-grained coatings and/or the fine-grained oxide scales show a fast creep rate at high temperatures, which can release the stresses accumulated in the scales, therefore reducing the scale spallation tendency. The oxides formed on nanocrystalline coatings are micro pegged onto the grain boundaries to form a complex interface that results in better scale adhesion to the metal substrate. Due to this reason nano- and microcrystal coatings possess superior high-temperature oxidation and corrosion resistance.

The oxidation mechanisms of sputtered microcrystalline Co-30Cr-5Al coatings were investigated **Wang et al. (1996)** by an acoustic emission technique, scratch test, transmission electron microscope (TEM), which was compared with CoCrAlY alloy. The results indicated that the beneficial effects of micro crystallization on the scale adhesion of Co-30Cr-5Al alloy are as follows: (1) The sputtered CoCrAl coating possesses a columnar structure, and oxidation along the columnar grains may form many micro pegs which can anchor the scale to the metallic substrate, enhancing bonding of the scale. (2) The grain size of the sputtered coating is several orders of magnitude smaller than that of the cast alloy, and the grain size of

oxide, scales formed on the former is finer than that of the latter. The finer oxide scale may relieve the growth stresses during isothermal oxidation and partial thermal stresses during cooling by plastic deformation through grain sliding. The microcrystalline coating is more plastic than the cast alloy, which may relieve a certain amount of thermal stresses of the oxide scales. On the basis of oxide adhesion and plasticity, micro crystallization is more beneficial than the addition of reactive elements.

Over the past two decades, there has been considerable research on the development of coatings with finer microstructures approaching the nanometer scale. Nanostructured coatings are more resistant to high-temperature oxidation and corrosion than their counterpart conventional coatings **(Gao et al. 2001, Liu et al. 1999, Zhang et al. 2005).** Short-term (50–200 h.) test results on Fe–Ni–Cr–Al and Ni–Cr–Al coatings have shown that the protective oxide layer formed on the nanocrystalline coatings exhibited better spallation resistance during cyclic oxidation testing compared to the conventional cast materials of the same chemical compositions of the coatings. The oxide layer formed on the nanocrystalline coating on 310 SS samples exhibited excellent spallation resistance during cyclic oxidation testing at 1000°C for up to 100 one hour thermal cycles **(Liu et al. 1999).**

Liu et al. (1998) have studied the effect of grain size on protective oxide scale formation and spallation behavior of oxide scale on a Ni–20Cr–3Al coating. Their 50 one-hour thermal cycling test results at a peak temperature of 1100°C showed that fine grain size promoted formation of either alumina (Al_2O_3) or chromia (Cr_2O_3) as opposed to formation of a mixed oxide scale. The oxide scale formed on the ultra fine grain coated surface varied from α-Al_2O_3 to Cr_2O_3 as the coating grain size increased from 50 to 500 nm. Specifically, the finer coating grain structure promoted selective oxidation of Al through rapid diffusion of Al along the grain and sub-grain boundaries.

The effects of Cr and Al contents on the oxidation behavior of nanocrystalline Ni–Cr–Al coatings were also investigated by **Chen and Lou (1999, 2000) and Liu and Gao (2004).** The results of these investigations showed that the formation of a protective α-Al_2O_3 oxide layer on the external surface of a nanocrystalline coating also depends on the Cr and Al content. The results of **(Liu and Gao et al. 1998)** showed that micro, or nanocrystalline,

grain size promotes an α-Al$_2$O$_3$ protective oxide scale formation even when the Al content in the coating is relatively low (Cr/Al>4). Formation of a continuous α-Al$_2$O$_3$ scale has been reported in a nanocrystalline Ni–20Cr-Al coating with an Al content as low as 2 wt %(**Liu and Gao et al. 1998**). Furthermore, it has been shown that the nanocrystalline structure reduced the critical Al content required for α-Al$_2$O$_3$ scale formation by increasing the diffusion rate of Al(**Chen and Lou 2000**).Contrary to the results **of(Liu and Gao et al. 1998), Chen and Lou(1999,2000)** reported formation of an Al$_2$O$_3$ and NiAl$_2$O$_4$ mixed scale on a Ni–3Cr-20 at% Al sputtered coating after 200 h exposure at 900°C, suggesting that the critical Al content for the formation of Al$_2$O$_3$ also depends on the Cr content in the coating.

The influence of sputtering on the high temperature oxidation resistance of the cast superalloy K17F has been studied by **(Hanyi Lou et al. 1995)**. The as-sputtered microcrystalline layer has a homogeneous γ phase structure with very fine grain size **(20-100 nm)**, while the as-cast alloy is composed of γ, γ' and carbides. The oxidation resistance of the microcrystalline coating of K17F alloy is much better than that of the as-cast alloy, and is even superior to that of the pack aluminized alloy. At the initial oxidation stage, the oxide scale which formed on the as-cast alloy is composed of complex oxides of Cr, Ti, Ni and Al. As the oxidation time is prolonged, the amount of α - Al$_2$O$_3$ increases and becomes the main product. However, the scale which formed on the microcrystalline coating consists only of α-Al$_2$O$_3$. Cyclic oxidation and acoustic emission examination showed that the oxide scale on the cast K17F alloy easily spalled during cooling, but the α-Al$_2$O$_3$ scale on the sputtered layer had excellent adhesion.

The corrosion resistance of the cast superalloy K38G and a sputtered nanocrystalline coating of the same material was investigated **(Wang Fuhui and Young D. J 1997)** in pure CO in the temperature range 850-1000°C and in CO-20 vol.% CO$_2$ at 900°C. The cast K38G alloy formed Cr$_2$O$_3$ and TiO$_2$ scales, and a zone of internal Al$_2$O$_3$ precipitation. Weight-gain kinetics followed the parabolic rate law under all conditions investigated. The sputtered K38G nanocrystalline coating, however, formed a single phase Al$_2$O$_3$ scale and no internal-oxidation zone. The parabolic rate constants for nanocrystalline coating oxidation were about one order of magnitude smaller than those of the cast alloy. The changes in reaction

morphology and rate are attributed to the more rapid grain-boundary diffusion of aluminum in the nanocrystalline material.

The rehealing ability of the protective oxide scales formed on a microcrystalline coating of the Ni-base superalloy K38G has been studied **(Hanyi Lou et al. 1995)**. The results indicated that the oxide scales on the coating may be rehealed when the original scales are destroyed, and the coating still has excellent resistance against high-temperature oxidation. When the original Al_2O_3 oxide scales spall, mixed-oxide scales of both $(Al, Cr)_2O_3$ and TiO_2 can form on the surface. The mixed scales are very protective and adherent.

The oxidation behavior of the sputtered NiCrAlY coating at 900°C, 1000°C and 1100°C was investigated **(Li M·H·et al. 2003)**. The oxidation kinetics of the coating showed phase transformation from θ-Al_2O_3 to α-Al_2O_3. The higher the oxidation temperature, the faster was the transformation from θ-Al_2O_3 to α-Al_2O_3. The rapid formation of α-Al_2O_3 which led to the mass gain of specimen at 1100°C was the lowest at the initial oxidation stage. Under steady-state condition, the oxidation reaction appeared to be controlled by diffusional transport in α-Al_2O_3 scale with activation energy of approximately 390 kJ/mol. The scale formed on the coating was alumina exclusively, though there exist different modifications of alumina. This favorable oxidation behavior could be mainly attributed to the high aluminum content, the third element Cr and the nanocrystallized microstructure of the coating. During oxidation, β-NiAl transformed to γ'-Ni_3Al and γ phase because of the diffusion and the formation of Al_2O_3.

Nanocrystalline coating on the cast K52 alloy was prepared by magnetron sputtering **(Wang F·et al. 2008)** from the target of the same alloy. The comparison of oxidation in air at 800–1000°C and hot corrosion under molten Na_2SO_4 +25 wt. % K_2SO_4 at 850°C of the cast alloy and its nano-grained counterpart was investigated by means of TGA and XRD. The result showed that the nanocrystallization of the cast alloy led to a transformation of the alloy from a chromia former to an alumina former, and consequently a greatly reduced oxidation rate. Besides, the alumina scale formed on the nanocrystalline coating was much adherent compared to the chromia scale on the cast alloy.

The hot-corrosion behavior of a nanocrystalline coating of K38G alloy, prepared by magnetron sputtering and cast K38G in molten 75 wt.% Na_2SO_4 +25 wt.% K_2SO_4 at 900°C was studied(**Geng S·et al. 2002**). The coating eliminated internal sulfidation during the early stage of corrosion as a result of the formation of a continuous and compact Al_2O_3 scale. The nanocrystallization of K38G alloy prolonged the incubation of breakaway corrosion and improved the corrosion resistance of K38G.

A nanocrystalline Ni–30Cr–8Al–0.5Y coating was deposited on a Ni-base superalloy by magnetron sputtering **(Ren Xin and Wang Fuhui 2006)**. Post-aluminizing was performed on the sputtered coating to improve the corresponding high-temperature properties. The isothermal oxidation behavior at 1000-1100°C and hot-corrosion behavior in the presence of 75 wt.% Na_2SO_4+25 wt.% K_2SO_4/NaCl film at 900°C of the sputtered coating with and without aluminizing have been investigated. The results indicated that the sputtered NiCrAlY coating possessed excellent oxidation resistance at 1000°C due to the presence of extensive amount of chromium and good amount of aluminum. Because of the excessive consumption of Al in the coating, it lost protection at 1100°C. The mass gain of the aluminized NiCrAlY coating was a little higher than that of the sputtered coating due to the formation of the rapid growth θ-Al_2O_3 phase at 1000°C. At 1100°C the oxidation resistance of the latter was better than that of the former. The sputtered coating provided much better hot-corrosion resistance in the presence of 75 wt.% Na_2SO_4+25 wt.% K_2SO_4/NaCl film as a result of the formation of a continuous and protective Al_2O_3 scale.

Ni–11Cr nanocomposite was fabricated **(Zhang C·et al. 2005)** through co-electrodeposition of Ni with Cr nanoparticles. Comparison of the hot corrosion of the nanocomposite and the arc-melted Ni–10Cr and Ni–20Cr alloys in air at 700°C under molten Na_2SO_4–K_2SO_4–NaCl demonstrated that the hot corrosion resistance of the three materials, from worst to best, is in the order of Ni–10Cr< Ni–20Cr< Ni–11Cr nanocomposite.

Microstructural investigation of the corroded samples indicated that a denser and higher chromia-enriched scale formed on the Ni–11Cr nanocomposite, whereas the scales on the Ni–Cr alloys were less protective, although the Cr contents of the alloys were similar to or much higher than that of the nanocomposite. The explanation lies in the exclusive

formation of a continuous chromia scale on the Ni–11Cr nanocomposite. This is probably due to the easy nucleation of chromia on chromium nanoparticles, a high concentration of metal grain boundaries, which are also nucleation sites, and then fast linking of the nuclei as a result of enhanced diffusion of Cr from the coating to the interface through those nanocomposite grain boundaries. Therefore, a dense chromia scale is formed before attack by the molten salt can occur. Although the Ni–20Cr alloy forms a continuous chromia scale; a longer time is needed for its development, which allows the molten salt to attack the metal. The Ni–10Cr alloy never forms a continuous chromia scale; therefore, the internal attack was the most significant in this case. The results suggest that it will be possible to develop a Ni–Cr nanocomposite which contains even less chromium and yet still has good resistance to hot corrosion.

2.7 PROBLEM FORMULATION

2.7.1 Scope

Hot corrosion is a serious problem, as steady, continuous increase in the operating temperatures of the hot sections of aero, marine and utility turbines focuses upon achieving its higher efficiency alone. This temperature rise has been met by the intelligent use of materials with high temperature stability through the use of advanced manufacturing technologies, including investment cast blades with improved cooling efficiencies and single-crystal technology, and the advanced coating systems. A wide range of turbine operating conditions exists in utility turbines, which makes use of multi-fuels. The industries pose demand mainly on the design of high efficiency power plant, capable of operating on a wide range of fuels. Under these service conditions, the engine may experience high temperature oxidation, which needs to be considered seriously **(Nicholls 2002).**

Modern gas turbine engines blades in aero, marine and industrial gas turbines are manufactured exclusively from nickel based superalloys and operate under the most arduous conditions of temperature and stress of many components in the engine. This is further complicated in marine applications due to the aggressive environment, which includes sulphur and sodium from the fuel and various halides contained in seawater. These features are known to drastically reduce the superalloy component life and reliability by consuming

the material at an unpredictably rapid rate, thereby reducing the load-carrying capacity and potentially leading to catastrophic failure of components **(Eliaz et al. 2002, Liu et al. 2006)**. Thus, in order to improve an efficiency of the gas turbine engine significantly, the hot corrosion resistance of superalloys is as important as its high temperature strength. **(Khajavia 2004, Guo 2006).**

Recent studies showed that the high temperature strength materials are highly susceptible to hot corrosion and the surface engineering plays a key role in effectively combating it **(Gurrappa 2006, Rocca 2003)**.Therefore, the combination two materials, i.e., base and coating must be considered as an integral system and the interface between them is equally important as it can be the limiting factor. An ideal system i.e, super alloy and coating should be able to survive the harsh corrosive environment to the designed service life **(Lin 1984).**

Different types of hot corrosion damages caused by vanadium have been encountered in all types of combustion equipments burning low-grade fuel oils. These include boilers, furnaces, diesel engines, and gas turbines. Indeed, petroleum crude and fuel oils can contain up to 4 percent sulfur, 500 ppm vanadium and several tens of ppm of sodium. The ash particles that result from their combustion consist of complex mixtures of vanadium pentoxide (V_2O_5) and sodium sulfate (Na_2SO_4) that exhibit low melting points down to 500°C. These compounds partly deposit on the hot gas path of the thermal equipment walls, tubes, piston/cylinder; turbine combustors. The resulting film acts as an ion-electrolyte and is conducive to fast attack of the substrate material by the oxidizing agents present in combustion gas and in the molten salt film. When the salt films (Na_2SO_4) contain vanadium, an acidic dissolution of the protective oxide scale would take place because V_2O_5 like MoO_3 or WO_3 acts as a strongly acidic oxide. Hence, the presence of vanadium in such molten salts causes a significant increase of the acidic solubility of the protective oxides **(Hussain et al. 1994).**

Nanostructured MCrAlY (M=Ni or Co or Fe) coatings provide a better corrosion resistance at high temperature due to the formation of continuous protective layer of scale assisted by the enhanced diffusivity of atoms in the coating **(Geng et al. 2002, Ren et al. 2006, Chen et al. 2000, Peng et al. 2003, Ajdelsztajn et al.2002)** which is unattainable with

the conventional MCrAlY (M=Ni or Co or Fe) coatings. Therefore, protective nanostructured MCrAl-type coatings are used for the hot section components of a gas turbine to protect their surfaces from oxidation and hot corrosion and to enhance the efficiency which in turns enhances the life of the components.

Owing to the aforementioned facts, there is a significant scope in understanding the reaction kinetics and the nature of the surface scales formed during oxidation, as they are important to evaluate the alloys for high temperature applications. The oxidation behavior of bare and nanostructured coated superalloy has not been studied extensively and is not well understood. Therefore, further studies are needed on oxidation behavior of nanostructured coated superalloy, particularly those used for high temperature applications.

The hot corrosion environment Na_2SO_4-60%V_2O_5 has been selected for the laboratory tests as the molten sulphate-vanadate deposits resulting from the condensation of combustion products of low grade fuels are extremely corrosive to the high-temperature materials (Rapp 1986). Furthermore, sodium vanadyl vanadate $(Na_2O.V_2O_4.5V_2O_5)$, which melts at a relatively low temperature 550 °C is found to be the most common salt deposit on the boiler super-heaters (Barbooti et al. 1988). This environment will also be pertinent to the gas turbines as the predominant species in the salt deposits forming on gas turbine surfaces are expected to be Na_2SO_4, V_2O_5 and $Na_2V_2O_6$.

The high temperature corrosion behavior of the sputtered deposited nanostructured coating on superalloy is very limited in the literature so far. Cobalt - Aluminum based metallic coatings are frequently considered for the protection against oxidation, corrosion, wear and erosion at high temperatures. Therefore, the present research work is envisaged to make a detailed investigation of Magnetron sputtered coatings (Cr/Co-Al and Co-Al coatings) on superalloy subjected to oxidation, and hot corrosion. The Ni- based superalloys such as Superni- 718 developed by Mishra Dhantu Nigham Ltd., Hyderabad have been chosen for the present work. It is very essential to investigate the hot corrosion behavior of sputtered nanostructured coatings on Superni-718 to assess its suitability for high temperature applications. Most industrial processes involve the use of metals and alloys at elevated temperature followed by cooling to room temperature numerous times. The operating

conditions in such plants are mostly cyclic, rather than to isothermal processes. Therefore, oxidation under cyclic conditions constitutes a more realistic approach towards solving the problem of metal corrosion **(Hocking and Sidky 1987).** Relatively fewer studies are reported under cyclic conditions, which actually simulate the working conditions of boilers and gas turbines. Owing to the aforementioned views, the present work has been focused to address the issues as given in following section.

2.7.2 Objectives

1. The objective of the present research work is aimed at studying the high temperature (900 $^{\circ}$C) oxidation (Air), and hot corrosion in Na_2SO_4-60%V_2O_5 environment in the laboratory tube furnace on superalloy such as Superni- 718 in bare conditions and after application of sputtered deposited nanostructured Cr/Co-Al and Co-Al coatings on the superalloy.

2. To compare the oxidation and hot corrosion performance of the sputtered deposited nanostructured coated superalloy with bare ones and assess its suitability for using it in the gas turbine engines, boiler super-heaters and re-heaters, and for other future hot section components to be used in similar corrosive environments.

3. To understand and propose mechanisms for the high-temperature corrosion of the substrate superalloy and coated superalloy, wherever possible. As far as the testing in air environment is concerned, the study could also provide useful information regarding the adhesion of the coatings and the spalling tendency of their oxide scales apart from air oxidation behaviour of the coatings.

4. The Cr/Co-Al and Co-Al coatings deposited on superalloy, after high temperature air

5. Oxidation and hot corrosion studies were characterized by the techniques such as XRD, FE-SEM/EDS and AFM to render an insight into the corrosion mechanisms based on the morphology of the corroded products formed on the coated superalloy. The similar characterizations studies were performed for the corroded uncoated superalloy.

6. To summarize the important contributions made in the present work on sputtered deposited nanostructured coatings on superalloy and highlight the scope for future work in the high temperature corrosion of coatings.

CHAPTER 3
EXPERIMENTAL
TECHNIQUES AND PROCEDURES

This chapter deals with synthesis and characterization techniques of the coatings. A detailed description of oxidation and hot corrosion studies of coated and bare superalloy in air and molten salt environments, respectively, is given in this chapter. The procedures for analyzing the corrosion products are discussed. The specifications of the equipments used are furnished.

3.1 SYNTHESIS OF NANOSTRUCTURED COATINGS

A wide variety of techniques have been used to synthesize nanostructured coatings including thermal evaporation, pulse laser deposition, rapid solidification, Magnetron sputtering, etc.. Among these techniques magnetron sputtering is widely used so far. The reasons for using magnetron sputtering are as follows:

❖ Precise control of coating composition and thickness

❖ Large area uniformity

❖ Deposition of coatings with properties close to bulk material

❖ Good adhesion to substrate

❖ High deposition rate
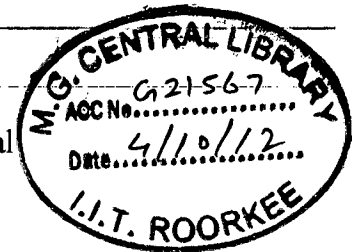
The intrinsic problems associated with sputtering of alloy coatings are difference in sputtering yield at a given sputtering power density, geometrical composition non-uniformity over substrate and along cross-sectional thickness of the coating, as well as wear, erosion and roughening of targets during sputtering **(Shih C. L. et al.2001 and Anders A. 2005)**. To combat these problems, following precaution have been taken: (a) separate element target of metals were used **(Shih C. L. et al. 2001 and Krulevitch P. et al. 1991)**; (b) substrate was kept on axial rotation during deposition; (c) good configuration of target and substrate

position and (d) precise control of sputtering conditions etc. Contamination is also one of the major problems; therefore, it is important to limit the impurities (like oxygen and carbon) to prevent the brittleness and degradation of mechanical properties. For this reason, the purity of Ar gas and targets is essential, and the base vacuum of the main chamber should be as high as possible. Pre-sputtering of targets before deposition effectively removes the surface oxides layer, thus constitutes one of the important steps in ensuring coating purity.

3.2 SPUTTERING

Sputter deposition is one of the physical vapor deposition processes for depositing coatings by sputtering, i.e. removal of atoms from a "target"(source), which then deposits onto a substrate. In other words, it is the ejection of atoms from the surface of material (the target) by bombardment with energetic particles, the process called 'sputtering'. The ejected or sputtered atoms get condensed on a substrate and form thin films. Sputtering is largely driven by momentum exchange between the ions and atoms in the material, due to collisions. The process can be thought of as atomic billiards, with the ion (cue ball) striking a large cluster of close-packed atoms (billiard balls). Although the first collision pushes atoms deeper into the cluster, subsequent collisions between the atoms can result in some of the atoms near the surface being ejected away from the cluster.

Sputtering process begins when inert gas atoms gets ionized due to the applied negative DC potential to the target material and these positive ions of inert gas hits the target atoms, the latter gains part of the momentum and transfer it to other atoms through further collisions, leading to a cascade which results in some of the target atoms to 'sputter' out of the target with secondary electrons. The sputtered atoms, those ejected into the gas phase, are not in their equilibrium state, therefore, they tend to condense back into the solid phase upon colliding with any surface in the sputtering chamber with maximum deposition taking place on the substrate, which is in the line of sight of the target to form a coating. It subtends the maximum area perpendicular to the momentum of ejected target atoms and clusters. These secondary electrons collide and ionize the inert gas atoms and plasma is generated. The initial positive ions needed to trigger the generation of secondary electrons are thought to be either

the stray ions always present in the atmosphere or the ions produced by field ionization of the inert gas atoms.

Other processes associated with the bombardment of a target by highly energetic ions include:

a) Generation of secondary electrons,

b) Ion reflection at the target surface,

c) Ion implantation with the ion permanently buried into the target surface,

d) Radiation damage in the structural rearrangement varying from simple vacancies and interstitial to gross lattice defects, and

e) Emission of X-rays and photons

These processes can be summarized as illustrated in **Fig. 3.1.**

To use sputtering as a useful thin film deposition process, some criteria have to be met. First, ions of sufficient energy must be created and directed towards the surface of a target to eject atoms from the surface of the material. To achieve this, an argon gas of ionization energy 15.76 eV, for example, can be used in a chamber and by application of a sufficiently large voltage between the target and the substrate; a glow discharge is set up in a way to accelerate the positive ions towards the target to cause sputtering.

Secondly, the ejected materials must be able to get to the substrate with little impedance to their movement. The pressure 'P' determines the mean free path of the sputtered particles which according to the Paschen's relation is proportional to $1/P$.
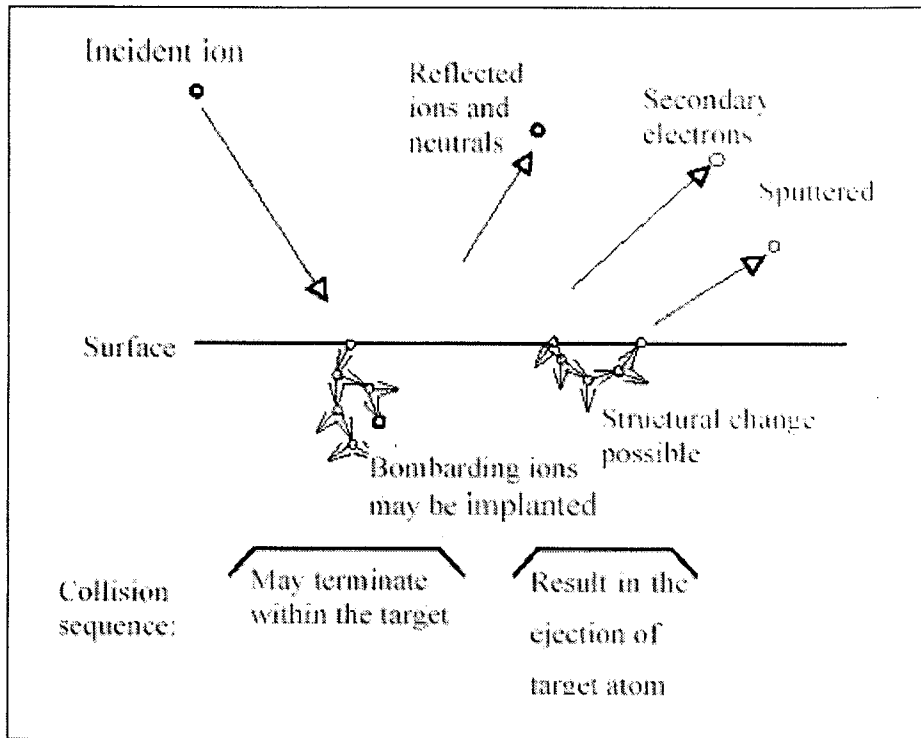
Fig. 3.1. Processes generated by the impact of highly energetic particle on a
   target surface. The collision may terminate at the target or cause
   particle sputtering.

In addition to pressure, the target-substrate distance determines the scattering of the sputtered particles on their way to the substrate and also the amount of energy with which they deposit on the substrate. Generally, the average energy of sputtered atom is 10-40 eV.

Sputtering is characterized by the sputter yield 'S', which is the ratio of the ejected atoms to the number of incoming energetic particles, which are predominantly ions. Sputter yield depends on the energy and direction of the incident (bombarding) ions, masses of the ions and target atoms and the binding energy of atoms in the solid. By Sigmund's theory, the sputter yield is given as

For E < 1 KeV,

$$S = \frac{3\alpha}{4\Pi^2} \frac{4M_1 M_2}{(M_1 + M_2)^2} \frac{E}{E_B} \qquad (3.1)$$

where, E_B is the surface binding energy of the target atom being sputtered, E is the ion bombardment energy, α. is a measure of the efficiency of momentum transfer in collisions, and M_1 and M_2 are the masses of the positive ion of the gas and target material, respectively. But for E > 1 KeV,

$$S = 3.56\alpha \frac{Z_1 Z_2}{Z_1^{2/3} + Z_2^{2/3}} \left(\frac{M_1}{M_1 + M_2} \right) \frac{S_n(E)}{E_B} \qquad (3.2)$$

where, Z_1 and Z_2 are the atomic numbers of the incident ion and sputtered target atom respectively and $S_n(E)$ is a measure of the energy loss per unit length due to nuclear collisions, and also it is a function of the energy as well as masses and atomic numbers of the atoms involved **(Ohring 2002).**

3.2.1 Magnetron Sputtering

Magnetron sputtering is a coating deposition technique based on the physical sputtering effects caused by the bombardment of a target material with accelerated ions produced in glow discharge plasma. A wide variety of coating materials, from metals to insulators, may be produced using this technique. In sputtering, not all of the electrons escaping the target contribute to the ionized plasma glow area. The wasted electrons fly around the chamber causing radiation and other problems, for example, the heating of the target. A magnetron sputtering source addresses the electron problem by placing a set of strong permanent magnets in the gun arranged in a circular geometry giving rise to a radial magnetic field parallel to the target surface as shown in **Fig. 3.2.**
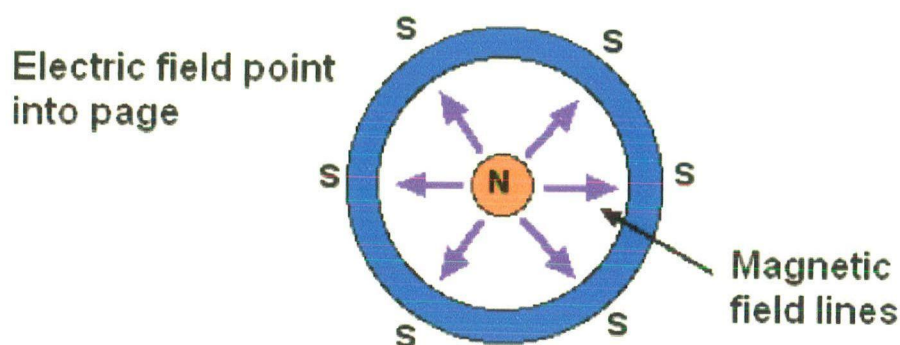
Fig. 3.2. Electric and magnetic field lines in a magnetron gun

A plate of a highly permeable material (such as iron) located behind the magnets, prevents the magnetic field flux from spreading into regions other than in front of the target surface. Thus the electrons are forced to follow a closed drift path caused by the crossed electric and magnetic fields, i.e. the electrons are trapped in a channel as shown in **Fig. 3.3(a)** of magnetron sputtering process **(Ohring 2002).** The effect of this is two fold:

a) The probability of ionizing the inert gas atoms will increase significantly and make the plasma more intense and sustainable at low pressure

b) An increase of the mean free path, which is inversely proportional to the pressure. Due to the confinement of secondary electrons, the larger number of sputtered atoms gets deposited as thin film on the substrate. **Fig. 3.3(b)** shows the collisions involved in a magnetron sputtering process near the target.

DC magnetron sputtering is used for conducting targets such as metals or doped semiconductors but not for non-conducting targets (non metals or insulators) because of its non-conducting nature, positive ions would lead to a charging of the surface and subsequently to a shielding of the electric field. Subsequently, the ion current would die off. Therefore, RF magnetron sputtering (radio frequency of 13.56 MHz) is used for non-conducting and semiconductor targets in which an AC-voltage is applied to the target. In one phase, ions are accelerated towards the target surface to sputter material.
In the other phase, charge neutrality is achieved.
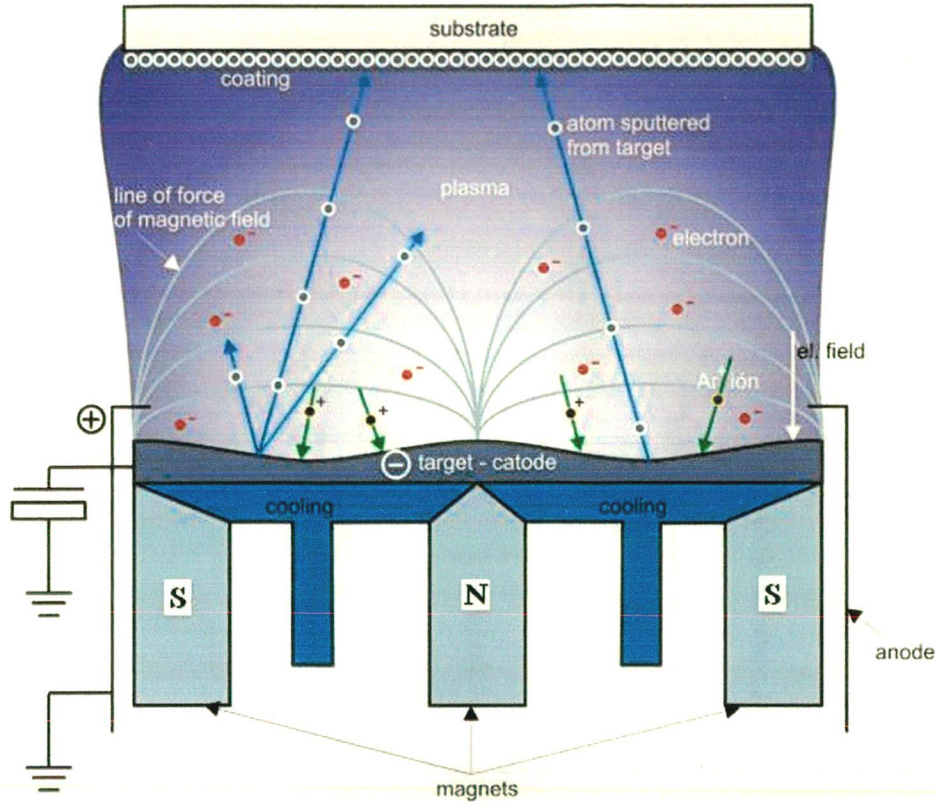
(a)
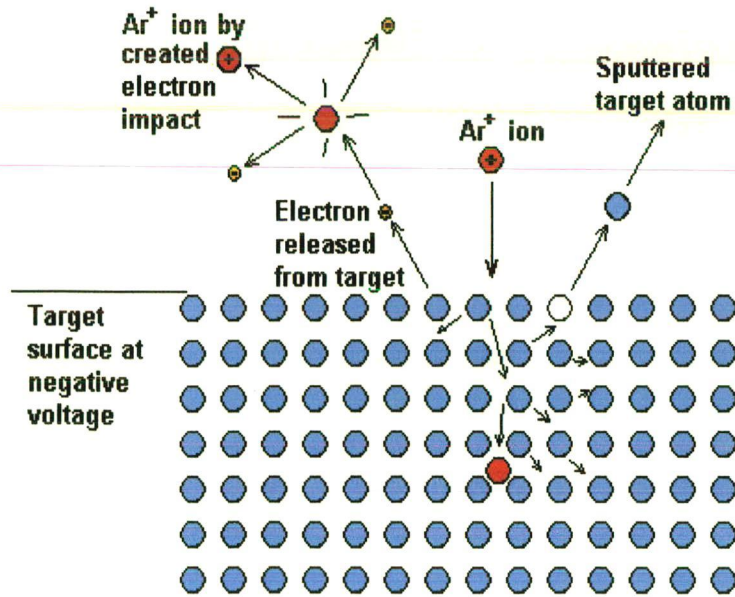
(b)

Fig. 3.3. (a) Magnetron sputtering process (b) Collisions in the sputtering
process near the target

The magnetron sputtering set up used for the present work is shown in Fig. 3.4(a).
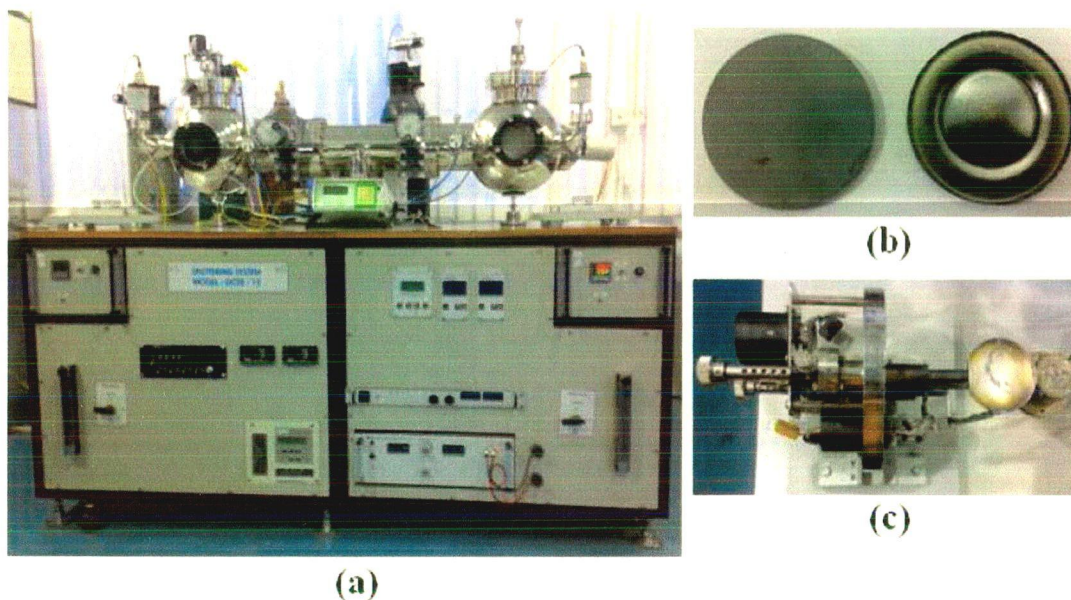
Fig.3.4. (a) DC/RF magnetron sputtering unit set up in our Nano Science Lab
(b) New & used sputtering target (c) Substrate holder/heater

A circular disc of diameter 2 inch and thickness 3-5 mm of pure material used as a target is shown in **Fig. 3.4(b),** which is mounted on the magnetron gun for sputtering. The target is eroded in a circular pattern due to the use of a set of strong permanent magnets in the gun arranged in a circular geometry behind the target. The substrate is fixed on a heater **(Fig. 3.4(c))** with the help of clips for the preparation of nanocrystalline coatings. The temperature of the substrate is controlled via the temperature controller of heater. After fixing the substrates, the chamber is evacuated using a turbo molecular pump, backed by rotary pump up to high vacuum ($>2 \times 10^{-6}$ Torr). After evacuation, an inert gas such as Argon (99.999% purity) is fed into the chamber via gas inlet valve. Simultaneously, the gate valve is brought into almost closed state (throttling) so as to match the gas influx and pumping-out rate. With proper throttling, the inert gas pressure and flow rate inside the chamber can be made very stable and then the process of sputtering is the same as discussed in the section **3.2.**

The advantages of sputtering as deposition technique are as follows: The deposited coatings have high uniformity at large area, better reproducibility of deposited coatings, good adhesion of coatings with substrate **(Kim S.K. et al .2004)**, high flexibility of large-scale as well as complex geometry shape production, easy deposition of materials with high melting points and high reactivity. A homogeneous multicomponent phases as well as multilayer coatings can be produced with completely new material properties and the deposited coatings show the same concentration as that of the target material **(Ohring 2002).** This might be surprising since the sputter yield depends on the atomic weight of the atoms to be sputtered as discussed earlier. It may result in one component of an alloy or mixture to sputter faster than the other components, leading to a higher concentration of that component in the deposited coating. Although the components are sputtered at different rates, however, since only surface atoms are sputtered, the faster sputtering of one element leaves the surface enriched with the other element, which effectively counteracts the difference in sputter rates resulting in deposited coatings with the same composition as the target.

3.3 BASIC STRUCTURAL CHARACTERIZATION TECHNIQUES

3.3.1 X-ray diffraction

X-ray diffraction is the non-destructive and most powerful technique for determining the crystal structure, preferred orientation, crystallite size, lattice constants, crystal defects, stress, layer thickness, phase analysis, etc. of solid matter. When a monochromatic beam of X-rays is incident upon a regular crystalline material, the beam will be scattered from the material at definite angles. This is produced by an interference effect called diffraction between the X-rays from different atomic layers within the crystal. These atomic layers are separated by distance in the order of angstroms and are comparable to the wavelength of X-rays. If the X-rays of a known frequency interacts with a crystalline solid then under particular circumstances of layer separation and angle of incidence to layer, the scattering from the different layers will constructively interfere at some angles and destructively interfere at most of the angles. This effect is characterized by the Bragg's equation

$$2d \sin \theta = n\lambda \qquad\qquad\qquad (3.3)$$

Where λ = wavelength of incident radiation and d = interplanar distance between the lattice planes), which is the base of X-ray crystallography.

In the present study, Bruker D8 Advance X-ray diffractometer **(Fig. 3.5)** was used to study the crystallite size and to identify the phases**(Yonghao Zhao et al. 2002)** present in coating before and after high temperature oxidation and hot corrosion. The radiation (Cu Kα) emanating from the X-ray tube is diffracted at the specimen and recorded by a detector. Bruker D8 Advance diffractometer uses NaI scintillation counter as a detector. It can detect the diffracted radiations in the wavelength ranging from 0.5 to 3 Å. Monochromators are used to suppress the undesired portions of radiation. To restrict the irradiated specimen area, aperture diaphragm is arranged between the tube and the specimen as shown in **Fig. 3.5**. The second aperture diaphragm shields the strong scattered radiation of the first aperture diaphragm. The scattered radiation diaphragm is used to suppress undesired scattered radiation. The resolution depends upon the detector diaphragm. The crystallographic information is obtained by evaluating'd' values and indexing of reflections. The characteristics diffraction pattern of a given substance can always be obtained whether the substance is present in pure state or as one constituent in a mixture of several substances. X-ray diffraction pattern is characterized by a set of line positions (2θ) and a set of relative intensities (I). The angular position of lines depends on the wavelength of the incident ray and spacing'd' of the lattice planes.

The technique can be used for quantitative analysis in which the concentration of phases is calculated by determining the area of the peak. The intensity of diffraction lines due to one constituent of a sample depend upon the concentration of that constituent in the specimen.
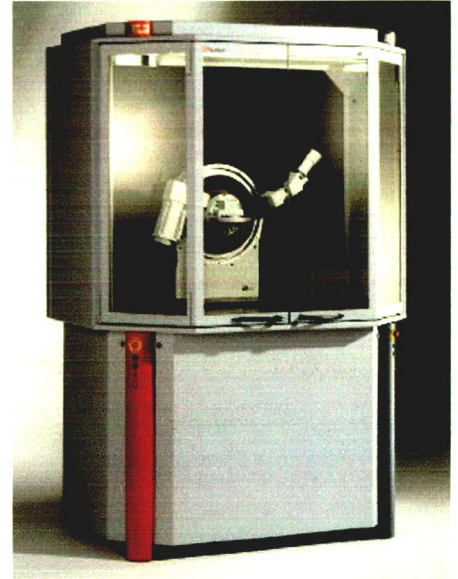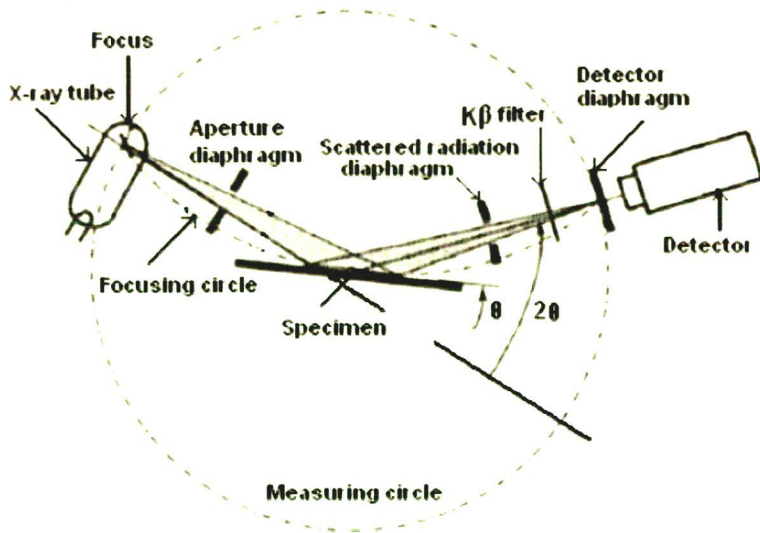
Fig. 3.5 Schematic diagram of beam path.   Photograph of X- ray

Diffractometer (Bruker AXS,D8

Advance)

The qualitative analysis for a particular substance is accomplished by identification of the pattern of that substance. The crystallite size is an important parameter, which can be determined using Scherrer's formula (**Cullity B. D. and Stock S. R.2001**):

$$t = \frac{0.9\lambda}{B\cos\theta} \qquad (3.4)$$

Where B (grain) is the corrected full-width at half maximum (FWHM) of a Bragg's peak, λ is the wavelength of X-ray, and θ is the Bragg's angle.

3.3.2 Field Emission Scanning Electron Microscopy

The scanning electron microscope (SEM) has a large depth of field, which allows a large amount of the sample to be in focus at one time. The SEM also produces images of high

resolution, which means that closely spaced features can be examined at a high magnification.

In the present study, field emission scanning electron microscope (FEI Quanta 200F model) with resolution of 2 nm and magnification 500000X was used to study the surface morphology of these thin films**(Kim Hyoung Soep et al.2004)**. **Fig. 3.6** shows a schematic diagram of the field emission scanning electron microscope (FE-SEM). FE-SEM uses field emission electron gun, which provides improved resolution of 2 nm i.e. 3 to 6 times better than conventional SEM and minimized sample charging and damage. In conventional SEM, electrons are thermionically emitted from a tungsten or
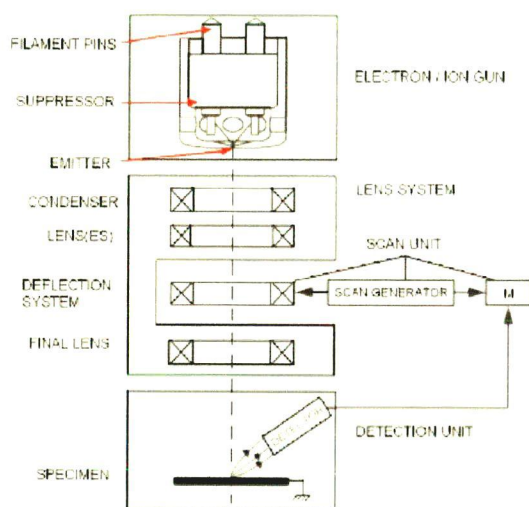
Fig. 3.6 Schematic diagram of   Photograph of FESEM

FE-SEM   (FEI Quanta 200F)

Lanthanum hexaboride (LaB6) cathode and are accelerated towards an anode, alternatively electrons can be emitted via field emission (FE). Tungsten is used as a filament because it has the highest melting point and lower work function, thereby allowing it to be heated for electron emission. The basic mechanism of field emission is that a high voltage applied between a pointed cathode and a plate anode caused a current to flow. The field emission tip is generally made of a single crystal tungsten wire sharpened by electrolytic etching. A tip

diameter of 100 to 1000 Å is used. The field emission process itself depends on the work function of the metal, which can be affected by adsorbed gases.

The electron beam, which typically has an energy ranging from a few hundred eV to 50 keV, is focused by two condenser lenses into a beam with a very fine focal spot size. The first condenser lens that works in conjunction with the condenser aperture helps to narrow the beam and also limit its current. The second condenser lens then forms the electrons into a very thin, coherent beam. The high energy beam of electrons scans the sample surface in a raster pattern using a set of scanning coils to obtain image. The objective lens does the final focusing of the beam onto the sample. At each point the numbers of secondary and back-scattered electrons reaching the detector are counted to be used for determining the relative intensity of the pixel representing that point in the final image.

Using the energy dispersive X-ray analysis (EDAX) attachment with the FE-SEM, elemental composition analysis was done. An EDAX spectrum normally displays peaks corresponding to the energy levels for which the most X-rays had been received. Each of these peaks is unique to an atom, and therefore corresponds to a single element. Higher the peak intensity, higher is the element concentration in the specimen. Insulator samples would be difficult to image using an SEM because of the fact that they would develop a negative charge (due to build-up of electrons), which would cause the image to become defocused due to deflection of the exciting electron beam, abnormal contrast in the image due to the uneven distribution of the negative charge on the sample and breaks or splitting of the image due to high negative charge on the sample which deflects the beam of electrons. Therefore, in order to enhance the number of secondary electrons from an insulating sample, the sample is often coated with a thin layer of gold- palladium or another electron-rich conducting material that produces abundant secondary electrons when struck by a focused electron beam. A thin metal coating will not mask surface features or the overall topology of the underlying sample. The conducting coating also conducts electrons away, so that the sample does not develop a significant charge when it loses secondary electrons and other types of electrons. This type of coating is essential for samples, which do not conduct charged particles.

3.3.2.1 Specimen- Electron Beam Interaction

When an incident electron beam strikes the specimen composed of a crystalline and amorphous structure, it undergoes a series of complex interactions with the nuclei and electrons of the atoms of the sample **(Fig. 3.7)**. The interactions produce a variety of secondary products, such as:

Secondary electrons: When the specimen is struck by the primary beam, electrons are freed from the specimen. The electrons released from the surface are mostly low energy secondary electrons between 0 and 50 electron volts. They will mainly give information of morphology and topology of the specimen.

Backscattered electrons: When the specimen is struck by the primary beam, electrons are elastically and non-elastically scattered back. Elastically means the primary electrons did not lose any of their primary energy. Back-scattered electrons release information on the composition of a material, the so-called Z contrast or atomic number contrast.

Photons: Photons or light quanta are freed when the primary beam strikes a material like some minerals. These light quanta can be detected using a cathode luminescence detector. The light detected can vary from infrared to ultraviolet.
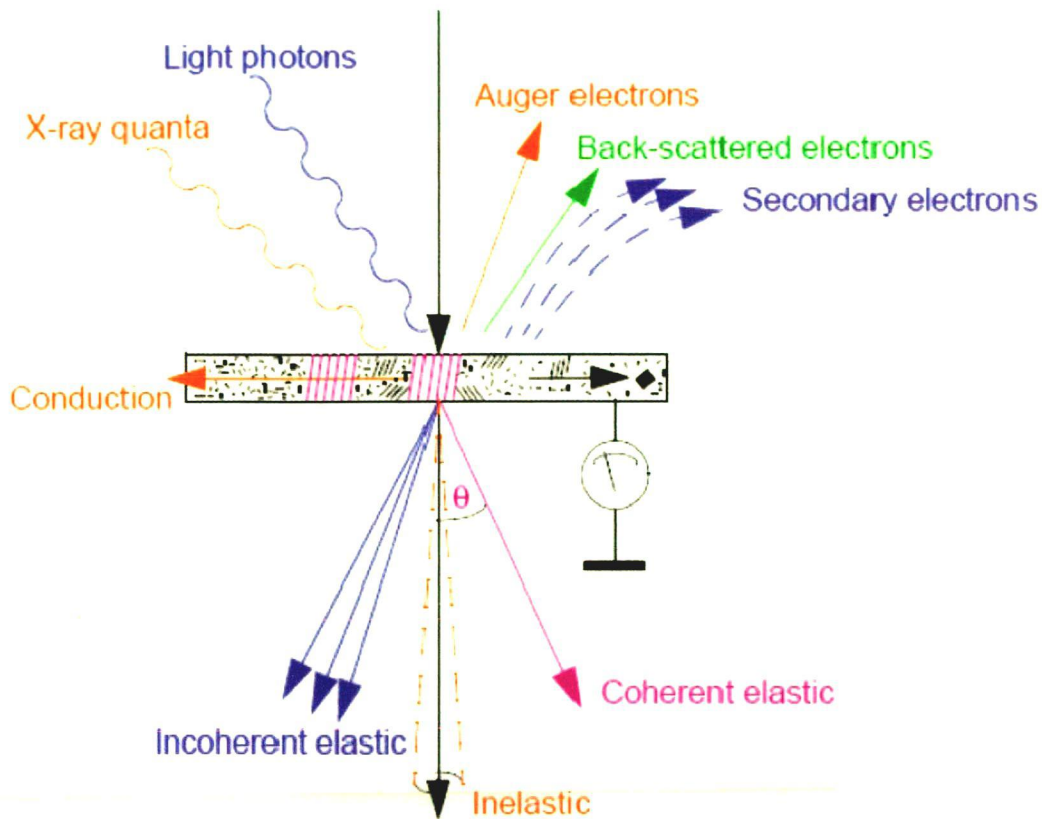
Fig.3.7 Specimen beam interaction.

Auger electrons: Due to collisions with the primary beam, auger electrons are freed. These electrons are element specific and their energy can be detected using an auger mass spectrometer. This technique is applied for detection of light elements and gives information on the top atomic layers of the specimen.

X-ray quanta: X-ray radiation takes place when an electron has received extra energy, e.g. due to a collision with an electron of the primary beam. As this is an unstable situation, the electron will fall back into its original orbit, the extra energy is released in the form of an X-ray quantum.

Conduction: Electrons that are stopped in the specimen must leave the specimen, therefore all specimens that are not conductive are made conductive by an extra layer of gold or carbon. If the specimen was non-conductive, it would start to become charged and thus an unwanted electrostatic lens would be made, which increases the inherent astigmatism.

Heat: The energy of the electrons stopped in the specimen is transferred to kinetic energy. The local temperature of the specimen can rise to temperature higher than 100 ^{o}C. The temperature depends on the acceleration voltage, the number of electrons (emission) and size (spot size) of the primary beam. If the temperature is too high for the type of specimen under investigation, the specimen will be damaged either in the form of contamination, evaporation, or complete tearing of the film layer.

Elastic scattering: Elastic scattering takes place when the negative charged electrons are scattered due to interaction with the positively charged atomic nucleus. Because the mass of the nucleus is much higher than the mass of the electrons, therefore a negligible energy transfer takes place. This means that the speed and thus the associated wavelength of the electron do not change. There are two types of elastic scattering:

(a) Incoherent elastic scattering: This is the case when the specimen has an amorphous structure. The deflected electron waves have no phase relation to the specimen.

(b) Coherent elastic scattering: This is the case when the specimen has a crystalline structure. There is now a phase relation between the specimen and waves are deflected under defined angles.

Inelastic scattering: Inelastic scattering takes place when the negative charged electrons are scattered due to interaction with the negative charged electrons. Now energy transfer takes place, this means that the speed and thus the associated wavelength of the electron changes.

3.3.3 Atomic Force Microscopy

The atomic force microscope (AFM) can be compared to traditional microscopes such as the optical or scanning electron microscopes for measuring dimensions in the horizontal axis. However, it can also be compared to profilers for making measurements in the vertical axis to a surface. One of the great advantages of the AFM is the ability to magnify in the X, Y and Z axes. Unlike traditional microscopes, the AFM does not rely on electromagnetic radiation such as photon or electron beams to create an image. An AFM is a mechanical imaging instrument that measures the two/three dimensional topography with a sharpened probe. In

the present study, atomic force microscope from NT-MDT: NTEGRA were used and the photograph is shown in **Fig. 3.8.** The sharpened probe attached to the lower side of a reflective cantilever, which is positioned close enough to the surface such that it can interact with the force fields associated with the surface. During imaging, light from a diode laser is focused on the cantilever and is reflected on to a four segmented photodiode. As the sample is scanned below the tip, the cantilever moves up and down which changes the ratio of light falling on the four elements of the photodiode. The difference in the intensity falling on the four segments is converted into a proportional voltage by the photodiode. This voltage serves as a feedback signal enabling the tip to maintain either a constant force or a constant height above the sample. An image of the surface is then reconstructed by monitoring the precise motion of the probe as it is scanned over the surface.
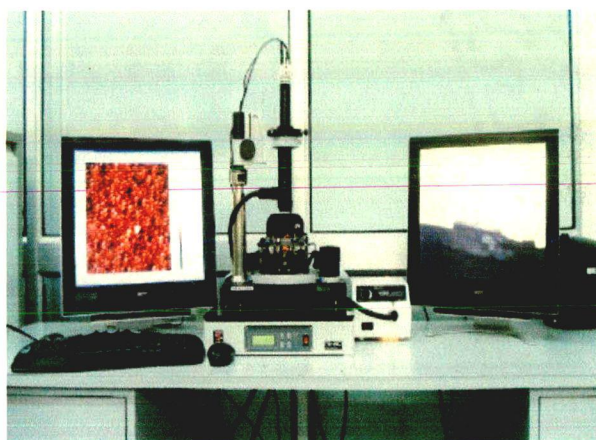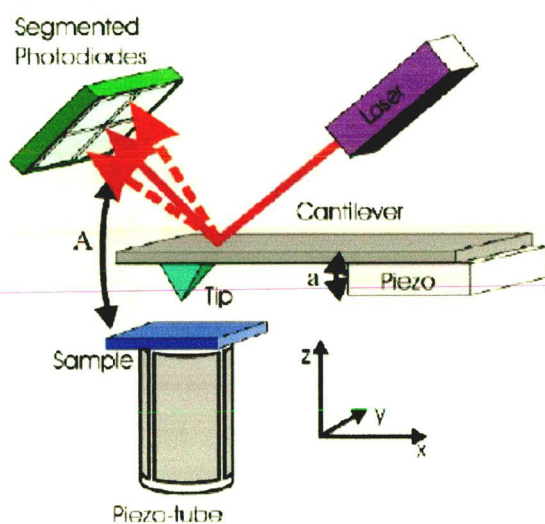
Fig. 3.8 Schematic diagram of AFM   Photograph of AFM (NT-MDT: NTEGRA)

For most applications, the instrument is operated in one of the following three modes:

(i) **Contact mode:** Contact mode is typically used for scanning hard samples and when a resolution of greater than 50 nanometers is required. In this mode, as the tip scans the sample in close contact with the surface, a repulsive force on the tip is set by

pushing the cantilever against the sample surface with a piezoelectric positioning element. During Scanning, the deflection of the cantilever is sensed and compared in a dc feedback amplifier to some desired value of deflection. If the measured deflection is different from the desired value, then the feedback amplifier applies a voltage to the piezo to raise or lower the sample relative to the cantilever to restore the desired value of deflection. The voltage applied by the feedback amplifier to the piezo, is a measure of the height of features on the sample surface. The typical problem with the contact mode is that the tip may scratch the surface and change its intrinsic features.

(ii) **Non-contact mode:** In this mode the tip is held at 50 - 150 Å above the sample surface. Attractive Vander Waals forces acting between the tip and the sample are detected, and topographic images are constructed by scanning the tip above the surface. Since the attractive forces from the sample are substantially weaker than the forces used by contact mode, therefore the tip is given a small oscillation so that AC detection methods can be used to detect the small forces between the tip and the sample by measuring the change in amplitude, phase, or frequency of the oscillating cantilever. For highest resolution, it is necessary to measure force gradients from Vander Waals forces which may extend only a nanometer from the sample surface.

(iii) **Semi-contact mode:** Semi-contact mode was developed as a method to achieve high resolution without including destructive frictional forces. In this mode, the cantilever is made to oscillate at its natural frequency by using a piezo-electric crystal. The change in oscillation amplitude during the tapping period is used as a feedback to maintain constant height or force between the tip and the sample. The feedback voltage serves as a measure of the surface features. The advantages of the semi-contact mode are that as the tip is not dragged over the sample, there is no damage caused to the sample and also the tip is prevented from sticking to the sample surface due to adhesion.

3.4 SUBSTRATE MATERIAL

The Ni-based superalloy namely, Midhani Grade Superni- 718 superalloy has been selected as the substrate material for the present study. This alloy was procured from Mishra Dhatu Nigam Limited, Hyderabad (India) in the rolled sheet form, for protecting them against high temperature corrosive environment applications. The nominal chemical composition of this alloy is given in **Table 3.1**. This superalloy find applications in steam boilers, heat exchangers, piping in the chemical industry, gas turbines, jet engines, furnace equipment, reformers and baffle plates/tubes in fertilizer plants.

Table 3.1 Chemical composition of superalloy used in study

Chemical composition, Wt-%

Midhani Grade	Fe	Ni	Cr	Ti	Al	Mo	Mn	Si	Co	Nb	P	C	S
Superni-718	19.8	Bal	17.6	0.96	0.53	3.23	0.02	0.03	0.01	4.91	0.005	0.02	0.007

3.5 HIGH TEMPERATURE OXIDATION AND HOT CORROSION STUDIES

3.5.1 Experimental Setup

Oxidation and hot corrosion studies were conducted at 900 °C in a laboratory silicon carbide tube furnace, Digitech, India make. The furnace was calibrated to an accuracy of ±5 °C using Platinum/Platinum-13% Rhodium thermocouple fitted with a temperature indicator of Electromek (Model-1551 P), India. The bare as well as the coated specimens were polished down to 1μm alumina wheel cloth polishing to obtain similar condition of reaction

before being subjected to corrosion run. The physical dimensions of the specimens were then recorded carefully with digital vernier caliper to evaluate their surface areas. Subsequently, the specimens were washed properly with acetone and dried in hot air to remove the moisture. During experimentation, the prepared specimen was kept in an alumina boat and the weight of boat and specimen was measured. The alumina boats used for the studies were pre-heated at a constant temperature of 1200 °C for 12 hours and it was assumed that their weight would remain constant during the course of high temperature cyclic oxidation/corrosion study. Then, the boat containing the specimen was inserted into hot zone of the furnace maintained at a temperature of 900 °C. The weight of the boat loaded with the specimen was measured after each cycle during the corrosion run, the spalled scale if any was also considered during the weight change measurements. Holding time in the furnace was one hour in still air followed by cooling at the ambient temperature for 30 minutes. Following this, weight of the boat along with specimen was measured and this constituted one cycle of the oxidation study. Electronic Balance Model CB-120 (Contech, Mumbai, India) having a sensitivity of 10^{-5} g was used to conduct the weight change studies. All oxidation and hot corrosion studies were carried out for 50-100 cycles. The reproducibility in the experiments was established by repeating hot corrosion experiments for three cases.

3.5.2 Oxidation Studies in Air

The oxidation tests at 900 °C were performed on Superni-718 bare superalloy (mirror polished) as well as magnetron sputtered Cr/Co-Al and Co-Al coated superalloy in laboratory furnace up to 100 cycles as discussed in section **3.5.1.**

3.5.3 Hot Corrosion Studies in Molten Salt (Na_2SO_4 - 60%V_2O_5)

3.5.3.1 Coating of Molten Salts

Magnetron sputtered coated as well as bare specimens (mirror polished) were prepared for studies as discussed in section 3.5.1. The specimens were then heated in an oven up to 250 °C and a salt mixture of Na_2SO_4-60%V_2O_5 dissolved in distilled water was coated on all the six surfaces of the warm polished specimens with the help of a camel hair brush. Amount of the

salt coating was kept in the range of 3.0 -5.0 mg/cm^2. The salt coated specimens as well as the alumina boats were then dried in the oven for 3 hours at 100 °C and weighed before being exposed to hot corrosion tests.

3.5.3.2 Hot Corrosion Studies

The bare as well as sputtered coated specimens after application of salt coating were subjected to hot corrosion in the laboratory furnace at 900 °C for 50-100 cycles as discussed in section **3.5.1.**

3.6 ANALYSIS OF CORROSION PRODUCTS OF OXIDATION IN AIR AND MOLTEN SALTS

All the specimens subjected to oxidation, and hot corrosion were analyzed for the characterisation of corrosion products. The surface and cross-section of the corroded specimens were analyzed by using various analytical techniques such as XRD, and FE-SEM/EDS.

3.6.1 Weight Change Studies

The weight change values were measured at the end of each cycle with the aim to establish the kinetics of oxidation and hot corrosion. The weight change data was plotted with respect to number of cycles for each specimen and the plots are given in the subsequent chapters. In this case, the weight change consists of a weight gain owing to the formation of the oxide scales and a weight loss due to the suspected spalling and fluxing of the oxide scales. Therefore, the net weight change in the industrial environment represents the combined effects of these two processes. The weight change data was plotted with respect to number of hours for each specimen and the plots are presented in subsequent chapter 4 and 5.

3.6.2 X-ray diffraction (XRD) Analysis

For identification of different phases formed in the oxides scales of oxidized/hot corroded specimens after 50-100 cycles in the laboratory, X-ray diffractometer has been used as described in section **3.3.1.**

3.6.3 FE-SEM/EDS Analysis

3.6.3.1 Surface Morphology

The surface morphology (**Biswas K et al.2008**) of some of the oxidized/hot corroded specimen surfaces after 50-100 cycles were studied with the help of a field emission scanning electron microscope (FE-SEM/EDS) (FEI Quanta 200F, Made in Czech Republic) and the details regarding the equipment are provided in section **3.3.2**. The specimens were scanned under the microscope and the critical areas of interests were photographed with an aim to identify the micro cracks, voids, inclusions and surface morphology of the scale. Point analysis by EDS was carried out at various locations on these identified areas of interest to understand composition (weight % and at %) of various phases in the oxide scales. Although these compositions correspond to selected points on the surfaces, the data could still be useful to support the formation of various phases in the oxide scales.

3.6.3.2 Cross-Sectional analysis

To understand the formation of elements, oxides and various other phases across the cross-section of oxidized and corroded samples, FE-SEM/EDS analysis for some of the selected specimens was carried out along their cross-sections using genesis EDAX software. Cross-sectional FE-SEM images were taken at some points of interest including scale/coating and substrate. The elemental composition (weight % and at %) was carried out by EDS analysis at various points along the cross-section. An approximate distribution of various elements across the thickness of the scales is estimated using these data.

CHAPTER 4
Cr/Co-Al COATINGS

4.1 EVALUATION OF HIGH TEMPERATURE OXIDATION BEHAVIOUR OF NANOSTRUCTURED Cr/Co-Al COATINGS

4.1.1 Introduction

Superalloys are used to fabricate the hot section components in industrial and aircraft gas turbine engines due to their excellent high temperature strength and creep resistance at high temperature. Since the superalloys provide only good structural integrity, protective coatings are required to obviate the high temperature corrosion problems for ensuring high efficiency and life of the turbine engines. Nanostructured MCrAlY(M = Ni, Co, or Fe) coatings have been identified as potential materials for providing good resistance against high temperature oxidation and hot corrosion **(Liu Z. et al. 1999, Liu Z. et al. 1999, Goa W. et al. 2001, Rahman A.et al. 2009, Rahman A. et al. 2011, Geng S.et al. 2002, Zhang C.et al. 2005)** as compared to conventional coatings due to the formation of dense, continuous, non-porous and adherent alumina and/or chromia scales over the coatings **(Cheruvu N. S. et al. 2010, Whittle D. P. 1978, Wang F. et al. 2008)**. The size effect of nanostructured coatings facilitates the enhanced diffusivity of atoms to form the continuous protective scales, which is normally discontinuous in the conventional coatings as reported in the literature **(Geng S.et al. 2003)**.

Short-term (50–200 hrs) test results on nanocrystalline Fe–Ni–Cr–Al coatings have shown that the continuous and protective Al_2O_3 scale formed on the coatings with Al content as low as 2 wt% exhibited better spallation resistance during cyclic oxidation testing **(Liu Z. et al. 1999, Liu Z. et al. 1999, Goa W. et al. 2001)** compared to the conventional cast materials of the same chemical compositions of the coatings. It is very essential that the oxide scales should be adherent to the coated substrate, under thermal cyclic conditions, and therefore its adherence is enhanced by addition of reactive rare earth elements such as Y, Ce to the superalloy coatings as reported in the literature **(Whittle D. P. and Stringer J. 1980).** The oxide layer formed on the nanocrystalline 304 SS-Al coatings on 310 SS samples exhibited excellent spallation resistance during cyclic oxidation testing at 1000 °C up to 100 hrs thermal cycles **(Cheruvu N. S. et al. 2009).**

Giggins and Petite (1969) and **Mertz M. D. (1979)** investigated the sputtered microcrystalline Ni–Cr alloy coatings deposited on 304 stainless steel and observed that it imparts higher oxidation resistance due to the formation of protective and adherent scale such as NiO and Cr_2O_3 over the coatings. Liu et al. **(1998)** have studied the effect of grain size on protective oxide scale formation and spallation behavior of oxide scale on a Ni–20Cr–3Al coating. The cyclic test results at a peak temperature of 1100 °C showed that fine grain size promoted formation of either Al_2O_3 or Cr_2O_3, as opposed to formation of a mixed oxide scale as reported in their work. **Wang F. et al. (1996)** and **Peng X. and Wang F. (2003)** have assessed the oxidation resistance of nanocrystalline Co–Cr–Al coatings and reported that the formation of a protective Al_2O_3 oxide layer on the external surface of a nanocrystalline coating depends on the Cr/Al ratio and grain size. Typically, ultra-fine grain promotes the formation of α- Al_2O_3 protective oxide scale even when the Al content in the coating is relatively low i.e. high ratio (Cr/ Al > 4). The formation of a continuous α-Al_2O_3 scale has been reported in nanocrystalline Ni–20Cr coating with an Al content as low as 2 wt% **(Liu Z and Gao W. 1998).** Furthermore, it has been shown that the nanocrystalline structure reduced the critical Al content required for α-Al_2O_3 scale formation by increasing the diffusion rate of Al **(Chen G. F. and Lou H. Y. 2000).**

The high temperature oxidation behaviour of sputter deposited nanostructured superalloy coatings has not been subjected to a detailed study so far. Therefore, the present work has been focused to evaluate the high temperature oxidation behavior of magnetron sputtered Cr/Co–Al coatings on the Superni-718 superalloy substrate. The formation of intermetallic β-CoAl phases in the Co–Al based superalloy coatings show high melting point (1640 °C), which is beneficial for providing oxidation resistance at very high temperature above 1000°C in the actual service applications, especially in gas turbines. The CoAl based nanostructured superalloy coatings could serve as potential protective coatings for the components in energy conversion systems such as stationary gas turbines of power plants, internal combustion engines, heat exchangers and jet engines operating at high temperatures, and in severe corrosive environments. The improved oxide spallation resistance on the nanostructured coatings has been attributed to the fine grain size of the scale formed on the microcrystalline and nanocrystalline coatings after thermal exposure **(Wang Z.B.et al. 2003, Cheruvu N. S.2009, Liu Z.et al. 1998, Wang F.1997).**

High efficiencies of engines, due to the application of protective coatings, would lead to a significant reduction of fuel consumption and a considerable decrease in exhaust gas emissions. High temperature resistant alloys based on the intermetallic compound CoAl alloyed with the refractory metals such as Cr, Mo or Re can be used as protective coatings for prospective energy conversion systems operating up to 1300°C in corrosive environments.

The development of Cr/Co–Al coatings consists of the following two stages namely (i) deposition of Cr coating on substrate, followed by (ii) co-sputtering of Co–Al, coatings on Cr coated substrate, in the present work. It is well known that the Al and Cr are two important inhibitors for high temperature applications. Above 900°C, Al forms stable Al_2O_3 scale, where as Cr forms unstable oxide Cr_2O_3, which oxidizes further into CrO_3. Since CrO_3 is volatile, it reaches to the top surface of Cr/Co–Al coatings, where aluminium is present in sufficient amount and facilitates the formation of Al_2O_3. Below 900°C temperature, Cr forms stable Cr_2O_3 scale. Cr coating deposited as an intermediate layer on the substrate form stable Cr_2O_3 scale, at 900°C temperature, which could act as diffusion barrier for outward diffusion of substrate element as well as inward diffusion of anions (O^{-2}). Thus, the Cr/Co–Al coatings may serve as a smart coating under fluctuating temperature during service conditions.

4.1.2 Experimental

Ni-based superalloy namely Superni-718 has been chosen to deposit Cr/Co–Al coating in the present work. The superalloy was procured from Mishra Dhatu Nigam Limited, Hyderabad, India in annealed and cold rolled sheet form and its chemical composition is shown in **Table 3.1 (discussed in section 3.4 of chapter 3 of thesis)**. Each specimen measuring approximately: 18 mm (L) × 15 mm (W) × 3 mm (T) were cut from the rolled sheet and ground by using 220, 320, 1/0, 2/0, 3/0, 4/0 grade SiC emery papers. Subsequently, it is polished on cloth polishing disc by using alumina powder followed by diamond paste. Commercially available Co Target (99.99 % pure) with dimension 2 inch diameter and 2.0 mm thickness and similarly, commercially available Al and Cr Target (99.99 % pure) with 2 in. diameter and 5.0 mm thickness were fixed at an angle of 45° to each other in the sputtering chamber. With the use of rotator, the substrate heater was rotated between Co and Al targets continuously to perform a co-sputtering. The target to substrate distance was fixed at 40 mm during deposition. Before starting the deposition, the targets were pre-sputtered for 15 min with a shutter located in between the targets and the substrate. The shutter is also used to control the deposition time. All the samples were cleaned in acetone, ethanol and deionized water prior to the deposition of Cr/Co–Al coatings. The process parameters used in DC/RF magnetron sputtering are given in Table **4.1.**

The sputtering parameters used for the deposition of the Cr/Co-Al coatings with varying substrate temperature, and deposition time are given in Table **4.2.**

Table 4.1 Sputtering parameters for Cr/Co-Al coatings on Superni-718 substrate

Target	Cr (99.99% pure, 2 inch diameter & 5 mm thickness)
	Al (99.99% pure, 2 inch diameter & 5 mm thickness)
	Co (99.99% pure, 2 inch diameter & 2 mm thickness)
Base pressure	3×10^{-6} Torr
Deposition gas pressure (Ar)	10 mTorr
Deposition power	100 W for Cr target
Deposition time for Cr Coating	30 minutes
Deposition power	50 W/100 W for Co/Al target
Deposition time for Co-Al Coating	60 minutes
Substrate	Superni718
Substrate Temperature	250 °C, 350 °C & 450 °C
Total Deposition time	90 minutes

Table 4.2 Sputtering parameters for Cr/Co-Al coatings with variation of substrate temperature and deposition time

Target	Al (99.99% pure, 50.8 mm diameter & 5 mm thickness)
	Co (99.99% pure, 50.8 mm diameter & 2 mm thickness)
	Cr (99.99% pure, 50.8 mm diameter & 5 mm thickness)
Base pressure	3×10^{-6} Torr
Deposition gas pressure (Ar)	15 m Torr
Deposition power	100 W for Cr target
Deposition time for Cr Coating	30 minute
Deposition power	70 W/150 W for Co/Al target
Deposition time for Co-Al Coating	90 minute
Substrate	Superni-718
Substrate Temperature	500°C & 700°C
Total Deposition time	120 minute

4.1.2.1 Characterization of Cr/Co-Al Coatings

XRD (Bruker AXS, D8 Advance) measurements were made using Cu k_α radiation to characterize the as deposited Cr/Co–Al coatings fabricated at 250, 350, 450, 500 and 700°C on Superni 718 substrate. The scan rate and the scan range used were 0.1 sec/step and from 20° to 100°, respectively. An average grain size of the Cr/Co–Al coatings is estimated using its XRD peak broadening according to Scherrer formula **(Zou D. et al. 2008)**, as given in Eq.

4.1. It was found to be in the range of 20–35 nm and 20.7, 26.2, 23.4, 28.7 and 19.3 nm at 250, 350, 450, 500, and 700°C respectively.

$$B(2\theta) = \frac{k\lambda}{DCos\theta} \qquad (4.1)$$

Where D is the average size of crystallite, B is the broadening of the diffraction line measured at half maximum intensity, k is constant (k = 1 is used in the present work), λ is the wavelength of the X-ray radiation (1.54052 A° , CuK_α) and θ is the Bragg angle. Instrumental broadening has been accounted for the calculation of grain size, and its value of 0.1(for standard Si sample) has been subtracted from the full-width half maximum (FWHM) value, from B value.

FE-SEM/EDS (FEI, Quanta 200F) has been used to characterize the microstructures of the as deposited Cr/Co–Al coatings at an acceleration voltage of 20 kV. The surface morphology of the Cr/Co–Al coatings has been characterized by AFM (NT-MDT, Ntegra) operated in a semi contact (tapping) mode in order to calculate its surface roughness. The root-mean-square (RMS) roughness of the surface of the sample was calculated from AFM scan at five different spots for each sample. The morphology and phase constituent of oxidized products of coatings and bare superalloy substrate were characterized by FE-SEM/EDS and XRD.

4.1.2.2 High Temperature Oxidation Studies

The weight change measurements were used to study the kinetics of high temperature oxidation behavior of the Cr/Co–Al coating as well as bare superalloy substrate in air at 900°C. The bare and Cr/Co–Al coated superalloy samples were kept in the alumina boats and then inserted inside SiC tube furnace. The bare substrate specimens were mirror-polished before oxidation. Cyclic high temperature oxidation studies were performed in air with each cycle consisting of 1 hour of heating at 900 °C followed by 30 min of cooling at room temperature for up to 50 -100 cycles. The cyclic loading was imposed to create the aggressive conditions, similar to the actual conditions, for oxidation/corrosion testing. Since Superni-

718 substrate can be used only up to maximum temperature of 800 °C due to the presence of Mo in it, temperature of 900 °C has been chosen for the cyclic oxidation studies. The duration of 50-100 cycles has been chosen to check if the continuous and protective alumina scale could form over the nanostructured coatings within the short-duration. The weight changes were monitored, using an electronic balance Model CB-120 (Contech, Mumbai, India) with a sensitivity of 10^{-5} g. During each cycle, the measured weight changes for bare and coated samples were used to calculate the oxidation rate. As spalled scales if any was also included in the weight change measurements. The kinetics of oxidation was determined from the weight change measurements. After oxidation studies, the oxidized samples were analyzed by using XRD and FE-SEM/EDS techniques to elucidate the oxidation mechanisms.

4.1.3 Results

4.1.3.1 XRD and AFM Analysis of the Coatings

The XRD pattern of as deposited Cr/Co–Al coatings on Superni 718 at 250, 350 and 450°C substrate temperatures are shown in **Fig. 4.1a.** The intermetallic β-CoAl phase is observed at different substrate temperatures, since outer layer of Cr/Co–Al coating contains high Co and Al as evident from the XRD results. The XRD results for the oxidized products of bare and Cr/Co–Al coated samples at 250, 350 and 450°C substrate temperatures after 50 hrs of cyclic oxidation at 900°C in air are shown in **Fig. 4.1b.** It is observed that the oxide scales such as Cr_2O_3, NiO, Fe_2O_3 are formed on the bare superalloy subjected to high temperature air oxidation at 900°C for 50 cycles. The oxide scale such as CoO, Cr_2O_3, $CoCr_2O_4$ and Al_2O_3 were observed in the oxidized Cr/Co–Al coated superalloy samples at 250, 350 and 450°C substrate temperatures after 50 cycles at 900°C in air. XRD pattern of as deposited Cr/Co-Al coatings on Superni 718 at 500 and 700°C substrate temperature are presented in **Fig.4.1 (c)** and the results revealed that the intermetallic β-CoAl phase is observed in coatings at two different substrate temperatures, which is in tandem with the intermetallic phase found in the CoAl binary phase diagram. The XRD patterns of the oxidized Cr/Co-Al coated sample at 500 and 700°C substrate temperature and oxidized bare substrate after 100 hrs of cyclic high temperature oxidation at 900°C exhibit the presence of several oxide phases **(Fig. 4.1(d)).** On

high temperature oxidation, the Cr/Co-Al coated sample at 500°C after 100 cycles gives rise to Cr_2O_3, Al_2O_3 CoO and $CoAl_2O_4$ as a major phase **(Fig.4.1 (d))**. The Cr/Co-Al coating at 700°C after 100 cycles give rise to similar phases namely Cr_2O_3, Al_2O_3 CoO and $CoAl_2O_4$ as a major phase, and also a minor phase of $CoCr_2O_4$. On the other hand, bare substrate after 100 cycles gives rise to phases namely Cr_2O_3, NiO, and Fe_2O_3 **(Fig.4.1 (d))**. XRD analysis **(Fig.4.1(d))** indicates that NiO and Fe_2O_3 phases were not present in oxidized Cr/Co-Al coated sample at 500 and 700°C substrate temperature, it means that intermediate Cr coating layer has worked as a barrier coating for substrate element (outward diffusion) during oxidation at 900 °C for 100 hrs, it forms protective Cr_2O_3 and spinel phase of $CoCr_2O_4$.
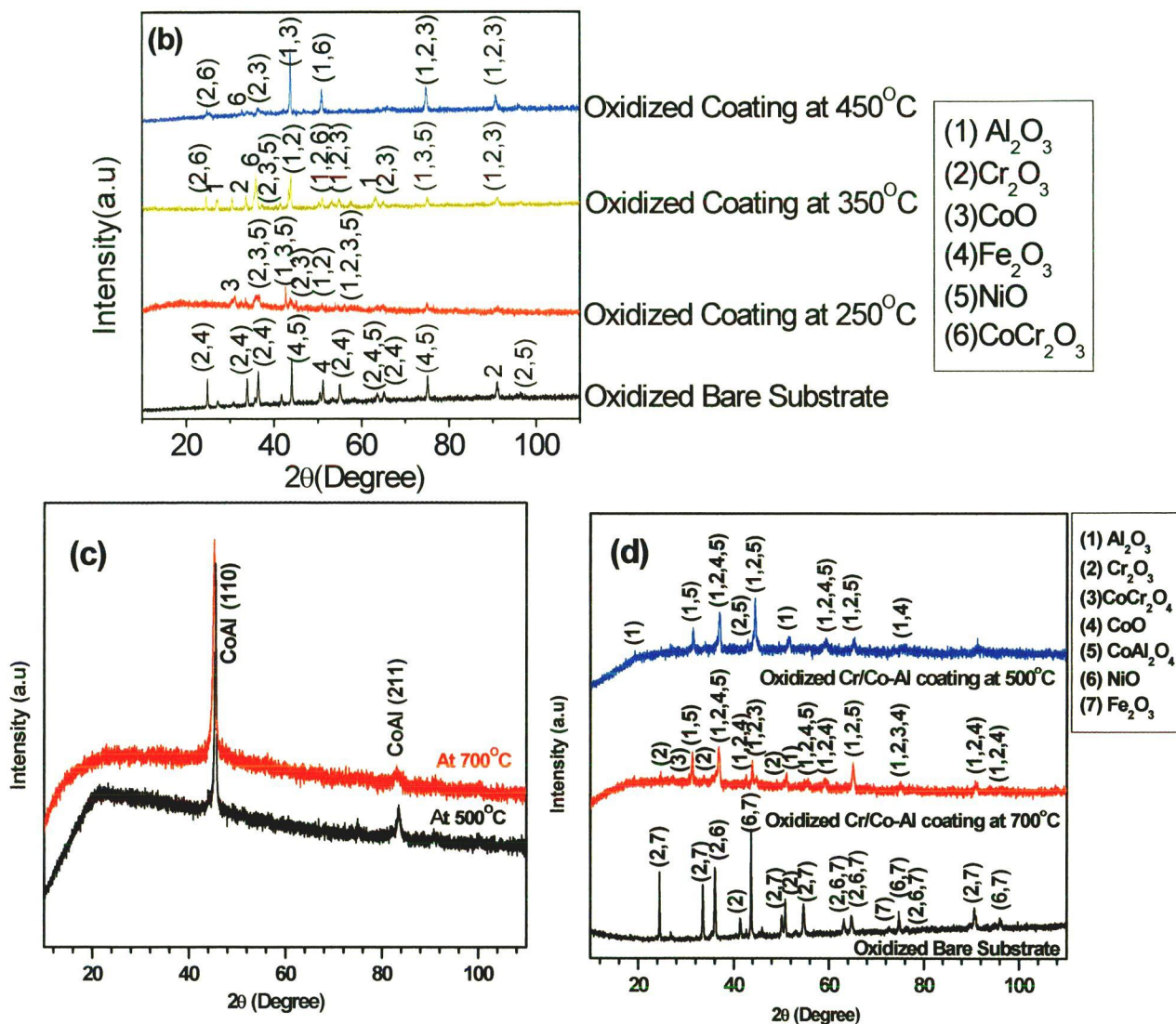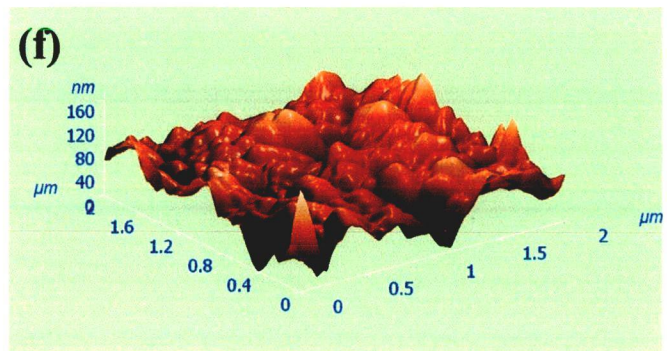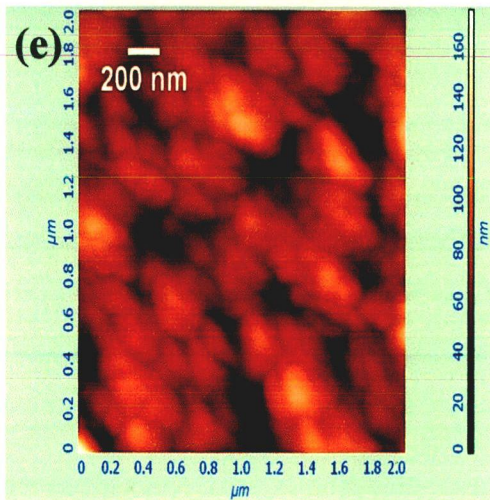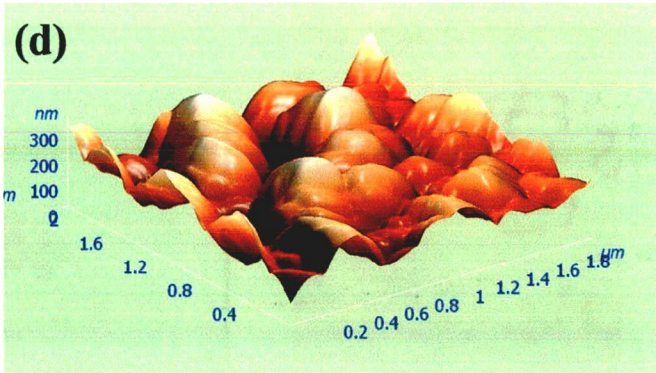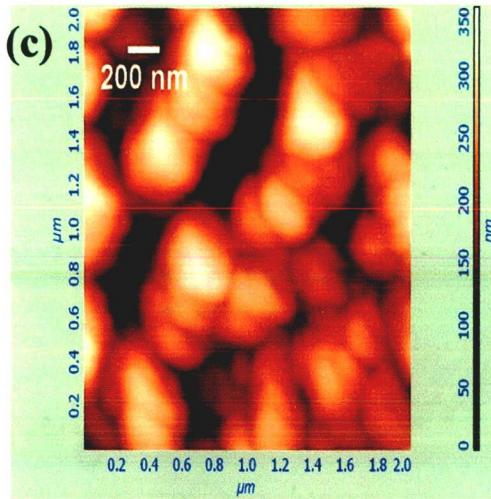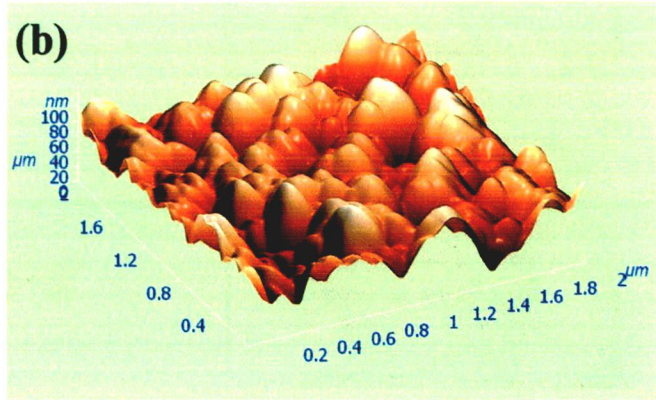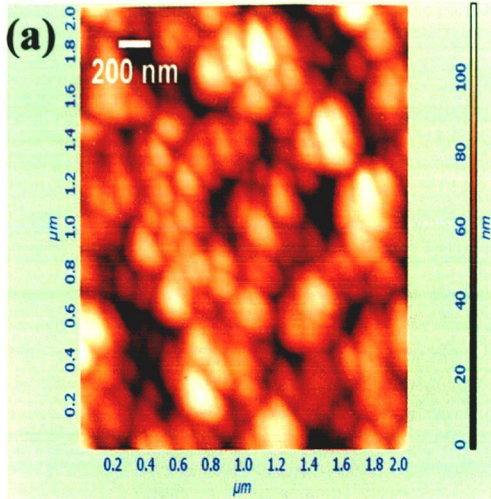

(a)
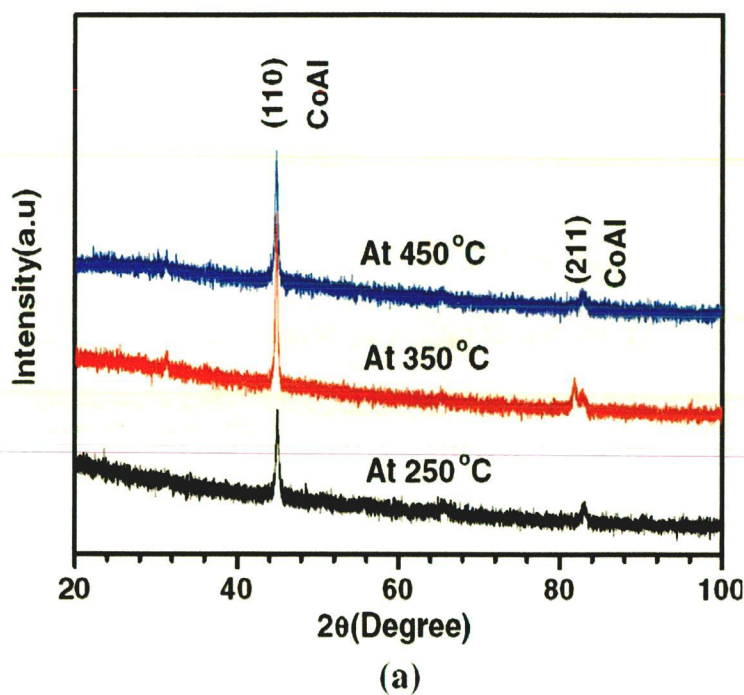
Fig.4.1 XRD pattern of (a) as deposited Cr/Co–Al coatings at 250, 350 and 450°C substrate temperatures and (b) oxidized Cr/Co–Al coatings on Superni-718 at 250, 350 and 450°C after 50 hrs and oxidized bare substrate after 50 hrs. XRD pattern of (c) as deposited Cr/Co-Al coatings at 500-700°C and (d) Oxidized Cr/Co-Al coatings on Superni-718 at 500-700°C substrate temperature after 100 hrs and oxidized bare substrate after 100 hrs
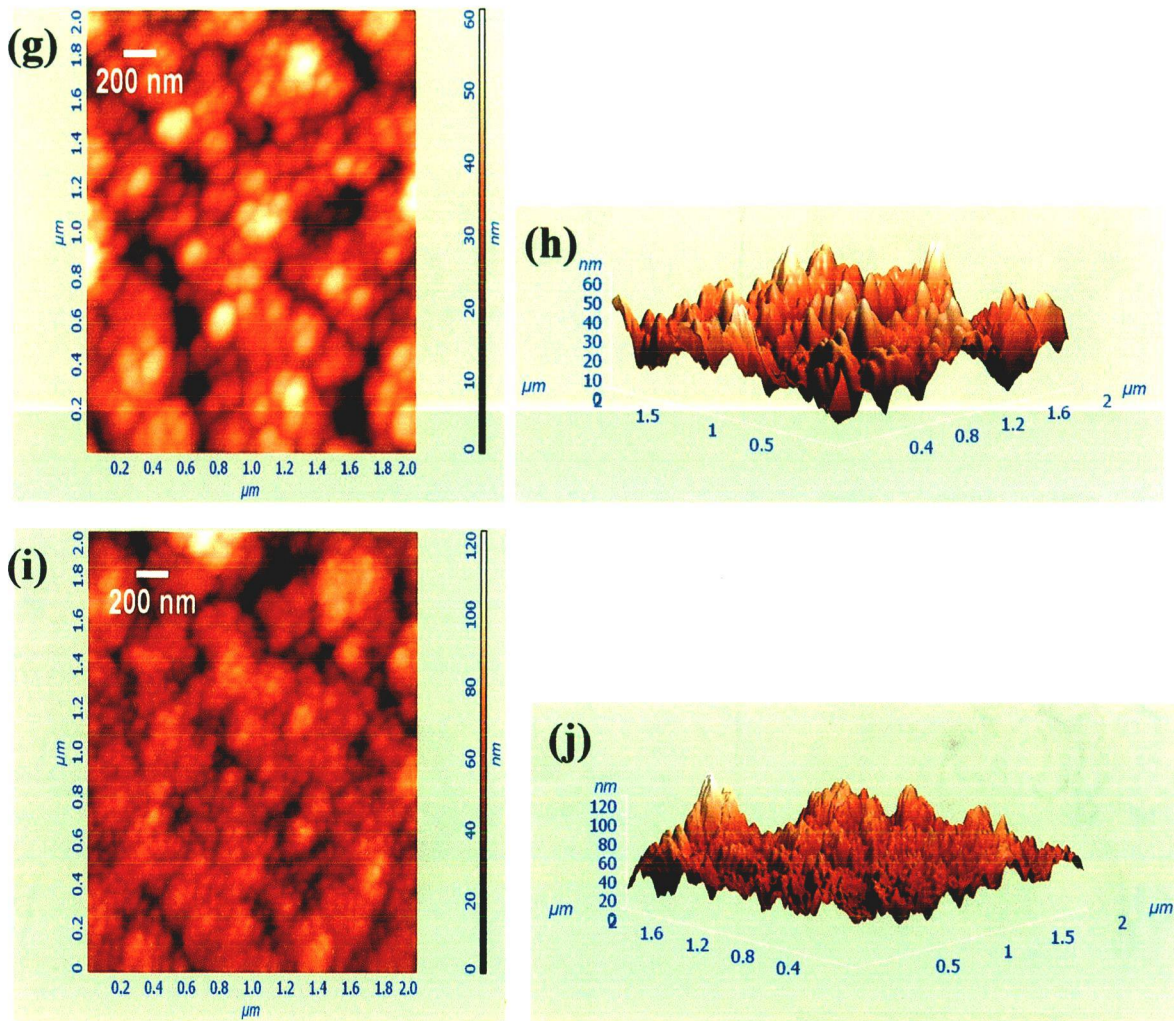
Fig.4.2 (a-j) AFM 2D & 3D images of Cr/Co–Al coatings on Superni-718 substrate at different substrate temperatures (a–b) at 250°C, (c–d) at 350°C , (e–f) at 450°C (g–h) at 500°C and (i–j) at 700°C

The 2D and 3D AFM images of the Cr/Co–Al coatings deposited at 250, 350, 450, 500 and 700°C substrate temperatures are shown in **Fig. 4.2(a–j).** The surface roughness of the coatings was found to be 18.3, 61.4, 19.9, 9.2 and 13.8 nm for the coatings deposited at 250, 350, 450, 500, and 700°C, respectively.

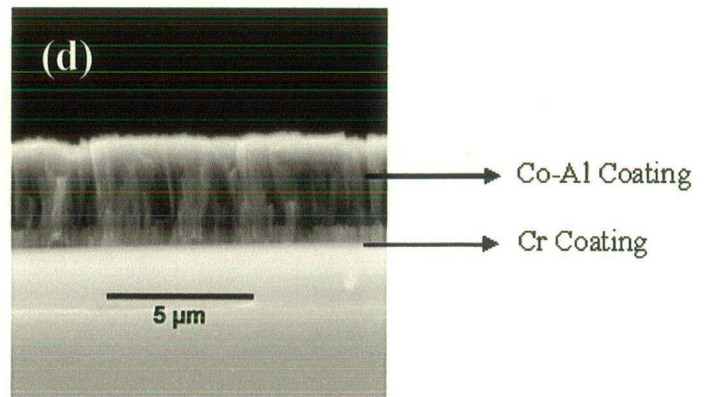## 4.1.3.2 Microstructural Characterization of Cr/Co-Al Coatings

FE-SEM surface micrographs with EDS at different points on the surface of Cr/Co–Al coatings at 250, 350 and 450 °C are shown in **Fig. 4.3(a–c)**. The observed microstructural features of the coatings can be classified by using the structure zone model proposed by Meissier **et al. (1984)**. The homogeneous temperature, (ratio of substrate temperature to melting point of the coating materials), is used to classify the coating microstructures observed at different substrate temperature during sputter deposition of the coatings. In the present work, the coating deposited at 250 °C exhibits a homogeneous temperature of 0.27 and showed globular shape grains and porous morphology, which approaches zone 1 structures as reported in Meissier's work. The homogeneous temperature (T_s /T_m) is 0.32 for the coatings deposited at 350°C and the elongated shape grains, looks like layer type deposition and dense morphology are observed at this deposition temperature, which comes under zone 2 structure. The coating deposited at 450°C exhibits a homogeneous temperature of 0.37 and showed spherical shape grains with dense morphology, which also approaches zone 2 structure. The cross-sectional FE-SEM/EDS micrograph of one of the as deposited coatings is shown in **Fig.4.3 (d)** which exhibits columnar structure. The thickness of coatings was calculated by its cross sectional FE-SEM images **(Fig.4.3 (d))** and it was found to be approximately 4.5 μ m.
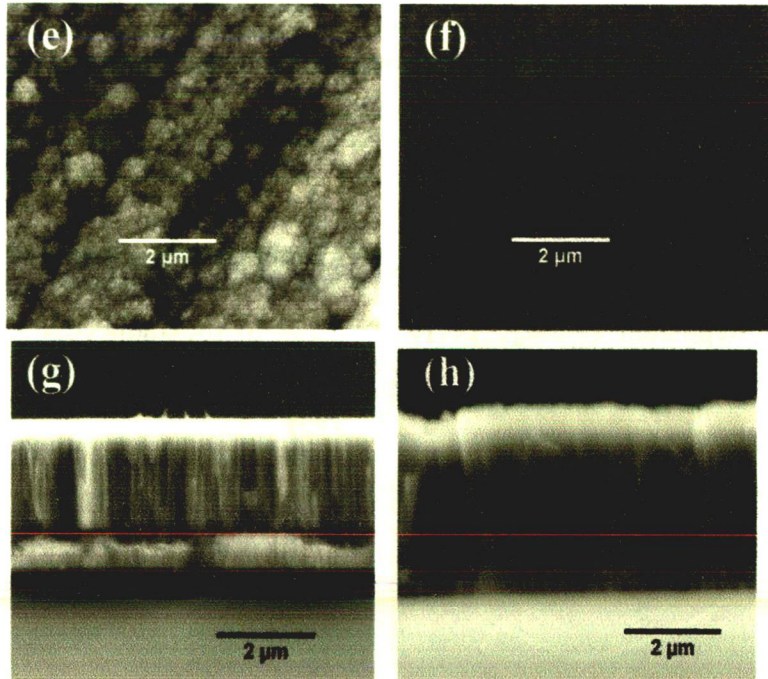
Surface morphology of Cr/Co-Al coated sample at 500 °C and 700 °C substrate temperature before oxidation was examined and the same is shown in **Fig.4.3 (e-f)**. The Cr/Co-Al coating deposited at 500 °C **(Fig.4.3 (e))** showed large spherical shape grains, where as the Cr/Co-Al coatings deposited at 700 °C **(Fig.4.3 (f)** showed smaller spherical shape grains with dense coating. Cr/Co-Al coating deposited at 500 °C and 700°C substrate temperature belong to zone 2 and zone 3, as structure zone model proposed by **Meissier et al. (1984)**. The cross-sectional morphology of Cr/Co-Al coating on Superni-718 at 500-700°C substrate temperatures before oxidation was examined and is shown in **Fig.4.3 (g-h)**. Coating deposited at 500 °C has fine columnar grains **(Fig. 4.3(g))**, whereas coating deposited at 700 °C has slightly thicker columnar grain **(Fig. 4.3(h))**. With increase in substrate temperature,

the surface mobility of condensed atoms increases, which could easily diffuse from island side to lower potential zone of substrate, resulting in denser coating with reduced porosity or voids in coatings. Thus AFM and FE-SEM (surface and cross-sectional) analysis indicate that the coatings deposited at 700 °C are denser as compared to coatings deposited at 250, 350, 450, and 500 °C. The thickness of coatings was calculated by its cross sectional FE-SEM images and it was found to be approximately 5 μm. It is observed that by increasing the deposition time of Co-Al co-sputter coating from 60 minute to 90 minute, thickness of coating has been increased to 0.5 μm. The chemical compositions of the as deposited Cr/Co-Al coating on Superni-718 substrate has been analyzed at the surface as well as the depth profile as shown in cross-sectional FE-SEM/EDS micrographs **(Fig. 4.3(i)).**
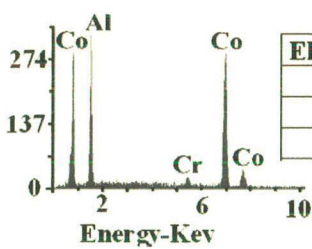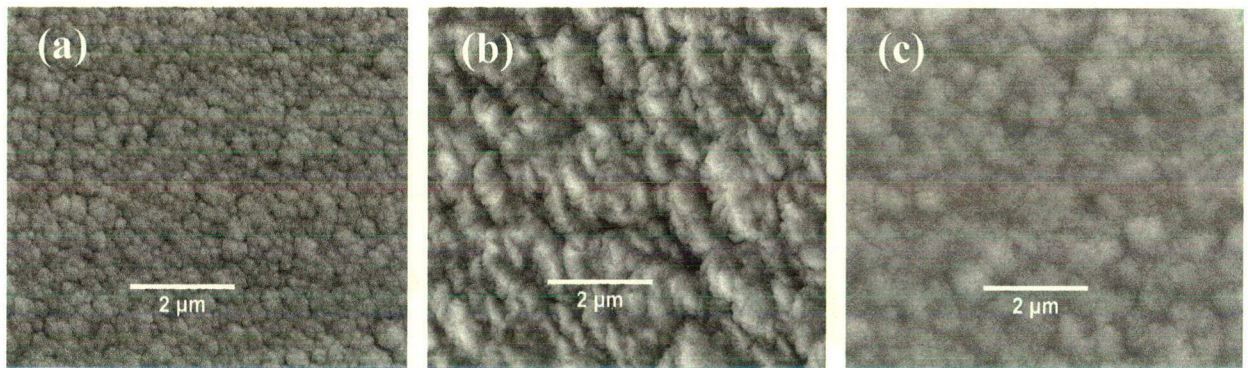
Element	Wt%	At%
Al	30.38	48.66
Cr	03.12	02.60
Co	66.49	48.75

Surface EDS analysis (i)   **Cross-sectional EDS analysis**

Element	Wt%	At%
AlK	23.89	40.67
CoK	76.11	59.33
Matrix	Correction	ZAF

Element	Wt%	At%
AlK	12.69	23.81
CrK	77.07	66.21
CoK	10.24	09.97
Matrix	Correction	ZAF
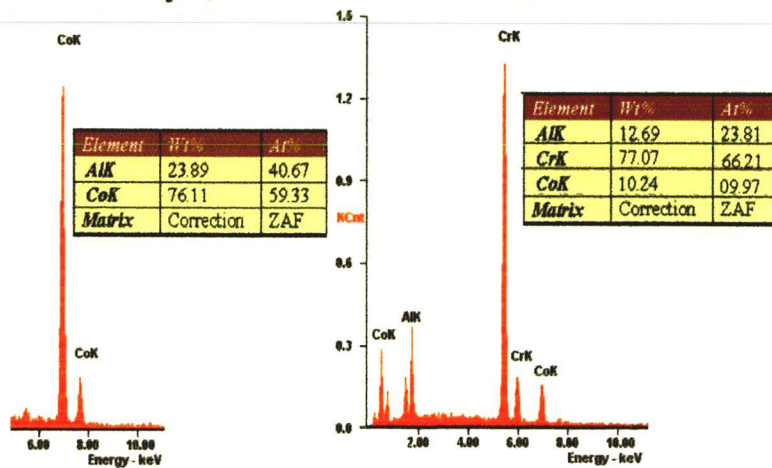
EDS surface micrographs of Cr/Co–Al coatings on Superni-718 substrate at different substrate temperatures (a) at 250°C, (b) at 350°C , (c) at 450°C, (d) Cross-sectional FE-SEM/EDS micrograph of as deposited

one of the Cr/Co-Al coating at 350°C , (e) at 500°C, and (f) at 700°C. And Cross-sectional FE-SEM/EDS micrograph of as deposited Cr/Co- Al coated sample at different substrate temperature, (g) at 500°C, and (h) at 700°C, (i) the detailed chemical compositions of the as deposited Cr/Co-Al coatings, on Superni-718 substrate (analyzed by depth profile on surface as well as cross-sectional).

The Cr/Co-Al coatings were deposited on Superni-718 at 800°C substrate temperatures, the deposited coatings peeled off due to the induced thermal stress in the coatings, which was confirmed by FE-SEM as shown in **Fig.4.4 (a-b).**
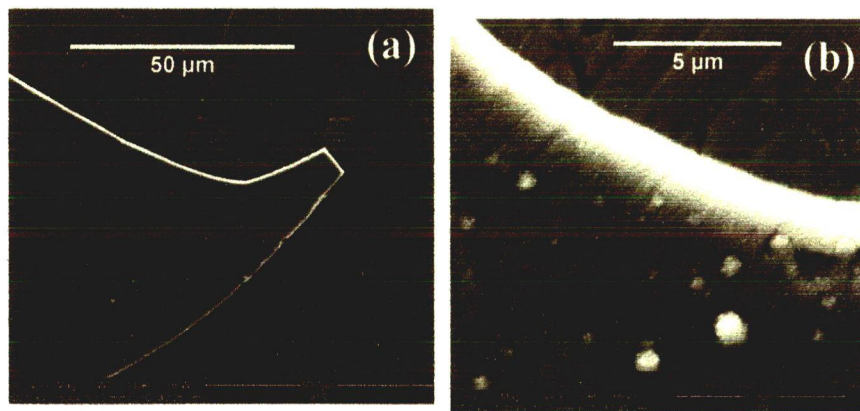

Fig.4.4 (a-b) FE-SEM surface micrographs at different locations of Cr/Co-Al coating deposited at substrate temperature 800°C.

## 4.1.3.3 Cyclic High Temperature Oxidation Studies in Air

The weight gain per unit area versus number of cycle's plots for the bare substrate and Cr/Co–Al coatings deposited at different substrate temperatures 250, 350 and 450°C on Superni-718 subjected to high temperature air oxidation studies at 900° C after 50 cycles is shown in **Fig.4.5(a).** It is observed that under cyclic conditions, the bare substrate is more

prone to oxidation/corrosion attack. The nature of oxidation kinetics of coatings and bare substrates was determined by using the changes in their weight measured as a function of different cycles. Mass gain results **(Fig.4.5(a))** of Cr/Co-Al coated specimen show that it follows nearly a parabolic law, where as bare substrate showed a deviation from the parabolic law. Parabolic law is diffusion controlled after the initial chemical controlled reaction of the coated specimens. Once a nearly constant weight gain is obtained, it indicates the parabolic law, which precludes further oxidation/corrosion process. The weight changes square (mg^2 / cm^4) verses time (number of cycles) plots are shown in **Fig.4.5 (b)** to establish the rate law for the oxidation. K_P value is calculated by a linear least-square algorithm to a function in the form of $(W/A)^2 = K_p$ t, where W/A is the weight gain per unit surface area ($mg\ cm^{-2}$) and 't' indicates the number of cycles represents the time of exposure. Bare substrate has $R^2 = 0.98$ **(Fig.4.5 (b))**, means that it follows 98% of linear law of oxidation, deviating mostly from parabolic law of oxidation, confirmed by weight variation /area ($mg\ cm^{-2}$) graph in **Fig.4.5(a)**. On the other hand, Cr/Co-Al coated sample at 250°C substrate temperature has $R^2 = 0.87$(Fig.4.5 (b)), means that it follows 87% of linear law of oxidation and 13% of parabolic law of oxidation. It is evident from Fig.4.5 (a) that after 30th cycles, weight gain is very less, almost constant up to 50 cycles, showing a parabolic nature. Where as Cr/Co-Al coated sample at 350°C substrate temperature has $R^2 = 0.043$(Fig.4.5 (b)), means that it follows 4.3% of linear law of oxidation and 95.7% of parabolic law of oxidation. It is evident from Fig.4.5 (a) that after 10th cycles, weight gain is very less, almost constant up to 50 cycles, showing a parabolic nature.

The R^2 value of Cr/Co-Al coated sample at 450°C substrate temperature is 0.14(Fig.4.5 (b)), revealing that it follows 14% linear law of oxidation and 86% of parabolic law of oxidation. It is shown in Fig.4.5 (a) that weight gain continues up to 25th cycles and afterwards, it is nearly constant up to 50 cycles, obeying parabolic law. The parabolic rate constant is calculated from the slope of the linear regression fitted line from (weight changes/area)^2 versus number of cycles as shown in **Fig.4.5(b)**. There is a visible deviation from the parabolic rate law in case of bare Superni-718 and a least deviation of coated sample deposited at 250, 350 and 450°C is observed up to 50 cycles. The weight gain data for the bare samples shows that it is prone to severe oxidation. The higher weight gain of bare alloy after 25th cycles is due to spallation of initial oxide scales and the continuous exposure of

fresh surface of the materials during oxidation. The evaporation of volatile impurities in bare substrate, during high temperature exposure, result in the formation of pores, which might also contribute to the enhanced reaction between the bare sample and oxygen. Cr/Co–Al coatings at 350°C substrate temperature on Superni-718 have shown a minimum weight gain as compared to other samples of Cr/Co–Al coating at 250 and 450°C substrate temperature and bare substrate The parabolic rate constant K_p was calculated by a linear least-square algorithm to a function in the form of $(W/A)^2 = K_p t$, where W/A is the weight gain per unit surface area (mg/cm^2) and 't' indicates the number of cycles represents the time of exposure. The calculated K_P for the Cr/Co–Al coating at 250, 350 and 450°C on superalloy after 50 cycles is found to be 10.889×10^{-12} gm^2/ cm^4 s^{-1}, 1.861×10^{-12} gm^2/ cm^4 s^{-1} and 2.361×10^{-12} gm^2/ cm^4 s^{-1}, respectively. It is very less as compared to the K_P value of 86.083×10^{-12} gm^2/ cm^4 s^{-1} obtained for the bare superalloy substrate. Thus, Cr/Co–Al coating at 350°C has provided a better protection to the Superni-718 during high temperature oxidation at 900°C in air environment for 50 cycles.
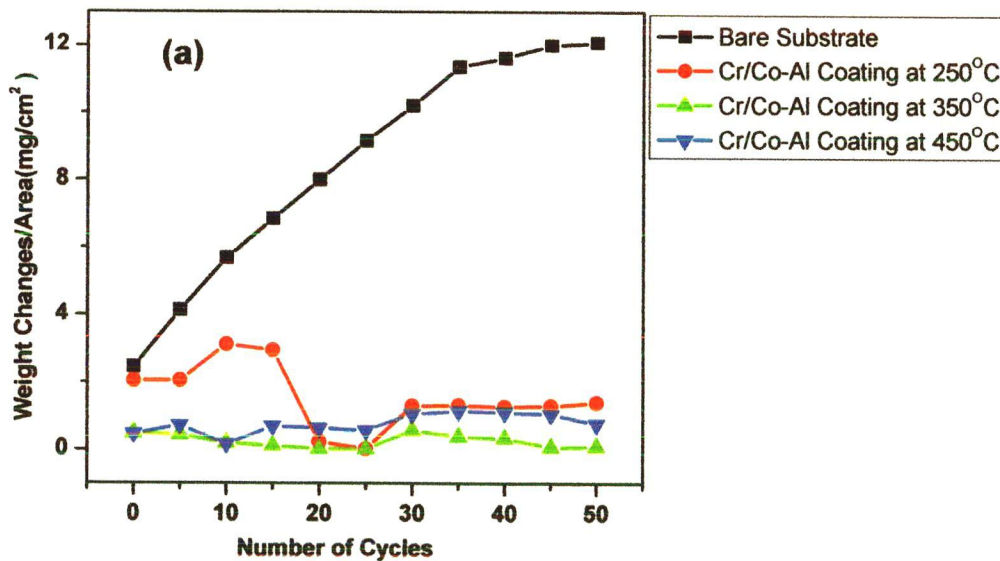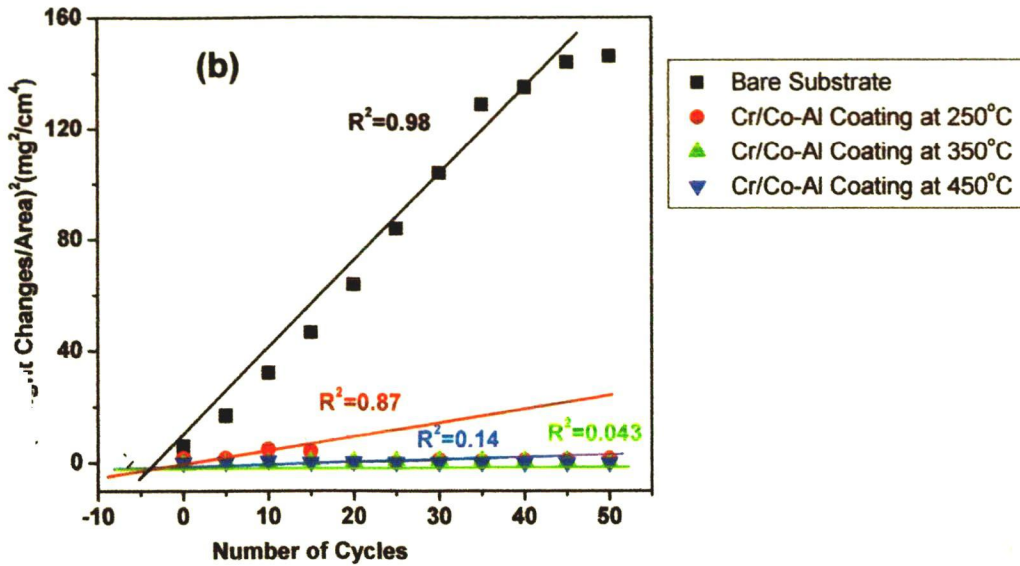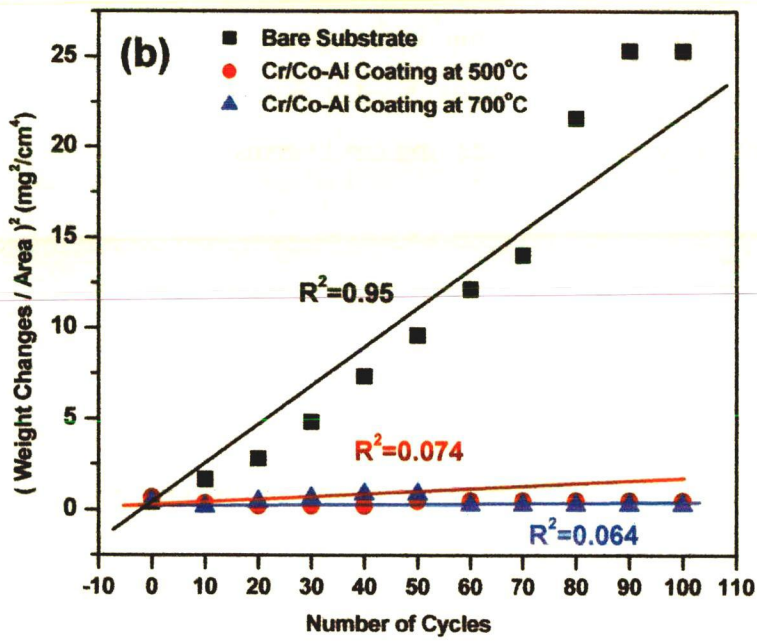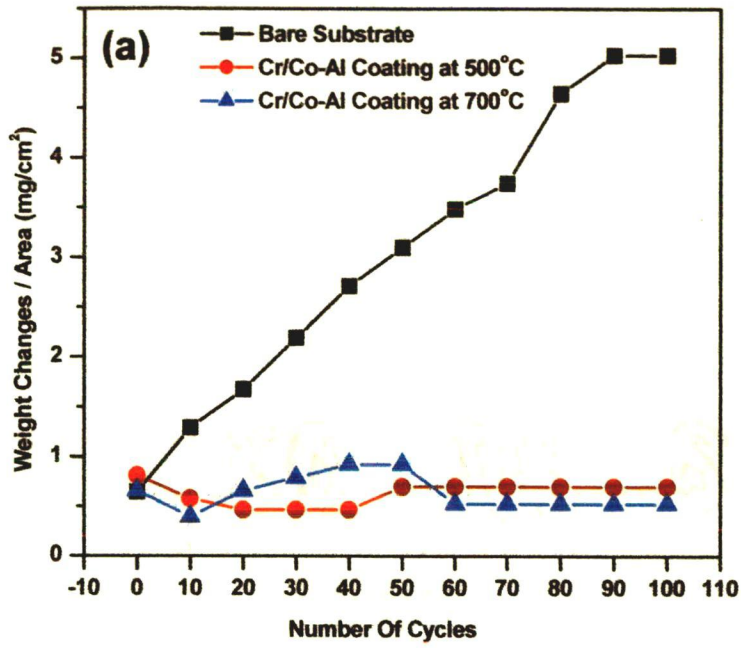
g.4.5 (a-b) Weight changes/area (mg/cm^2) versus number of cycles and Parabolic rate constant, K$_P$ (Weight change/area)^2, mg^2/cm^4 versus number of cycles, for bare and coated samples at 250,350 and 450°C oxidized in air at 900°C, for 50 cycles.

Further, the oxidation kinetics of the bare superalloy (Superni-718) and Cr/Co-Al coating deposited on superalloy substrate, at 500 and 700°C substrate temperatures were studied in air environment at 900°C for 100 cycles. Weight gain data as a function of time of all specimens is shown in **Fig. 4.6(a).** The weight gain plots of Cr/Co-Al coated sample at different substrate temperature and bare substrate are compared in order to demonstrate the influence of high temperature oxidation behavior of the coated samples. The **Fig.4.6 (a)** shows that the Cr/Co-Al coated sample at 500-700°C has lower weight gain as compared to bare substrate. The Cr/Co-Al coating at 700°C shows the lowest weight gain as compared to bare substrate and Cr/Co-Al coating at 500°C after 100 cycles **(Fig.4.6 (a)).** This implies that the bare substrate is more susceptible as compared to Cr/Co-Al coated sample with respect to high temperature oxidation in air at 900°C. From the **Fig.4.6(a),** it may be inferred that the Cr/Co-Al coating at 700°C is more oxidation resistant at 900°C after 100 cycles. The high temperature oxidation kinetic behaviour of the bare Superni-718 substrate and Cr/Co-Al coating on Superni-718 at 500-700°C substrate temperature was further examined and shown

in **Fig.4.6(b)** as (weight gain/area)^2 versus time plots). K_P value is calculated by a linear least-square algorithm to a function in the form of $(W/A)^2 = K_p\, t$, where W/A is the weight gain per unit surface area (mg cm^{-2}) and 't' indicates the number of cycles represents the time of exposure. Bare substrate has $R^2 = 0.95$ (Fig.4.6 (b)), means that it follows 95% of linear law of oxidation, deviating mostly from parabolic law of oxidation, confirmed by weight variation /area (mg cm^{-2}) graph in Fig.4.6 (a).On the other hand, Cr/Co-Al coated sample at 500°C substrate temperature has $R^2 = 0.074$(Fig.4.6 (b)), means that it follows 7.4% of linear law of oxidation and 92.6% of parabolic law of oxidation. It is evident from Fig.4.6 (a) that after 50th cycles, weight gain is very less, almost constant up to 100 cycles, showing a parabolic nature. Where as Cr/Co-Al coated sample at 700°C substrate temperature has $R^2 = 0.064$(Fig.4.6 (b)), means that it follows 6.4% of linear law of oxidation and 93.6% of parabolic law of oxidation. It is evident from Fig.4.6 (a) that after 55th cycles, weight gain is very less, almost constant up to 100 cycles, showing a parabolic nature. The calculated K_p for the Cr/Co-Al coating at 500 °C and 700 °C after 100 cycles at 900°C in air environment was found to be 0.511×10^{-12} g^2 cm^{-4} s^{-1}, and 0.333×10^{-12} g^2 cm^{-4} s^{-1}, respectively. It is very less as compared to the K_p value of 75.122×10^{-12} g^2 cm^{-4} s^{-1} obtained for the bare superalloy substrate. The total weight gain at the end of the 100 cycles for bare Superni-718 substrate has been found to be 33.55 mg/cm^2. However, the total weight gain in case of Cr/Co-Al coated sample at 500°C and 700°C was found to be 6.97 and 4.75 mg/cm^2 respectively. **Fig.4.6(c)** shows the cumulative weight gain per unit area for Cr/Co-Al coated sample at 500-700°C substrate temperature and bare Superni-718 substrate subjected to cyclic high temperature oxidation for 100 cycles in air at 900 °C. It is inferred from the cumulative weight gain per unit area plot that total weight gain in case of Cr/Co-Al coating on Superni-718 substrate at 700 °C after 100 hrs cyclic oxidation at 900°C was lower than the Cr/Co-Al coating at 500 °C and bare Superni-718 substrate. This aspect is further examined using microscopy studies.
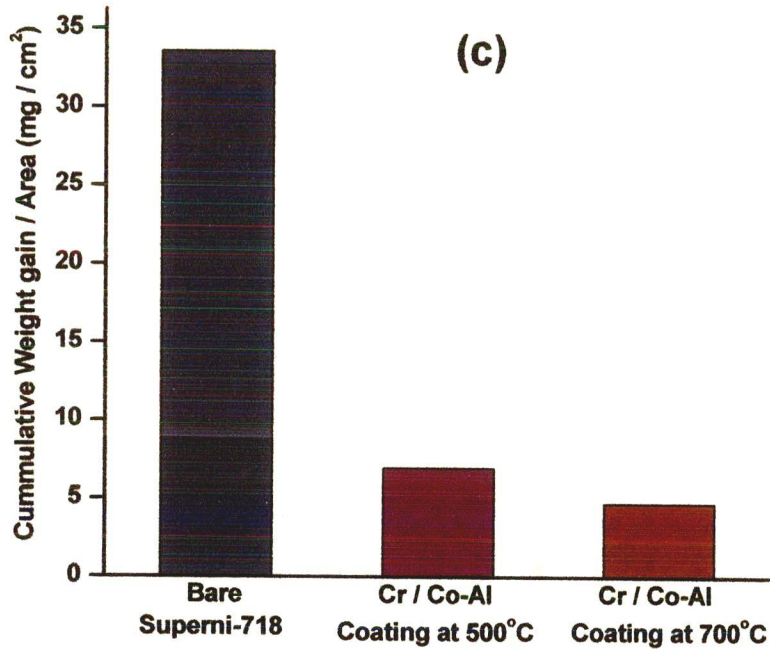
Fig.4.6 (a-b) Weight changes/area (mg/cm^2) versus number of cycles and Parabolic rate constant, K_P (Weight change/area)^2, mg^2/cm^4 versus number of cycles, for bare and coated samples at 500-700°C oxidized in air at 900°C after 100 cycles, and (c) Cumulative weight gain/area (mg/cm^2) versus number of cycles, for bare and coated samples at 500-700°C oxidized in air environment at 900°C, for 100 cycles.

4.1.3.4 Surface Scale Analysis

FE-SEM/EDS surface micrographs at the selected points of interest of oxidized bare substrate Superni-718 after 50 cycle's oxidation in air at 900°C are shown in **Fig.4.7 (a–b)**. The scale formed on bare Superni-718 has spalled and the cracks were formed as shown in **Fig.4.7b.** The EDS result showed that scale on the surface of oxidized bare substrate has chromium rich oxide and also iron and nickel oxide are present. These results are also confirmed by XRD results which are shown in **Fig.4.1b.** The large numbers of small pores on the surface of the specimen are observed from **Fig.4.7a.** The FE-SEM surface micrographs of oxidized Cr/Co-Al coatings at 250, 350 and 450°C substrate temperature after 50 cycles oxidation in air (at 900°C) at the selected points of interest are shown in **Fig.4.8 (a-c)** along